



NÚMERO: 438/2011
UNIVERSIDADE ESTADUAL DE CAMPINAS
INSTITUTO DE GEOCIÊNCIAS

JOSÉ PAULO DONATTI FILHO

**PETROGÊNESE DO CAMPO KIMBERLÍTICO BRAUNA,
CRÁTON DO SÃO FRANCISCO**

TESE DOUTORADO APRESENTADA AO
INSTITUTO DE GEOCIÊNCIAS DA UNICAMP
PARA OBTENÇÃO DO TÍTULO DE DOUTOR EM
CIÊNCIAS NA ÁREA DE GEOLOGIA E
RECURSOS NATURAIS

ORIENTADOR: PROF. DR. ELSON PAIVA DE OLIVEIRA

Campinas, Outubro de 2011

FICHA CATALOGRÁFICA ELABORADA POR
CÁSSIA RAQUEL DA SILVA – CRB8/5752 – BIBLIOTECA “CONRADO PASCHOALE” DO
INSTITUTO DE GEOCIÊNCIAS
UNICAMP

D715p Donatti Filho, José Paulo 1981-
 Petrogênese do campo kimberlítico Brauna, Cráton do
 São Francisco / José Paulo Donatti Filho--
 Campinas,SP.: [s.n.], 2011.

Orientador: Elson Paiva de Oliveira.
Tese (doutorado) - Universidade Estadual de
Campinas, Instituto de Geociências.

1. Crátions - Bahia. 2. Kimberlito. 3. Petrologia. 4.
Geocronologia. 5. Geoquímica. I. Oliveira, Elson Paiva
de, 1947- II. Universidade Estadual de Campinas,
Instituto de Geociências. III. Título.

Informações para a Biblioteca Digital

Título em inglês: Petrogenesis of the Brauna Kimberlite Field, São Francisco craton..

Palavras-chaves em inglês:

São Francisco craton

Kimberlite

Petrology

Geochronology

Geochemistry

Área de concentração: Geologia e Recursos Naturais

Titulação: Doutor em Ciências

Banca examinadora:

Elson de Oliveira Paiva (Presidente)

Darci Pedro Svisero

Excelso Ruberti

Roberto Perez Xavier

Ticiano José Saraiva dos Santos

Data da defesa: 30-08-2011

Programa de Pós-graduação em Geociências



UNIVERSIDADE ESTADUAL DE CAMPINAS
INSTITUTO DE GEOCIÊNCIAS
PÓS-GRADUAÇÃO EM GEOCIÊNCIAS NA
ÁREA DE GEOLOGIA E RECURSOS NATURAIS

AUTOR: José Paulo Donatti Filho

"Petrogênese do Campo Kimberlítico Braúna, Cráton do São Francisco".

ORIENTADOR: Prof. Dr. Élson Paiva de Oliveira

Aprovada em: 30 / 08 / 2011

EXAMINADORES:

Prof. Dr. Élson Paiva de Oliveira

A handwritten signature in blue ink, appearing to read "Elson Paiva Oliveira", followed by the title "Presidente".

Prof. Dr. Ticiano José Saraiva dos Santos

A handwritten signature in blue ink, appearing to read "Ticiano José Saraiva dos Santos".

Prof. Dr. Roberto Perez Xavier

A handwritten signature in blue ink, appearing to read "Roberto Perez Xavier".

Prof. Dr. Darcy Pedro Svizzero

A handwritten signature in blue ink, appearing to read "Darcy Pedro Svizzero".

Prof. Dr. Excelso Ruberti

A handwritten signature in blue ink, appearing to read "Excelso Ruberti".

A handwritten signature in blue ink, appearing to read "Excelso Ruberti".
Campinas, 30 de agosto de 2011

*Aos meus pais,
que me ensinaram a ter responsabilidade e objetivo na vida.*

*... e se cheguei mais longe, foi porque inicialmente me enganei,
pensando estar muito perto.*

AGRADECIMENTOS

Deixo aqui meu agradecimento a todos aqueles que contribuíram de alguma forma para a minha formação e pesquisa. Agradeço principalmente ao meu orientador professor Elson Paiva de Oliveira por insistir em me ensinar a geologia com paciência e didática ímpar, e a me “lapidar” como um pesquisador de competência. Agradeço profundamente ao Nelson Angeli meu grande amigo e professor de graduação que um dia abriu meus olhos para a ciência e acreditou no meu potencial. Ao estimado professor Asit Choudhuri por me incentivar a continuar tentando entender muitas vezes o inexplicável, me ensinando a filosofia mais profunda que ronda a existência do ser. Agradeço também as pessoas que me abriram portas, forneceram novas oportunidades e acreditaram no meu trabalho: Brent Jellicoe, José Ricardo Pisani, Kenneth Johnson, José Fernando Tonoli (in memoriam), Alfredo Perin, Christian Schobbenhaus, Homero Braz Silva e Fernanda Prendin Ochika. Aos professores Larry Heaman (University of Alberta), Neal McNaughton (University of Western Australia) e Hirochika Sumino (University of Tokyo), pela atenção, colaboração e co-autoria nos trabalhos. Aos críticos e relatores Roger H. Mitchell, Kenneth Tainton, Stephen E. Harggerty, Darcy Pedro Svisero, Ticiano Saraiva, Excelso Ruberti, Roberto Perez Xavier pelos valiosos conselhos e contribuições ao meu trabalho. Aos amigos de laboratório, sala de estudos, discussões e trabalho de campo: Sebastian Tappe, Judy Schultz, Barry Herchuk, Homero Braz Silva, Juliana Finoto Bueno, Marcelo Furlan, Leandro B. Vieira, Rogério Marcon, Carina Siqueira, Marcos Mansueto, Erica Tonetto, Aloísio Cotta, Cristiano Gonçalves, Aparecida Vendemiatto, Lúcia dos S. Carvalho. As queridas amigas secretárias da Pós-graduação, Valdirene Pinotti, Maria Gorete Bernardelli e Edinalva de Novaes, pelo auxílio em todos os momentos. A toda equipe Vaaldiam Resources Ltd. Brasil e Canadá pela importante

colaboração e à Fundação de Amparo à Pesquisa do Estado de São Paulo (FAPESP) pela concessão da minha bolsa de doutorado.

Quero também deixar minha homenagem àqueles da minha família que se foram durante o período em que eu estava estudando e muitas vezes não estava por perto para o adeus: grande homem meu avô Nelson Bayod; Moacir Donatti; minha avó querida Yolanda Ghezzi Donatti; meu estimado tio Benedito Donatti e meu tio-avô Laércio Costa.

Agradeço também a todos os membros da minha família pelo apoio nos momentos mais difíceis, em especial minha amada avó Irene Costa Bayod e minha tia do coração Sueli Bayod. E é claro, não poderia deixar de agradecer ao “meu” Deus, que me protegeu e que me contemplou inexplicável, gentil, e elegantemente, com o talento da insistência e da arte mais bela dentre todas as outras, a “minha” Música. Estes sim foram meus parceiros em todos os momentos de inspiração, alegrias e baixos senoidais de minha vida, e que sem eles não suportaria viver neste pequeno Planeta de história tão enigmática que assombra os humanos pelo fato de ser simplesmente belo e auto-suficiente.

Peço desculpas àqueles que não foram lembrados neste momento de pura ansiedade, adrenalina e excitação, porém estou ciente da importância que todos tiveram e que sempre irão morar em meus pensamentos.

PREFÁCIO

Este projeto de doutoramento teve início durante o trabalho de campo final do meu projeto de Mestrado pelo IG-UNICAMP, onde estudei a geoquímica e geocronologia de basaltos do Greenstone Belt do Rio Itapicuru orientado pelo professor Elson Paiva de Oliveira. Neste trabalho de campo, professor Elson e eu tomamos conhecimento da existência de uma empresa que estava reativando um projeto de pesquisa de diamantes (i.e. Vaaldiam Resources Ltd.), iniciado pela De Beers no início da década de 80, um ano antes do meu nascimento. Fizemos uma visita ao projeto e fomos muito bem recebidos por duas pessoas incríveis que se tornaram meus grandes amigos, o meu chefe José Ricardo Pisani e a gerente do projeto Brauna, Fernanda Prendin Ochika. Naquela ocasião, conseguimos recuperar duas amostras frescas de kimberlitos em furos de sondagem, tarefa essa muito difícil se tratando deste tipo de pesquisa por ser altamente sigilosa. No último dia de campo, professor Elson e eu estávamos pernoitando na praia Jardim de Alá em Salvador, em ordem a esperar nosso vôo no dia seguinte. Foi naquela ocasião de areia e brisa do mar que cantava em uníssono em função da quebra das ondas, que meu brilhante orientador sugeriu a possibilidade em me aprofundar no estudo sobre kimberlitos, e que esta seria uma grande oportunidade para a minha formação como pesquisador. Sem titubear, portando um semblante espantado, respondi prontamente que sim. A partir deste dia o objetivo da minha vida passou a ser entender a gênese dos kimberlitos, diamantes e rochas associadas, culminando nesta tese de doutoramento que possuía o seguinte título provisório: “*Caracterização geoquímica e isotópica dos kimberlitos e xenólitos associados, Província Kimberítica Brauna, Bahia*”.

Logo após meu ingresso no doutoramento, comecei a me envolver com ensino de geologia assumindo o programa Super PED na época, que consistia em ministrar aulas de Geologia Geral e Mineralogia para os cursos de Biologia e Química da UNICAMP. Adicionalmente, aproveitando esta experiência, assumi a cátedra das mesmas disciplinas na Faculdade Maria Imaculada, localizada na interiorana cidade de Mogi Guaçu. Um ano se passou e recebi uma proposta de emprego na Vaaldiam Resources Ltd., me colocando em uma posição confortável para dar continuidade em minha tese de doutoramento. Aceitei imediatamente e abandonei a bolsa e o cargo de catedrático nas duas Instituições. Envolvendo-me profundamente com o assunto sobre kimberlitos, fui enviado a outro projeto de pesquisa de diamantes no Canadá chamado “Candle Lake Project”, durante o inverno mais rigoroso e incrível da minha vida, e vivendo em um container de navio a -40°C. Foi lá que conheci um chefe maravilhoso e muito competente, Brent Jellicoe, que apostou e acreditou no meu potencial e me levou em uma viagem de intermináveis oito horas para me apresentar ao Dr. Larry Heaman em Edmonton (University of Alberta). Foi em seu laboratório, um ano depois, que aprendi a metodologia para se datar kimberlitos utilizando fenocristal de perovskita, culminando na primeira datação deste gênero publicada no Brasil. Após esta temporada no gelo, voltei para o Projeto Brauna para terminar minhas descrições, modelos e relatórios finais. Neste ínterim, escrevi um projeto de doutorado para FAPESP, pois estava percebendo a decadência da empresa em função do mercado mundial de diamantes. Foi a partir daí que resolvi sair da empresa e voltar a ser bolsista com a aprovação do meu projeto após um longo período de análise pelos relatores da referida fundação de fomento à pesquisa. Tendo mais tempo para minha pesquisa, participei em congressos nacionais e internacionais e viajei para a Perth-Austrália aprender a operar a microssonda iônica (SHRIMP) e obter dados mais robustos para meu projeto de doutorado, freqüentemente auxiliado pelo sempre presente e simpático professor Neal McNaughton da Curtin University of Technology & University of Western Australia.

Após todos esses anos de dedicação, chego até aqui carregando uma bagagem pesada de informações, experiências, responsabilidades profissionais e acadêmicas, que me dão orgulho e fazem brilhar meus olhos e aguçarem meus mais primitivos instintos quando testado em quaisquer circunstâncias associadas à minha competência. Sou inteiramente grato a essa minha trajetória e as pessoas que me ajudaram, e me orgulho de ter chegado até aqui com os meus acertos e, principalmente, assumindo com humildade todos os por mim cometidos. Posso dizer assim que cheguei ao fim de uma jornada que me levará e me guiará certamente ao começo de um novo e brilhante plano de vida, desta condição *sine qua non* eu tenho a absoluta certeza.

SUMÁRIO

AGRADECIMENTOS-----	v
PREFÁCIO-----	viii
RESUMO-----	xii
ABSTRACT-----	xii
INTRODUÇÃO-----	1
ANEXO 1: Age and Origin of the Neoproterozoic Brauna Kimberlites: magma generation within the metasomatized base of the São Francisco craton, Brazil-----	3
Abstract-----	4
Introduction-----	5
Geological Setting-----	6
Kimberlite Occurrence and Facies-----	7
Pipe Morphology-----	11
Petrography-----	13
Mineral Composition-----	15
Garnet-----	15
Ilmenite-----	16
Clinopyroxene-----	16
Spinel-----	18
Phlogopite-----	18
Whole Rock Geochemistry-----	20

U-Pb Perovskite Geochronology-----	26
Sr-Nd Isotope-----	27
Discussion-----	30
Brauna Kimberlite Classification-----	30
Petrogenesis-----	31
Brauna Kimberlite Magma Classification-----	34
Conclusions-----	35
Acknowledgements-----	37
References-----	38

ANEXO 2: Zircon xenocrysts U-Pb dating from the Neoproterozoic Brauna Kimberlite Field, São Francisco Craton, Brazil: geodynamic implications for kimberlitic intrusion-----	46
Abstract-----	47
Introduction-----	48
Geological Settings-----	50
Brauna Kimberlite Zircon Sources-----	52
U-Pb SHRIMP Zircon dating-----	54
Nordestina Granodiorite Zircon Geochronology-----	55
Brauna Kimberlite Field Zircon Geochronology-----	58
Discussion-----	61
Acknowledgements-----	63
References-----	64



UNIVERSIDADE ESTADUAL DE CAMPINAS

INSTITUTO DE GEOCIÊNCIAS

Pós-Graduação em Geologia e Recursos Naturais

PETROGÊNESE DO CAMPO KIMBERLÍTICO BRAUNA, CRÁTON DO SÃO FRANCISCO

RESUMO

A presente tese concentrou-se na classificação do magmatismo kimberlítico do Campo Kimberlítico Brauna no nordeste do Craton do São Francisco, e sua relação com as rochas encaixantes, xenólitos (e.g. crustais e mantélicos), mineralizações diamantíferas e contexto tectônico regional associado ao Greenstone Belt do Rio Itapicuru e Bloco Serrinha. O escopo do estudo refere-se à utilização de técnicas analíticas convencionais como microscopia, microscopia eletrônica de varredura, microssonda eletrônica e difratometria de raios-X para a classificação da mineralogia e da química mineral dos kimberlitos e xenólitos associados. Somado a isto, utilizou-se técnicas analíticas mais avançadas aplicadas ao estudo de kimberlitos, como a obtenção de dados geoquímicos de alto poder interpretativo (e.g. HFSE e REE) por ICPMS e XRF, com a finalidade de se entender a petrogênese dessas rochas. Além de análises isotópicas de Sr-Nd em rocha total e perovskita da matriz kimberlítica, e U-Pb em grãos de zircão e perovskita por SHRIMP e TIMS respectivamente, para definir e determinar fontes geradoras do magmatismo do campo kimberlítico.

Este volume foi organizado sob forma de dois artigos completos, onde a grande maioria dos resultados desta tese foram apresentados. O primeiro artigo intitulado “Age and Origin of the Neoproterozoic Brauna Kimberlites: magma generation within the metasomatized base of the São Francisco craton, Brazil”, teve como principal objetivo a classificação petrogenética dos kimberlitos e xenólitos associados do Campo Kimberlítica Brauna, desde então superficialmente explorada por empresas de exploração de diamantes na década de 80 e 90. Neste artigo foram utilizadas técnicas convencionais de classificação de rocha bem como: descrições petrográficas, relações de campo, microscopia eletrônica de varredura, microssonda RAMAN, difratometria de Raio-X e geoquímica de elementos maiores e traços. O artigo contempla também a utilização de técnicas mais avançadas até então inexistentes na literatura sobre kimberlitos no Brasil, são elas: datação radiométrica U-Pb em fenocristais de perovskita por Termal Ionization Mass Spectrometry (TIMS), dados isotópicos de Sr-Nd em rocha total e isótopos de Nd em fenocristal de perovskita. Além disso, o artigo contribui de forma representativa para uma discussão frequente entre a comunidade internacional de kimberlítólogos sobre tipos de magmas kimberlíticos heterogêneos.

O segundo artigo intitulado “Zircon xenocrysts U-Pb dating from the Neoproterozoic Brauna Kimberlite Field, São Francisco Craton, Brazil: geodynamic implications for kimberlitic intrusion”, foi contemplado com dados isotópicos precisos de U-Pb em xenocristais de zircão do kimberlito e fenocristais de zircão do granodiorite encaixante por Sensitive High Resolution Ion Microprobe (SHRIMP II). Este artigo teve como principal objetivo a identificação das diferentes idades registradas nos xenocristais de zircão trazidos à superfície da Terra pelo magmatismo kimberlítico com o intuito de se entender a constituição da litosfera sob o Bloco Serrinha, onde o campo kimberlítico Brauna encontra-se intrudido. Além disso, o estudo isotópico detalhado do granodiorito encaixante também se fez importante para o entendimento da mecânica de colocação e forma de contaminação crustal desse tipo de magmatismo tão peculiar, tornando este artigo o segundo no mundo com esse tipo de abordagem.

Palavras-chaves: Craton do São Francisco; kimberlito; petrologia; geocronologia U-Pb; geoquímica do manto.



UNIVERSIDADE ESTADUAL DE CAMPINAS

INSTITUTO DE GEOCIÊNCIAS

Pós-Graduação em Geologia e Recursos Naturais

**PETROGENESIS OF THE BRAUNA KIMBERLITE FIELD,
SÃO FRANCISCO CRATON**

ABSTRACT

The present thesis deals with the classification of the Brauna Kimberlite Field magmatism, northeast São Francisco Craton, and its relationship with the host-rock, xenoliths (e.g. crustal and mantelic), diamondiferous mineralization and the regional tectonic context associated to the Rio Itapicuru greenstone belt and Serrinha Block. The scope of this study refers to conventional methodologies such as scanning electron microscope, electronic microprobe and X-ray difratometry for the mineralogy classification of the Brauna kimberlites and the related xenoliths. Additionally, we have used more robust analytical techniques applied to the kimberlite study, such as ICPMS and XRF and also isotopic analysis of whole rock and perovskite Sr-Nd isotope, and also zircon U-Pb geochronology, using TIMS and SHRIMP respectively, to understand the kimberlitic source and magma generation process.

This volume was organized under paper form where the results, discussions and conclusions are reported. The first manuscript entitle “Age and Origin of the Neoproterozoic Brauna Kimberlites: magma generation within the metasomatized base of the São Francisco craton, Brazil”, had the main subject the Brauna kimberlites and xenoliths petrogenetic classifications, since then superficially explored by the exploration Companies during the 80’s and 90’s decades. In this article we have utilized conventional techniques for rock classification such as petrographic descriptions, field relationships i.e. SEM, RAMAN and X-Ray difratometry for major and trace elements geochemistry. Also we have analysed the samples by most advanced techniques inexistent in the Brazilian literature so far, for example: trace elements using ICPMS, U-Pb perovskite dating and whole rock Sr-Nd and perovskite Nd isotope by TIMS. Furthermore, this manuscript has contributed for the international kimberlite community discussion about the heterogeneous kimberlitic magma types.

The second manuscript entitled “Zircon xenocrysts U-Pb dating from the Neoproterozoic Brauna Kimberlite Field, São Francisco Craton, Brazil: geodynamic implications for kimberlitic intrusion”, was awarded with U-Pb isotopic data in zircon xenocrysts in Brauna kimberlites and its host rock Nordestina granodiorite batholith using the SHRIMP. This article had the principal objective, to place constraints on the lithosphere beneath the Archean Serrinha Block. Furthermore, the detailed isotopic study on the host-rock was important to improve our understanding about the form and dynamic of the kimberlitic intrusion. It is important to note that this paper is the second published paper with this subject in the world.

Keywords: São Francisco craton; kimberlite; petrology; U-Pb geochronology; mantle geochemistry.

INTRODUÇÃO

O estudo de kimberlitos, sempre foi tema de enorme interesse, no que se refere à sua procedência, se do manto inferior, manto astenosférico ou manto litosférico, forma de ocorrência ao longo do tempo geológico, relações com as rochas hospedeiras, origem dos xenólitos crustais e mantélicos, além de a sua relação com a gênese e procedência de diamantes. Os kimberlitos mais estudados da Terra, em torno de 80%, são Mesozóicos/Cenozóicos (200-50 Ma) e são freqüentemente relacionados à quebra de supercontinentes e a formação de bacias oceânicas e intra-cratônicas.

Kimberlitos e rochas alcalinas na Plataforma Brasileira e Sul Africana são bem conhecidos em função de suas relações com a abertura do Oceano Atlântico Sul durante o Mesozóico (Le Roex 1986), e são geralmente associados ao lineamento do AZ-125. Muitos destes kimberlitos são mineralizados a diamante e fazem parte desta suíte ultrapotássica associada a este evento vulcânico restrito. Curiosamente, a maior parte das fontes primárias para diamantes no Brasil continuam desconhecidas. Estudos isotópicos recentes culminaram no reconhecimento de outro episódio kimberlítico principal ocorrido durante quebra/extensão continental no Proterozóico entre 520 Ma e 1100 Ma. As hipóteses mais plausíveis são: i) kimberlitos relacionados à quebra de supercontinentes e rifteamento litosférico; ii) associação à magmatismo alcalino ultrapotássico contemporâneo aos kimberlitos. Adicionalmente, o evento kimberlítico mais antigo conhecido até o momento foi reconhecido na Índia por volta de 1100 Ma (Rao et al., 2011), que pode estar associado à um período global de atividade de plumas do manto com vida curta e/ou mudança e reorganização do regime de convecção do manto neste período.

No Brasil, o Campo Kimberlítico Brauna revelou-se através deste estudo ser a fonte primária de diamantes mais antiga (642 Ma), além disso, representa um registro importante como provável evidência de quebra do supercontinente Rodínia na Plataforma Sul-America. Trabalhos sobre kimberlitos no Cráton do São Francisco são raros, portanto, o presente estudo faz-se importante por constituir uma ferramenta de grande potencial não só para compreender a origem das mineralizações diamantíferas na área, mas também para investigar a natureza do próprio manto aos quais os kimberlitos se originaram, além de sua relação tectônica / geodinâmica com as rochas do Bloco Serrinha, mais restritamente às rochas do terreno granito greenstone belt do Rio Itapicuru, ao qual o referido Campo Kimberlítico Brauna encontra-se hospedado.

Desta forma, os principais objetivos da presente tese de doutoramento foram: classificar petrograficamente, geoquimicamente e isotopicamente os kimberlitos e xenólitos associados do Campo Kimberlítico Brauna, e caracterizar os processos petrogenéticos envolvidos na evolução e gênese dessas rochas. Esta pesquisa também contribuiu para a evolução do conhecimento sobre o terreno granito-greenstone belt do Rio Itapicuru e a natureza da litosfera sob o Núcleo Serrinha, cujos vestígios estão registrados nos xenólitos aprisionados pelo magma kimberlítico. Nesse quadro, o estudo dos kimberlitos do CKB é relevante tanto do ponto de vista econômico, quanto do ponto de vista científico, pois esta pesquisa está inserida em um projeto de auxílio à pesquisa FAPESP (Proc. No. 06/06222-1) intitulado: “Evolução geológica pré-colisional do greenstone belt do Rio Itapicuru Núcleo Serrinha, Bahia: relações de campo, geocronologia e geoquímica”, coordenada pelo orientador deste projeto Prof. Dr. Elson Paiva de Oliveira.

ANEXO 1:

“Age and Origin of the Neoproterozoic Brauna Kimberlites: magma generation within the metasomatized base of the São Francisco craton, Brazil”

Age and Origin of the Neoproterozoic Brauna Kimberlites: magma generation within the metasomatized base of the São Francisco craton, Brazil

José Paulo Donatti Filho^a, Sebastian Tappe^b, Elson Paiva Oliveira^a, Larry Heaman^b

^a *Institute of Geosciences, P.O. Box 6152, University of Campinas – UNICAM, 13083-970 Campinas, SP, Brazil*

^b *Department of Earth and Atmospheric Sciences, University of Alberta, 1-26 Earth Sciences Building, Edmonton, Alberta, Canada T6G 2E3*

Abstract

The Brauna kimberlite field is situated in the northeast part of the São Francisco craton, Bahia State, Brazil, and ongoing exploration revealed three pipe-like bodies and nineteen complex dykes oriented along a N30W trend. U-Pb perovskite dating yielded a high-precision emplacement age of 642 ± 6 Ma and documents the first Neoproterozoic kimberlitic magmatism and the oldest diamond source in this craton. Brauna kimberlite mineralogy comprises olivine, ilmenite, spinel, phlogopite, serpentine, perovskite, apatite, magnetite as well as xenocrysts of Cr-diopside, pyrope garnet, and olivine set in a phlogopite rich matrix. The most common xenoliths are the host-rock granodiorite, eclogites, and mantle peridotites. The kimberlites have three distinct textures: aphanitic, porphyritic and segregationary. The Brauna kimberlites have uncommon geochemical and isotopic signatures with negative $\epsilon_{\text{Nd}}(t)$ values of -5.8 to -8.1 and variable $^{87}\text{Sr}/^{86}\text{Sr}$ ratios (0.7045 – 0.7063), plotting between “anomalous” and heterogeneous kimberlites. Low Al_2O_3 , high Ni and Cr contents, and high Mg# (85.4 - 90.1) in the kimberlites indicate strongly depleted refractory peridotitic mantle sources. Brauna kimberlites do not fit into the classical subdivision of kimberlites and orangeites based on the South African occurrences and their mantle source was metasomatized prior to kimberlite eruption. The incompatible trace element data are consistent with origin of the Brauna kimberlites as partial melts from a transitional zone between the asthenosphere and the sub-continental lithospheric mantle that was

enriched by metasomatic fluids prior to melt extraction, during Neoproterozoic lithosphere extension probably triggered by a deep mantle thermal anomaly.

Keywords: São Francisco craton; kimberlite; petrology; U-Pb perovskite geochronology; mantle geochemistry.

Corresponding author. Tel.: +55 19 97732250

E-mail address: donatti@ige.unicamp.br (José Paulo Donatti Filho)

1. Introduction

Kimberlites are rare but widespread magmatic rocks of great scientific and economic importance owing to the mantle xenoliths and diamonds they may entrain, thus providing direct information about the Earth's inner structure and composition.

Diamond-rich sedimentary strata of Phanerozoic and Precambrian ages have been exploited in South America since the colonial times but the diamond sources in kimberlites and lamproites are virtually unknown. With the exception of the Mesozoic alkalic rocks and diamond-bearing kimberlites that are associated with the South Atlantic opening and occur along the >2000 km long Az 125° igneous corridor (e.g. Bardet 1977; Buzzi et al. 1994; Gibson et al. 1995) little is known about Precambrian kimberlites in South America. So far the Guaniamo kimberlite in Venezuela is the only Precambrian kimberlite well characterized in South America with the age of 712 ± 6 Ma (Kaminski et al. 2004).

In the Brazilian shield there are no information reporting on Precambrian kimberlites or on the primary sources of Precambrian detrital diamonds. For instance, the kimberlite sources of diamonds recovered from sedimentary rocks in the historical diamond region of Espinhaço Range in Minas Gerais (Chaves et al., 2001), Chapada Diamantina in Bahia (Svizero, 1995), and within the Roraima Supergroup (Santos et al. 2003) are not yet known. However, extensive diamond exploration over the past two decades using kimberlite indicator minerals and geophysical techniques (e.g., gravity and magnetic properties) has resulted in the discovery of 22 kimberlite intrusions in the São Francisco craton, Brazil (Fig. 1a). These bodies form the Brauna Kimberlite Field (BKF) and they are the first well-defined Precambrian diamond source in Brazil.

Nevertheless, a detailed description of the age and petrogenetic characteristics of the Brauna kimberlites is not yet available.

This paper reports on new U-Pb perovskite age, mineral compositions, whole-rock geochemistry, including major and trace elements, and isotopic data for the Brauna kimberlites, with the objective of placing new constraints on their origin.

2. Geological Setting

The Brauna Kimberlite Field is a confined region of ultrapotassic magmatism that forms part of the Archean Serrinha block, in the northeast São Francisco craton (Fig. 1).

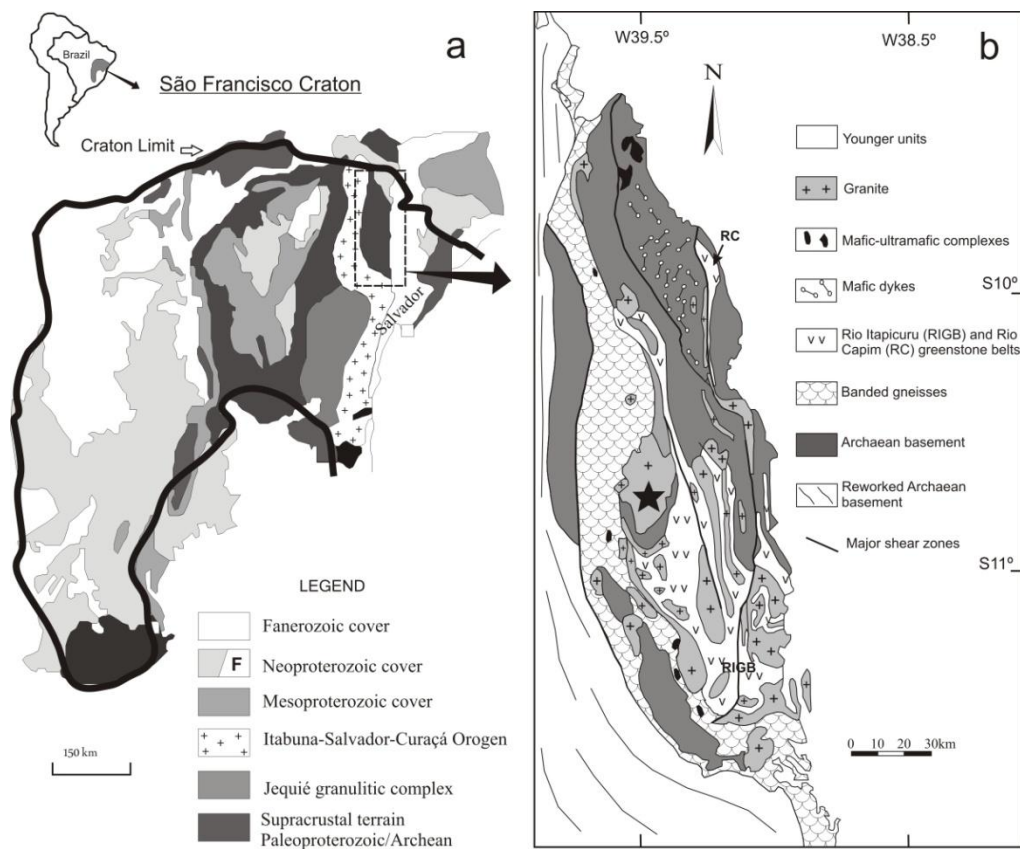


Figure 1: Geological setting of the Brauna Kimberlite Field. **A)** Geological map of the São Francisco Craton and the location of the Serrinha block (after Souza et al., 2003). **B)** Geological map of the Serrinha Block and the Rio Itapicuru greenstone belt (after Oliveira et al., 2004) with location of the Brauna kimberlite field (black star).

The Serrinha block forms a mega-ellipsoidal structure ($> 21,000 \text{ km}^2$) that has remained relatively rigid during Paleoproterozoic collision of at least three blocks to form the Itabuna-Salvador-Curaça orogen (Barbosa and Sabaté, 2004; Oliveira et al., 2010). The lithostratigraphic succession of the Serrinha block consists dominantly of: (i) an Archean basement of migmatitic gneisses and calc-alkaline to tonalite-trondhjemite-granodiorite (TTG) plutons, mostly granodiorite with N-S foliation; (ii) volcanic-sedimentary sequences of the Paleoproterozoic Rio Itapicuru greenstone belt and the Rio Capim Group (Oliveira et al. 2011; Costa et al. 2011) and, (iii) Paleoproterozoic granitic intrusions (Silva et al. 2001; Mello et al. 2006; Oliveira et al. 2010). Syenites make up a distinct but minor rock assemblage in the western part of the Serrinha block; they post-date the major volcanic-plutonic cycles and much of the early deformation (Rios et al. 2007). BKF is hosted in the southern part of the volumetric most important Paleoproterozoic trondhjemite batholith of the Rio Itapicuru greenstone belt (i.e. the Nordestina batholith).

3. Kimberlite Occurrence and Facies

The kimberlites occur as discrete intrusions, crosscutting the 2155 to 2132 Ma Nordestina granodiorite batholith (Pisani et al. 2001; Donatti Filho et al. 2008; Donatti Filho et al. in prep.) of the Paleoproterozoic Rio Itapicuru greenstone belt (Fig. 2).

The BKF is controlled by a NW-SE fracture system. This system hosts three kimberlite pipes (Brauna 03, 04 and 07) and nineteen dykes oriented about N30W (Pisani et al. 2001; Donatti Filho et al. 2008). Pipe morphologies range from circular to elliptical and are strongly controlled by joints and faults. The volumetrically most significant pipe is Brauna 03, consisting of three lobes with a combined surface area of approximately 17,500 m². The dykes form segments up to 300m long and 0.5 to 5 meter wide, and can be traced over a strike length of 15 kilometers (Fig. 2). Owing to tropical weathering, surface exposure of pipes and dykes is poor, and fresh rock is only available through drilling.

The kimberlite facies classification adopted here was based on Clement and Skinner (1979). Accordingly, the kimberlite facies are divided into crater, diatreme and hypabissal facies. In the BKF only the hypabissal facies is present because no pyroclastic structures or textures were observed. Massive (coherent) and brecciated kimberlite types are also present as well as

autholiths, xenoliths and xenocrysts. Several textures were recognized: aphanitic, fine- to coarse-grained, porphyritic, segregationary, and the combination of two or more of these textures. The term microcryst was applied for crystals smaller than 0.5 mm in size, macrocryst for crystals between 0.5 mm and 10 mm, and megacryst for crystals larger than 10 mm (Clement and Skinner 1979, Dawson 1980) independent of their origin, whether xenocryst or not.

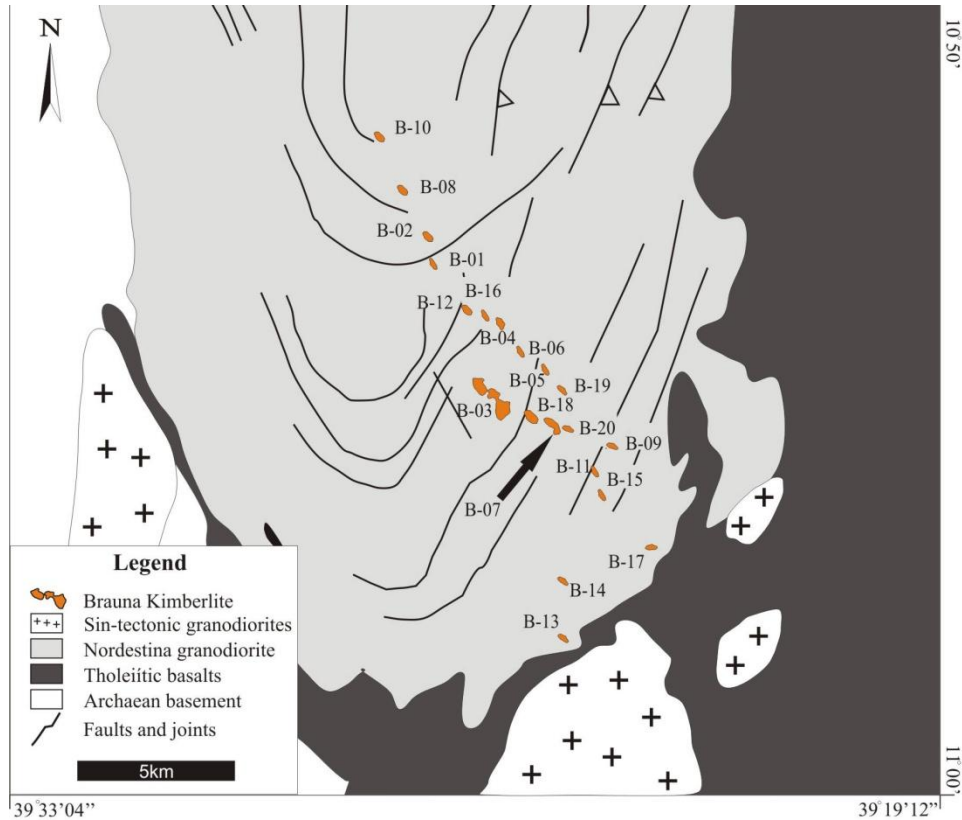


Figure 2: Geological map and surface exposure of the Brauna Kimberlite Field pipes (B-03, 04 and 07) and dyke system (remaining B localities). Arrow highlights the dated kimberlite pipe (B-07).

Aphanitic kimberlites are commonly observed in the BKF (Fig. 3a) but the most abundant type is the porphyritic kimberlite (PK), which is composed of phlogopite and olivine macrocrysts (Fig. 3b). Kimberlites with segregationary, globular segregationary and brecciated textures were also observed representing about 20-30 vol.% of the kimberlitic sequence (Fig. 3b/c). The groundmass of most PKs contains variable but significant proportions of calcite, serpentine and secondary pyrite. In the aphanitic and fine-grained kimberlites, groundmass calcite and serpentine occur bordering anhedral olivine and ilmenite grains. Calcite and serpentine typically encloses

groundmass olivine, apatite, spinel and phlogopite. The majority of kimberlites contain altered/serpentinized olivine macrocrysts and microcrysts in a fine-grained groundmass that includes primary serpentine and calcite. Fresh olivine microcrysts are rare, but do also occur as irregular fragments in the kimberlitic groundmass and/or in the core of serpentinized olivine. Groundmass serpentine does not display pseudomorphic textures, thus ruling out an origin by alteration after mafic minerals, such as olivine.

The segregationary PKs are characterized by globular and diffuse segregations (Fig. 3d) consisting largely of earlier crystallized minerals including olivine, phlogopite, green to brown spinels and perovskite set in an inter-globular matrix of late minerals such as apatite, calcite and serpentine. PK breccias (Fig. 3c) contain abundant “kimberlitized” granodiorite boulders from the Nordestina batholith with carbonate and serpentine inclusions. The latter mineral is occasionally polygonal (i.e. serphophite) and surrounded by a very fine-grained phlogopite reaction rim. The boulders represent approximately 30-60 vol.% of the sequence and are often crosscut by irregular secondary calcite + serpentine + pyrite veins.

The porphyritic kimberlites are quite altered and characterized by 10-25 vol.% macrocrystic olivine, garnet and phlogopite set in a medium-grained matrix, and include rare cumulate olivine grains associated with garnet xenocrysts. In some macrocrystic samples, calcite displays a segregationary texture that is either globular or homogeneous fine-grained in the groundmass. Diopside is rare in PK. In summary, most of the BKF kimberlites have uniform magmatic textures but segregationary textures do occur. In contrast, the aphanitic varieties are extremely fine grained, although some contain 5–10 vol. % olivine macrocryst.

Xenoliths are very common in the Brauna Kimberlite Field, of which xenoliths from the lower and upper crustal wall-rocks are the most abundant. In general, their textures are obliterated by pervasively alteration. Typically, the most frequent crustal xenoliths are granodiorites from the Nordestina Batholith, into which the kimberlite magma was emplaced (Fig. 3e). Occasionally these xenoliths are highly altered with extensive replacement by kimberlitic minerals and the term ‘kimberlitized’ can be applied to describe this feature (Skinner and Marsh 2004). Mantle xenoliths in BKF are relatively rare and highly altered, and they are represented by garnet-bearing serpentinised peridotites. Other important xenolith occurrences are rocks from the Rio Itapicuru greenstone belt, such as basalt, andesite, and less often pervasively altered granitic rocks.

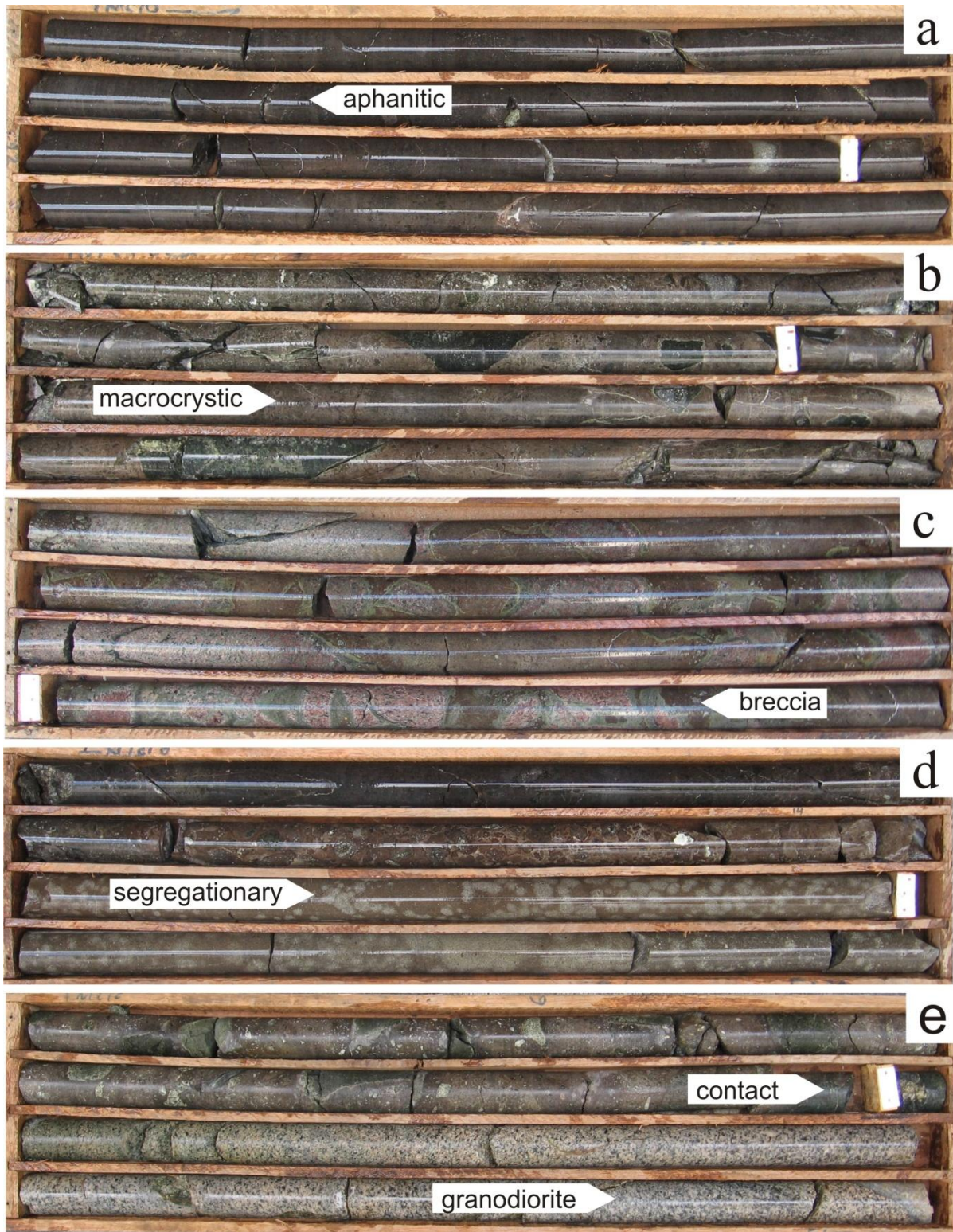


Figure 3: Characteristic textures of the Brauna kimberlites. **a)** Aphanitic kimberlite; **b)** Porphyritic kimberlite; **c)** kimberlite breccia; **d)** Segregationary kimberlite; **e)** Contact between the kimberlite and the Nordestina granodiorite.

4. Pipe Morphology

Three pipes were recognized in the Brauna Kimberlite Field (Brauna 03, 04, and 07). However, the volumetrically most significant are the Brauna 03 and Brauna 07 pipes. These are composed of three lobes of hypabyssal kimberlite with steeply dipping contact (75° to 85°) with the Nordestina granodiorite.

The three-dimensional models for the Brauna 03 and Brauna 07 pipes at current drilling levels (200 m) were produced by Wardrop Engineering Inc. using core loggings and the software Gemcom™. The models are shown in Fig. 4 and indicate that the kimberlite bodies continue to even deeper levels. The size of the pipes becomes relatively reduced at depth exhibiting clear evidence of complex root zones. Breccia is typically observed along the pipe contacts, and in rare cases in the central portions of the pipes. Kimberlite dykes less than 3 m wide are commonly observed between kimberlite pipes, and in some cases they represent connections between pipes, suggesting that they acted as feeders during pipe growth (Lorenz and Kurszlaukis 2008). Pipe and dyke shapes variably follow local faults and joints, thereby causing the elongate and irregular pipe geometries, and locally outward-dipping contacts.

The BKF kimberlite pipes and dykes are relatively small with surface area generally not exceeding $10,000 \text{ m}^2$. The relatively small size of the BKF pipes is similar to many Canadian kimberlite pipes (cf., Scott-Smith 2008) including active mines in the Slave (Lac de Gras cluster) and Superior cratons (Attawapiskat cluster). The BKF pipes are much smaller than the majority of their Kaapvaal craton analogues, which reach surface areas of up to $15,000 \text{ m}^2$, e.g. Orapa mine (Jakubec, 2008).

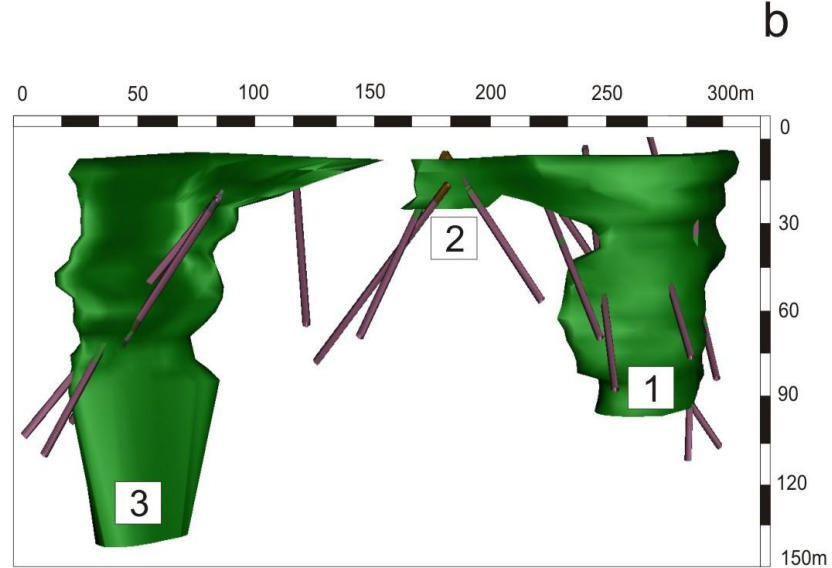
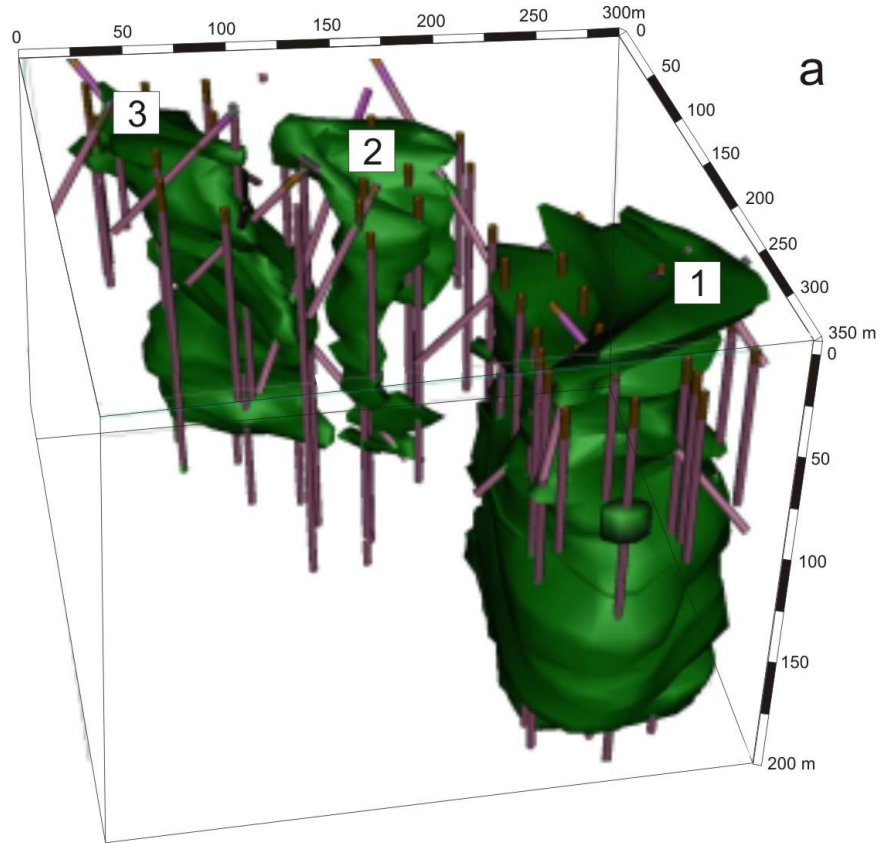


Figure 4: Three-dimensional model of the Brauna 03 and 07 kimberlite pipes. **a)** 1: Brauna 03 south, 2: Brauna 03 central, 3: Brauna 03 north; **b)** 1: Brauna 07 south, 2: Brauna 07 central, 3: Brauna 07 north.

5. Petrography

The petrographic classification of kimberlitic rocks was first defined in South Africa where their mineralogical compositions were divided into two main groups: kimberlite and orangeite (Smith 1983; Mitchell 1995). In addition to olivine, pyroxene, and perovskite, the kimberlite group contains spinel, Fe-poor phlogopite (kinochitalite), monticellite, and abundant calcite, whereas the orangeite group contains Fe-bearing phlogopite (tetraferriphlogopite), Mn-bearing ilmenite, less calcite, rare spinel, and no monticellite. A third, relatively rare, group of transitional kimberlites on the Kaapvaal craton, and within the Proterozoic Namaqua-Natal mobile belt is also described containing mixed mineralogical compositions (Skinner et al., 1992; Becker and Le Roex, 2007).

Dykes and pipes of the Brauna Kimberlite field are composed mainly of olivine, tetraferriphlogopite, spinel, Cr-diopsid, ilmenite, perovskite, garnet, apatite, calcite, and serpentine. The groundmass of all samples consists predominantly of phlogopite, perovskite, magnetite, secondary chlorite and pyrite. Other common groundmass phases include calcite + serpentine + ilmenite +/- apatite. The kimberlite groundmass is phlogopite-rich (Fig. 5a).

Olivine is the most abundant phase, ranging from 0.1 to 3.5 cm in size and is typically rounded to subangular (Fig. 5b). It is generally pervasively altered and can be completely replaced by serpentine and/or calcite (Fig. 5c). Despite the extensive alteration caused by magmatic fluids around rims and along fractures, fresh olivine cores (macro and megacrysts) are preserved in some samples (Fig. 5b). Olivine megacrysts are xenocrysts and can be up to 3.5 cm long and frequently have garnet inclusions. Clinopyroxene is rare and when preserved it shows reaction relationships with serpentine (Fig. 5d). Phlogopite is the most relevant phenocryst phase (< 10%) in all samples; it occurs with a perfect cleavage and less common as nodules or xenomorphic segregations with traces of deformation. Phlogopite can comprise >5% of the kimberlite mineral mode and be up to 0.5-5cm long; they often show corroded or altered rims, or very fine-grained kimberlitic reaction halo. Anhedral green-brown spinel phenocrysts/microphenocrysts occur in the groundmass of a few samples or as inclusions in altered olivine macrocrysts (Fig. 5e). Euhedral perovskite can be locally abundant in the kimberlite groundmass often forming clusters (Fig. 5f). Altered perovskite typically exhibits a reaction halo of phlogopite and barite.

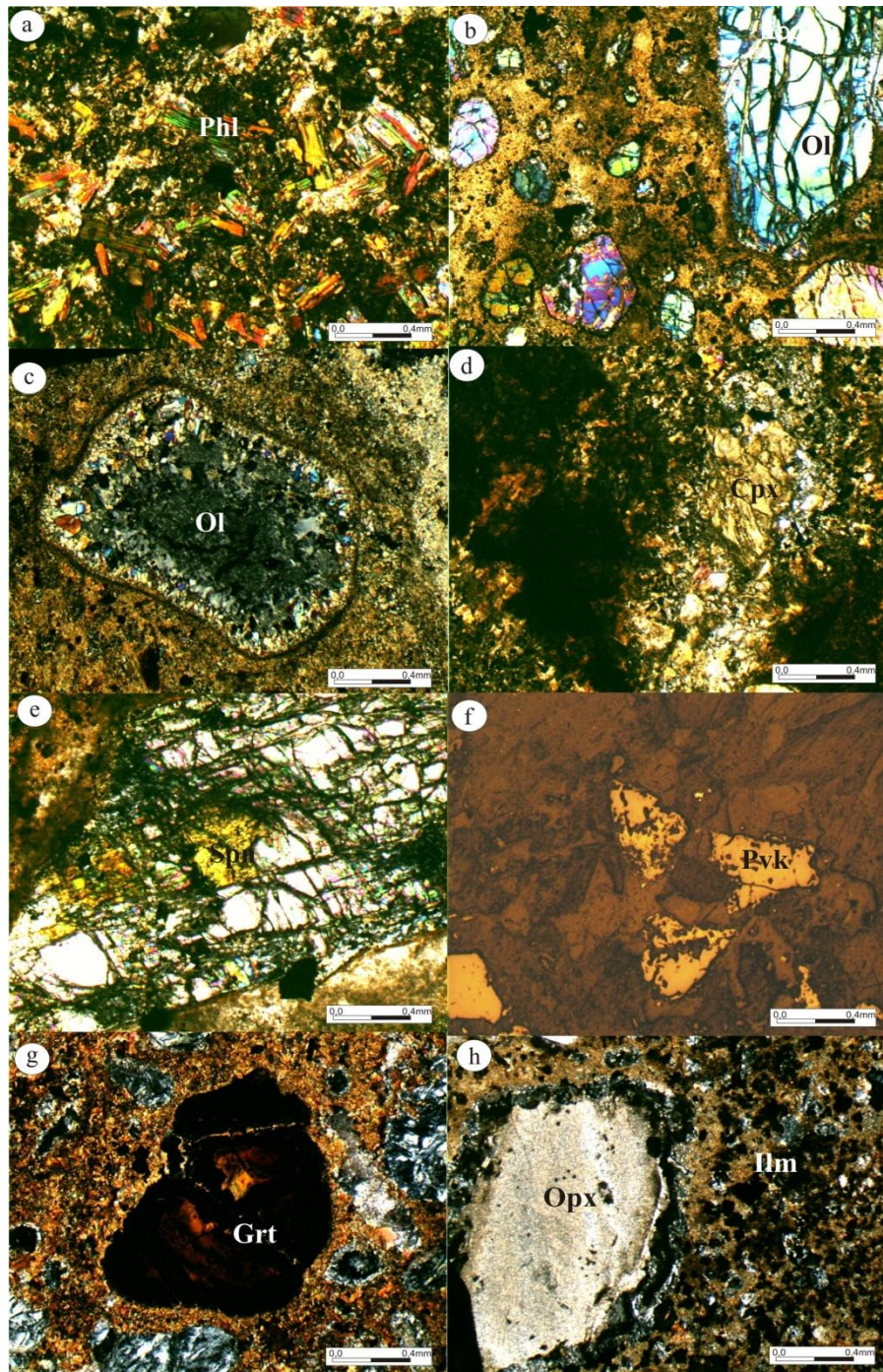


Figure 5: Photomicrographs illustrating overall petrographic features of the Brauna kimberlites. **a)** Typical hypabyssal kimberlite facies with very fine-grained phlogopite-rich groundmass. **b)** Preserved olivine macrocrysts. **c)** Serpentized olivine macrocryst. **d)** Pervasively altered clinopyroxene xenocryst. **e)** Subangular partially altered spinel phenocryst. **f)** Euhedral perovskite phenocryst. **g)** Garnet xenocryst surrounded by groundmass phlogopite and olivine pseudomorphs. **h)** Subangular orthopyroxene xenocryst with altered rim in an ilmenite-rich groundmass.

Srp=serpentine; Qtz=quartz; Opx=orthopyroxene; Cpx=clinopyroxene; Ol=olivine; Ilm=ilmenite; Grt=garnet; Phl=phlogopite; Pvk=perovskite.

The main xenocrysts are garnet, olivine and less often pyroxene. They are all recognized as xenocrysts by a dark colored reaction rim. The most common xenocryst is olivine (Fig. 5c). Eclogitic and peridotitic garnets, including the harzburgitic (red to orange) and lherzolitic (pink to purple) types range in size from 0.2 to 4 cm (Fig. 5g). Pyroxene xenocrysts are subangular in shape with altered rims and may reach 1 cm in size (Fig. 5h).

6. Mineral Composition

Mineral compositions were determined using a Jeol Superprobe JXA-8600 electron microprobe at University of São Paulo, but data acquired by Vaaldiam Resources Ltd during the exploration campaigns were also used. Operating conditions at University of São Paulo included an accelerating voltage of 15 kV, beam current of 20.10 ± 0.10 nA, and beam diameter of $5\mu\text{m}$. Matrix corrections were carried out using online software with PAP corrections. Detection limits for low abundance elements were typically 0.02 wt. %. Counting times were 40 s for all peaks and 10 s for backgrounds. Representative mineral compositions are shown in Table 1 and the full data are available from the authors upon request. Figure 6 illustrates the results.

6.1.Garnet

Crustal and upper mantle garnets have been extensively studied in terms of major element chemistry, and the most important type is the peridotitic garnet that has been used to constrain mantle processes (Schulze 2003), as well as to aid diamond exploration programs (Gurney and Zweistra 1995; Grüttner et al. 2004). Brauna kimberlite garnets are xenocrysts and were separated into two types: mantle source ($(\text{Mg}/(\text{Mg}+\text{Fe}) = 0.30-0.80$; $\text{Ca}/(\text{Ca}+\text{Mg}) = 0.10-0.80$) and crustal source ($(\text{Mg}/(\text{Mg}+\text{Fe}) = 0.01-0.5$; $\text{Ca}/(\text{Ca}+\text{Mg}) = 0.1-1.0$) (Fig. 6a). Following the classifications of Schulze (2003) and Grüttner et al. (2004), the mantle garnets are further separated into eight distinct groups: (G10) harzburgitic garnet; (G9) lherzolitic garnet; (G12) wehrlitic garnet, (G1) low-Cr megacrysts; (G5, G4) pyroxenitic, websteritic and eclogitic garnets; (G3) eclogitic garnet; (G0) not recognized garnet type. Figure 6b shows the garnet classification diagram with data for the Brauna kimberlites. The most common populations are garnets of the G4, G5 and G9 groups,

and less often G10 and G12 garnets. The G1, G3 and subcalcic G0 garnets comprise less than 10% of the total analysed garnets. The data define two major trends: the Iherzolitic trend (Sobolev, 1977) of positive correlation between Cr_2O_3 and CaO , and the eclogitic trend (Grutter et al, 2004) of Ca-only enrichment. The Iherzolitic trend is common in kimberlites and is believed to reflect distinct garnet compositions from the garnet Iherzolite stability field in the mantle, where garnet is in equilibrium with clinopyroxene (Sobolev et al. 1973).

6.2. Ilmenite

Wyatt et al., (2004) use on-craton and off-craton ilmenites in kimberlites around the world to define a simple and practical classification scheme to discriminate between ilmenites derived from kimberlitic sources and those from other sources. The key major elements used in this distinction are MgO and TiO_2 .

Here, we analysed ilmenites grains are from Brauna kimberlite pipes and dykes. Following this arguments, two groups of ilmenite are recognized from Brauna kimberlites: (i) kimberlitic source: High TiO_2 and MgO contents ($\text{TiO}_2 = 40\text{-}55$ and $\text{MgO} = 6\text{-}18$); and (ii) non kimberlitic source: high TiO_2 and low MgO contents ($\text{TiO}_2 = 42\text{-}57$ $\text{MgO} = 0.1\text{-}8$), typical of calcite kimberlites and carbonatites (Fig. 5C). It is important to note that only ilmenite phenocrysts from Brauna kimberlites are reported in Table 1.

6.3. Clinopyroxene

Clinopyroxene is represented by Cr-diopside; it is rare and occurs as apple green to brown xenocrysts. On the basis of their Cr_2O_3 and Al_2O_3 contents, used to discriminate between clinopyroxenes from garnet peridotites, “off-craton” peridotites, eclogitic-megacrystic and cognate clinopyroxenes (Ramsay and Tompkins, 1994), the clinopyroxene grains are all of the type “on-craton” garnet peridotite (Fig. 6c,d).

Table 2: Representative mineral analysis of Brauna kimberlites

Sample	SiO ₂	TiO ₂	Al ₂ O ₃	FeO	MnO	MgO	CaO	Na ₂ O	Cr ₂ O ₃	K ₂ O	BaO	Total
<i>Garnet xenocrysts</i>												
BRA-04*	43.51	0.34	19.28	6.37	0.17	20.90	4.37	n.d.	4.97	n.a.	n.a.	99.91
BRA-05*	42.94	0.47	20.40	6.44	0.11	21.66	4.65	n.d.	3.64	n.a.	n.a.	100.31
BRA-07*	41.56	0.07	19.95	6.96	0.24	19.27	5.34	n.d.	4.68	n.a.	n.a.	98.07
BRA-11*	42.04	0.25	21.65	8.91	0.88	18.69	4.62	0.05	3.32	n.a.	n.a.	100.41
B3D31**	41.85	1.42	20.76	9.02	0.27	21.61	4.94	0.09	1.34	n.a.	n.a.	101.29
DH5B**	41.19	0.52	22.30	7.00	0.34	22.52	4.31	0.05	1.05	n.a.	n.a.	99.29
B3D30**	40.06	0.50	22.09	17.95	0.37	16.09	2.72	0.13	0.09	n.a.	n.a.	100.00
B3D32**	41.07	0.59	22.50	12.72	0.31	18.93	4.03	0.15	0.22	n.a.	n.a.	100.52
<i>number of cation results based on 24 Oxygen atoms</i>												
<i>Clinopyroxene xenocrysts*</i>												
BRA-01	54.68	0.38	1.95	2.85	0.10	17.9	19.2	2.11	1.25	n.a.	n.a.	100.38
BRA-03	54.2	0.20	0.71	1.94	0.09	17.67	21.4	0.88	1.77	n.a.	n.a.	98.87
BRA-04	54.87	n.d.	0.35	2.49	0.02	19.66	21.11	0.34	0.78	n.a.	n.a.	99.62
BRA-05	54.32	0.09	1.74	2.36	0.00	17.74	19.4	1.49	1.52	n.a.	n.a.	98.69
BRA-07	54.8	0.14	0.73	2.46	0.11	17.87	19.4	1.46	2.09	n.a.	n.a.	99.02
BRA-11	54.87	0.17	0.29	3.63	0.09	15.99	20.4	1.6	2.66	n.a.	n.a.	99.66
<i>number of cation results based on 6 Oxygen atoms</i>												
<i>Ilmenite phenocrysts*</i>												
BRA-01	n.d.	52.8	0.49	36.01	0.20	10.86	0.08	n.d.	0.01	n.a.	n.a.	100.41
BRA-03	0.03	54.8	1.3	26.67	0.09	15.26	0.83	n.d.	0.02	n.a.	n.a.	98.98
BRA-04	0.01	53.1	0.45	30.54	0.09	13.56	2.80	n.d.	0.03	n.a.	n.a.	100.54
BRA-05	n.d.	54.8	n.d.	38.27	0.47	6.82	0.07	n.d.	0.15	n.a.	n.a.	100.53
BRA-07	0.13	56.1	0.02	28.14	0.30	13.57	0.98	n.d.	0.09	n.a.	n.a.	99.36
BRA-11	n.d.	46.9	0.22	41.05	2.28	3.91	4.38	n.d.	0.00	n.a.	n.a.	98.75
<i>number of cation results based on 3 Oxygen atoms</i>												
<i>Spinel phenocrysts*</i>												
BRA-01	0.06	1.14	11.31	30.96	0.14	12.48	0.01	n.d.	41.98	n.a.	n.a.	98.08
BRA-03	0.44	0.32	16.64	20	0.64	13.67	0.01	n.d.	43.93	n.a.	n.a.	95.65
BRA-04	0.21	3.04	7.81	19.84	0.06	14.38	0.02	n.d.	54.47	n.a.	n.a.	99.83
BRA-05	0.03	0.47	8.00	18.65	0.25	10.17	n.d.	n.d.	61.53	n.a.	n.a.	99.10
BRA-07	0.03	0.13	28.90	16.03	0.31	13.3	n.d.	n.d.	40.34	n.a.	n.a.	99.04
BRA-11	0.15	0.42	6.04	18.16	0.35	12.93	0.06	n.d.	61.32	n.a.	n.a.	99.43
<i>number of cation results based on 4 Oxygen atoms</i>												
<i>Phlogopite phenocrysts**</i>												
B3D45	39.31	3.27	10.02	8.98	0.12	22.01	n.d.	0.096	n.a.	10.20	0.04	94.44
B21D3	39.09	3.47	10.80	7.85	0.03	23.05	n.d.	0.038	n.a.	9.69	0.40	94.87
B16D1	38.70	3.24	10.17	8.55	0.06	21.84	0.01	0.067	n.a.	10.01	0.45	94.01
B3D51	40.10	2.76	10.60	8.72	0.06	23.55	0.04	0.033	n.a.	10.08	0.33	96.77
B3D50	43.74	0.04	3.58	11.43	0.08	26.83	0.03	0.317	n.a.	10.58	0.12	97.27
B3D29	40.49	2.23	10.96	10.42	0.12	21.59	0.04	0.029	n.a.	9.49	0.51	96.33
<i>number of cation results based on 22 Oxygen atoms</i>												

Total Fe reported as FeO based on crystal chemistry; n.d. = not detected; n.a. = not analysed

* data from Vaaldiam Resources Ltd.; ** data from this study.

6.4. Spinel

Spinel is Cr-rich and has MgO and Cr₂O₃ contents of 5 to 19 wt. % and 27 to 75 wt. %, respectively; a few grains contain low MgO and Cr₂O₃ abundances. The TiO₂ versus 100 Cr / (Cr + Al) diagram from Ramsey and Tompkins (1994) shows that the majority of the spinels from the BKF plot within the garnet peridotite field (Fig. 6e) exhibiting a magnesiochromite composition in the range 0.80 < Cr/(Cr + Al) < 0.99. This is also the compositional range of most spinel-group minerals in depleted peridotite (Shulze, 2001). In the Cr-spinel binary diagram that displays both the diamond intergrowth and diamond inclusion field of Fipke et al. (1995), the BKF spinels fall in the two fields (Fig. 6f).

6.5. Phlogopite

The phlogopite megacrysts (2 to 6 cm) have low-Al (Al₂O₃ = 7.36 – 13.1 wt. %) but high TiO₂ contents (1.2 – 4.09 wt. %); Mg# varies between 82 and 94.5. There are no significant geochemical differences between fresh and altered phlogopite. The groundmass phlogopites have high contents of Fe compared to the macrocrysts and megacrysts. In general the cores are iron- and barium-poor (FeO = 3.04 – 3.31 wt. % and BaO = 0.1 – 0.404 wt. %) and the rims enriched in these elements (FeO = 8.28 – 9.88 wt. % and BaO = 0.041 – 0.425 wt. %). Phlogopite macrocrysts and groundmass phlogopite have similar Al and Ti contents (Al₂O₃ = 8.07 – 11.21 wt. %; TiO₂ = 1.2 – 3.59 wt. %), and compositionally they are classified as tetraferriphlogopite. Additionally, we have analysed altered phlogopite rims and some matrix phlogopite aggregates; they were also classified as tetraferriphlogopite.

In the FeO versus Al₂O₃ diagram (Fig. 6g), the majority of phlogopite grains fall in between the fields of microphenocrysts from orangeites/lamproites and microphenocrysts from transitional kimberlites. Additionally, the analysed grains show high iron contents (FeO = 10.42 - 13.16 wt. %) and low aluminum contents (Al₂O₃ = 3.58 – 8.83 wt. %). In summary, given their pronounced titanium enrichment and aluminum depletion (Fig. 6h), as well as the occurrence of tetraferriphlogopite rims the BKF phlogopite has heterogeneous composition with affinities to phlogopite from South African orangeites, worldwide ultramafic lamprophyres, and olivine lamproites.

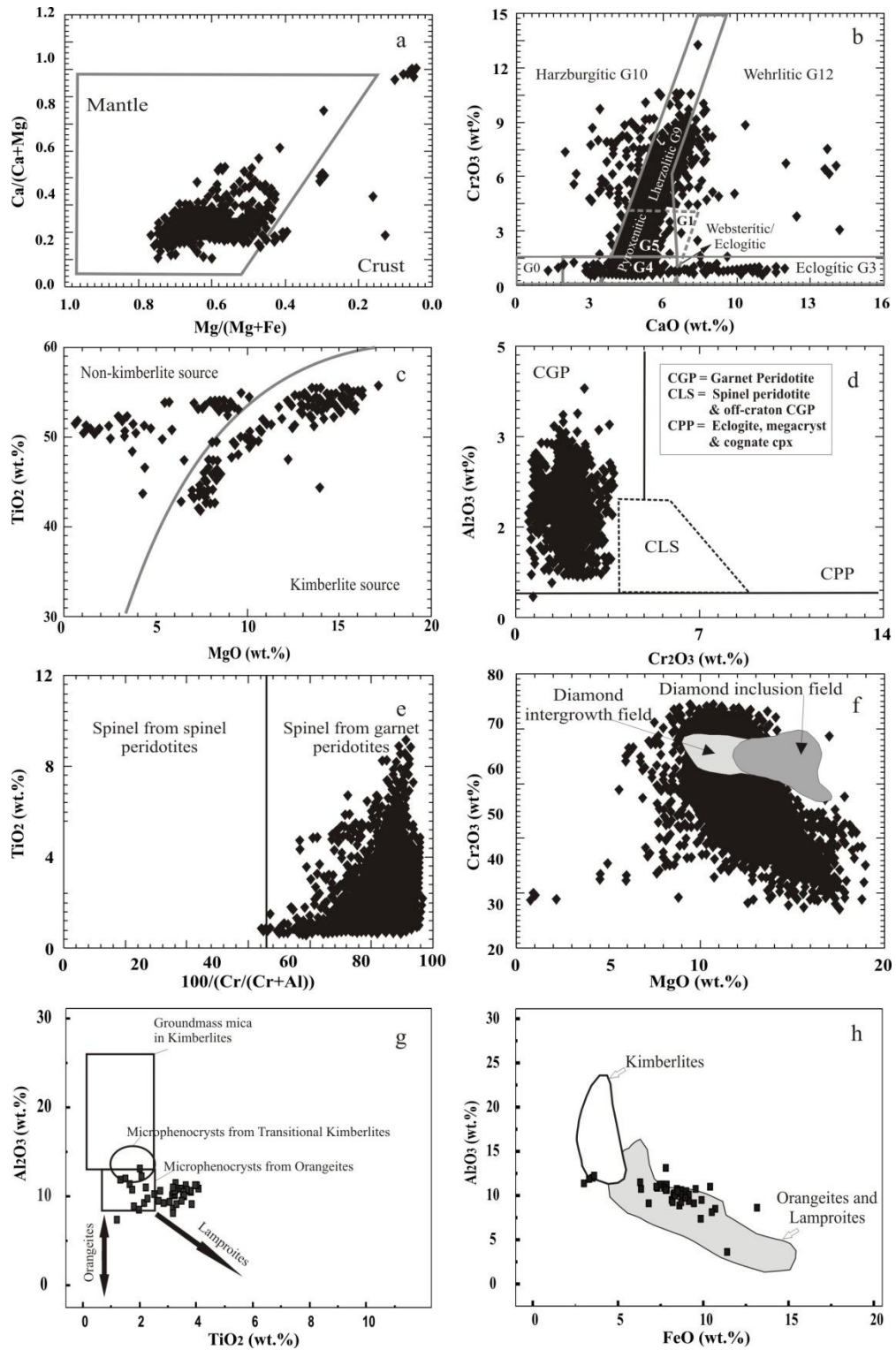


Figure 6: Chemical characteristics of minerals from the Brauna Kimberlite Field. **a)** Mg/(Mg + Fe) vs. Ca/(Ca + Mg) diagram distinguishing mantle-derived and crustal garnets, after Schulze (2003). **b)** Cr₂O₃ vs. CaO classification diagram for Brauna kimberlite garnets, showing the G0, G1, G3, G4, G5, G9, G10 and G12 suites (after Schulze 2003 and Grütter et al. 2004). **c,d)** Cr-diopside plotted on Ramsay and Tompkins (1994) discriminant diagram using Cr₂O₃ and Al₂O₃ contents in Cr-diopside for peridotitic pyroxenes from BKF. **e)** TiO₂ vs. 100Cr / (Cr+Al) diagram of Ramsey and Tompkins (1994) showing that BKF

spinels plot within the garnet peridotite field. **f)** Cr₂O₃ vs. MgO diagram for Cr-spinels with BKF spinels plotting within fields for diamond inclusion and diamond intergrowth (after Fipke et al., 1995). **g,h)** Discriminant diagram using TiO₂ and FeO versus Al₂O₃, showing the geochemical similarities of the BKF phlogopites with the group II phlogopites (after Beard et al. 2000).

7. Whole-Rock Geochemistry

The analysed kimberlite samples are from dykes and the root zones of pipes including all textural varieties, i.e., aphanitic, porphyritic and segregationary kimberlites. Eighteen samples of fresh kimberlite were selected for chemical analysis at the Geosciences Institute of the University of Campinas, following the analytical procedures of Vendemiatto and Enzweiler (2001). Fragments with visible xenolithic material, veining or external weathering were not considered. Major elements were analysed on fusion beads by X-ray fluorescence spectrometry (XRF). The trace elements Cu, Ni, Co, Cr, V, Zn and Nb were also analysed by XRF using pressed powder pellets. Data quality was controlled through routine analyses of the international rock standards W-2 and BHVO for major elements, and RGM-1 and WSE for trace elements. The relative errors are 0.4 - 1.5% for major and minor elements, while for trace elements they range within 1.5 - 10%. Rare earth elements (REE), Th, Ta, U, Hf and Nb were analysed by inductively coupled plasma mass spectrometry (ICP-MS), after total digestion with HF/HNO₃ (Paar bombs, 4 days, 180 °C), following the procedures of Navarro et al. (2008). Data quality control was performed by simultaneous analysis of the international reference materials BRP-1 and BHVO-2; deviation of most results differ from the reference values typically less than 10%. The data are reported in Table 1.

BKF kimberlites from both the pipes and dykes are rich in MgO (18.6 – 34.1 wt. %). When the Mg# number is considered, pipe and dyke samples are very primitive and show similar variation from 80.12 to 90.11 (Tab. 1). Aluminum oxide (1.96 – 4 wt. %), CaO (2.41 – 11.93 wt. %), Fe₂O₃ (8.44 – 10.43 wt. %), and K₂O (0.71 – 3.74 wt. %) contents show negative correlation with Mg# in both pipes and dykes. In general, dyke samples are more enriched in TiO₂ than the pipe samples. The compatible trace elements Ni and Cr (Ni = 940-1655 ppm, Cr = 984-1520 ppm) define very good correlations with MgO.

Table 2 Whole-rock geochemical data for Brauna kimberlites including pipes and dykes samples.

Sample	B4D1-75.55	B7D15-30.00	B7D15-45.00	B3D34-37.50	B3D34-85.40	B3D34-132.30	B3D34-186.60	B3D54-40.60	B8D1-77.35
Type	pipe	pipe	pipe	pipe	pipe	pipe	pipe	pipe	dyke
SiO ₂	34.67	37.61	34.76	35.59	36.24	33.67	35.64	39.35	38.49
TiO ₂	3.37	3.26	4.38	2.23	2.47	2.88	2.88	2.59	3.50
Al ₂ O ₃	2.46	4.00	3.66	2.86	2.97	2.09	3.10	3.25	3.25
Fe ₂ O ₃	9.04	9.49	9.62	8.70	9.35	8.77	9.34	8.83	9.81
MnO	0.13	0.10	0.18	0.14	0.13	0.12	0.15	0.09	0.10
MgO	31.13	26.80	26.30	27.04	29.85	32.03	24.76	22.88	22.14
CaO	4.84	5.70	5.90	7.48	5.60	5.04	8.51	8.89	8.93
Na ₂ O	0.12	0.05	0.10	0.08	0.08	0.11	0.15	0.40	0.15
K ₂ O	2.17	2.90	3.00	3.09	3.10	1.80	3.74	2.15	2.69
P ₂ O ₅	0.04	0.04	0.07	0.81	1.17	0.21	1.21	0.82	1.70
BaO	0.17	0.14	0.09	0.21	0.25	0.14	0.33	0.09	0.16
Cr ₂ O ₃	0.42	0.29	0.39	0.34	0.32	0.43	0.31	0.22	0.20
SrO	0.11	0.02	0.04	0.12	0.08	0.05	0.19	0.06	0.09
LOI	11.07	8.92	10.32	10.47	8.28	11.92	9.12	9.50	7.50
Total	100.10	99.50	99.10	99.50	100.20	99.60	99.70	99.40	98.90
Mg#	88.59	86.43	86.04	87.51	87.80	89.17	85.67	85.38	83.57
<i>XRF (ppm)</i>									
V	47.0	17.1	n.d.	116.0	127.0	63.0	66.0	66.0	89.0
Cr	1452	984	1328	1149	1094	1459	1066	762	683
Ni	1459	940	1329	1366	1393	1655	1136	1010	909
Cu	42.0	6.4	31.0	50.0	88.0	14.6	46.0	54.0	10.6
Zn	63	40	58	67	69	54	77	58	59
Ga	6.7	16.2	7.6	9.6	8.1	6.6	9.9	10.8	13.4
Rb	194	220	263	190	189	157	206	114	189
Sr	908	172	305	1026	645	406	1632	536	729
Y	n.d.	4.7	6.1	7.5	9.4	6.4	13.4	13.2	15.1
Zr	221	276	282	278	313	182	395	436	600
Nb	169	129	174	111	127	136	110	129	175
Pb	11.1	4.7	2.5	13.4	9.9	7.2	15.3	14.8	21.6
Ce	250	171	235	107	117	137	159	245	207
Nd	112	53	117	51	47	53	77	96	76
<i>ICP-MS (ppm)</i>									
Sc	6.06	4.01	6.37	8.41	2.34	13.39	6.36	11.0	14.1
Cs	3.31	1.15	2.93	2.11	2.13	2.10	4.77	2.90	1.30
Co	86.77	72.36	88.06	82.94	85.11	90.65	77.62	70.00	57.40
La	215.3	166.4	266.3	113.9	120.2	182.6	143.7	163	140
Pr	38.42	30.56	44.89	20.11	21.50	33.56	25.47	30.10	24.60
Sm	15.68	12.91	19.90	8.90	9.57	13.98	11.39	13.10	12.00
Eu	3.75	3.20	5.18	2.36	2.54	3.42	3.05	3.5	3.3
Gd	8.21	7.58	11.93	5.29	5.86	7.49	7.08	8	8.0
Tb	0.90	0.89	1.41	0.65	0.70	0.87	0.89	0.9	0.9
Dy	3.79	3.88	6.10	2.95	3.20	3.68	4.14	4.1	4.6
Ho	0.51	0.56	0.88	0.48	0.52	0.53	0.68	0.6	0.8
Er	1.03	1.13	1.76	1.08	1.19	1.09	1.58	1.3	1.8
Tm	0.11	0.11	0.19	0.13	0.14	0.11	0.18	0.14	0.21
Yb	0.57	0.52	0.90	0.75	0.74	0.57	0.97	0.78	1.19
Lu	0.08	0.07	0.12	0.11	0.10	0.07	0.08	0.10	0.16
Hf	6.48	5.44	9.82	8.92	5.09	10.68	8.18	12.3	16.4
Ta	6.79	10.21	7.70	9.89	15.08	7.27	13.05	6.10	10.80
Th	25.51	20.05	32.19	15.30	17.17	25.48	19.54	20.20	20.20
U	2.45	2.71	3.09	3.58	3.54	3.34	4.81	2.90	4.20

Mg# = atomic proportion for an Fe₂O₃/FeO ratio of 0.15; n.d. = not detected

Table 2 continued

Sample	B8D1-79.70	B8D2-17.95	B8D2-20.45	B16D1-82.30	B16D1-91.30	B21D1-20.15	B21D1-21.93	B21D3-20.25	B21D3-23.20
Type	dyke	dyke	dyke	dyke	dyke	dyke	dyke	dyke	dyke
SiO ₂	36.01	35.87	35.51	40.66	45.15	38.23	36.46	34.76	38.47
TiO ₂	3.57	1.92	3.73	4.10	3.18	3.83	4.04	3.08	3.71
Al ₂ O ₃	3.12	1.96	2.14	4.00	2.27	3.26	3.72	2.74	3.25
Fe ₂ O ₃	8.49	8.44	9.18	10.39	10.22	10.43	8.73	8.73	9.57
MnO	0.19	0.13	0.16	0.13	0.18	0.14	0.12	0.18	0.13
MgO	32.62	34.12	32.13	18.57	19.61	20.12	23.00	29.37	22.85
CaO	2.41	2.88	3.16	10.82	11.93	9.73	10.02	5.45	9.56
Na ₂ O	0.03	0.02	0.02	0.19	0.11	0.23	0.17	0.04	0.18
K ₂ O	1.60	0.99	1.41	3.08	0.71	2.80	3.51	2.16	3.19
P ₂ O ₅	0.65	0.58	0.73	0.48	1.14	1.44	0.74	1.20	0.48
BaO	0.09	0.06	0.07	0.07	0.16	0.25	0.32	0.14	0.32
Cr ₂ O ₃	0.45	0.30	0.33	0.35	0.21	0.20	0.21	0.34	0.22
SrO	0.04	0.02	0.03	0.05	0.07	0.09	0.09	0.08	0.09
LOI	10.80	12.60	11.70	6.40	4.10	8.10	7.80	11.30	7.20
Total	100.40	100.30	100.60	99.70	99.30	99.10	99.10	99.90	99.40
Mg#	89.65	90.11	88.75	80.12	81.22	81.31	85.59	88.35	84.33
<i>XRF (ppm)</i>									
V	68	60	92	96	66	89	58	115	59
Cr	1549	1017	1131	1198	711	674	716	1147	749
Ni	1607	1951	1548	1810	882	885	867	1437	930
Cu	26.60	10.10	7.30	79.00	28.90	75.00	34.00	39.00	30.00
Zn	40	50	59	88	67	86	67	67	67
Ga	8.4	7.6	6.7	8.9	15.5	12.7	13.4	10.5	13.4
Rb	156	91	136	54	244	208	279	185	252
Sr	342	190	236	456	604	768	752	655	735
Y	4.2	4.9	4.5	12.0	6.6	24.3	5.1	9.5	4.9
Zr	277	262	226	167	728	1304	693	685	699
Nb	182	116	174	181	157	171	164	152	159
Pb	12.6	8.4	17.9	3.9	7.9	11.4	10.5	16.4	11.1
Ce	256	142	232	174	191	182	181	213	186
Nd	115	61	103	82	82	81	87	92	84
<i>ICP-MS (ppm)</i>									
Sc	11.9	6.9	7.4	23.4	11.2	14.7	26.2	9.5	13.9
Cs	1.00	0.60	0.90	0.60	1.80	1.90	1.80	1.30	1.90
Co	86.3	68.1	73.1	78.7	61.9	64.2	58.8	76.6	64.6
La	234	123	211	142	160	182	172	191	158
Pr	46.00	23.40	43.00	32.20	31.10	33.50	32.90	35.80	30.50
Sm	19.70	10.10	18.70	14.30	14.50	15.30	15.40	15.80	13.70
Eu	5.00	2.50	4.70	3.70	4.00	4.50	4.40	3.90	4.00
Gd	11.00	5.80	10.40	8.20	9.40	10.60	9.60	9.10	8.80
Tb	1.10	0.60	1.10	0.90	1.00	1.30	1.00	1.00	0.90
Dy	4.70	2.60	4.50	3.90	4.50	6.60	4.70	4.30	4.20
Ho	0.70	0.40	0.60	0.60	0.70	1.10	0.70	0.60	0.60
Er	1.30	0.80	1.20	1.30	1.40	2.70	1.40	1.40	1.30
Tm	0.13	0.09	0.12	0.15	0.16	0.33	0.16	0.15	0.16
Yb	0.64	0.48	0.60	0.85	0.88	1.92	0.85	0.79	0.87
Lu	0.08	0.07	0.07	0.11	0.13	0.25	0.11	0.10	0.12
Hf	6.20	4.50	6.40	19.20	5.20	24.60	13.40	8.30	18.20
Ta	15.60	7.40	15.90	12.50	12.30	12.50	13.00	12.70	12.50
Th	35.80	19.00	31.50	23.70	23.30	23.40	26.70	27.90	24.00
U	4.20	2.50	3.70	3.40	3.10	4.20	4.10	3.30	3.10

Mg# = atomic proportion for an Fe₂O₃/FeO ratio of 0.15; n.d. = not detected

Selected major and trace element diagrams to distinguish between South African orangeite and kimberlites (Smith, 1983; Smith et al., 1985) are shown in Figure 7 for the studied samples. Figure 7a shows a plot of TiO_2 versus K_2O , wherein the BKF samples spread over the fields of South African orangeites and kimberlites, with a significant amount of samples plotting in between the two fields. However, when silica contents are considered, the BKF samples are more similar to the South African orangeites. If silica is plotted against Pb and the ratios Th/Nb, Nb/La and Ce/Sr (Fig 7b-e) the BKF samples are not unambiguously similar to the South African orangeites; the BKF samples plot outside the fields of the South African rocks or in between the two fields. The geochemical characteristics of the Brauna kimberlites are probably related to their unique anomalous nature.

High field strength elements (HFSE) and the light rare earth elements (LREE) are all high in abundance (e.g. La = 113.9 - 266.3 ppm, Zr = 182 - 395 ppm, Nb = 110 - 180 ppm). On the other hand, the dyke samples are more enriched in LREE contents than the pipe samples (see table 1). In general, both varieties present REE values similar to the South African orangeites, where it is evident that all samples show sub-parallel patterns and are strongly enriched in the light REE relative to the heavy REE ($(\text{La}/\text{Sm})\text{N} = 8.4$; $(\text{La}/\text{Yb})\text{N} = 182.8$) (Fig. 8a). Normalised La abundances range between 480 and 1123 times chondrite, whereas Lu ranges between 2.8 and 4.7 times chondrite. The REE patterns for individual samples are parallel, with the Brauna 04 and Brauna 07 pipe samples showing uniformly higher concentrations relative to Brauna 03.

Primitive mantle-normalised trace element patterns (Fig. 8b) are generally sub-parallel and strongly enriched in highly incompatible elements (~150 to 600 times primitive mantle), with HREE (Tb to Lu) showing the least enrichment (2–20 times primitive mantle). A representative sample of the Nordestina granodiorite (sample 1406 of Cruz Filho et al. 2003) was also plotted in Fig. 8 to show that the high trace element abundances of all kimberlite samples cannot have been acquired through contamination with the Nordestina granodiorite, which show considerably lower trace element abundances than the kimberlites. The majority of kimberlite samples show negative anomalies (relative to adjacent elements) of K, Sr, and Y, and most sample show positive anomalies of Ta and Nb (Fig. 8b), excluding the negative anomaly from the aphanitic kimberlite sample B3D34-186,60. The above anomalies are probably a characteristic of the original kimberlite mantle source and they will be recalled later.

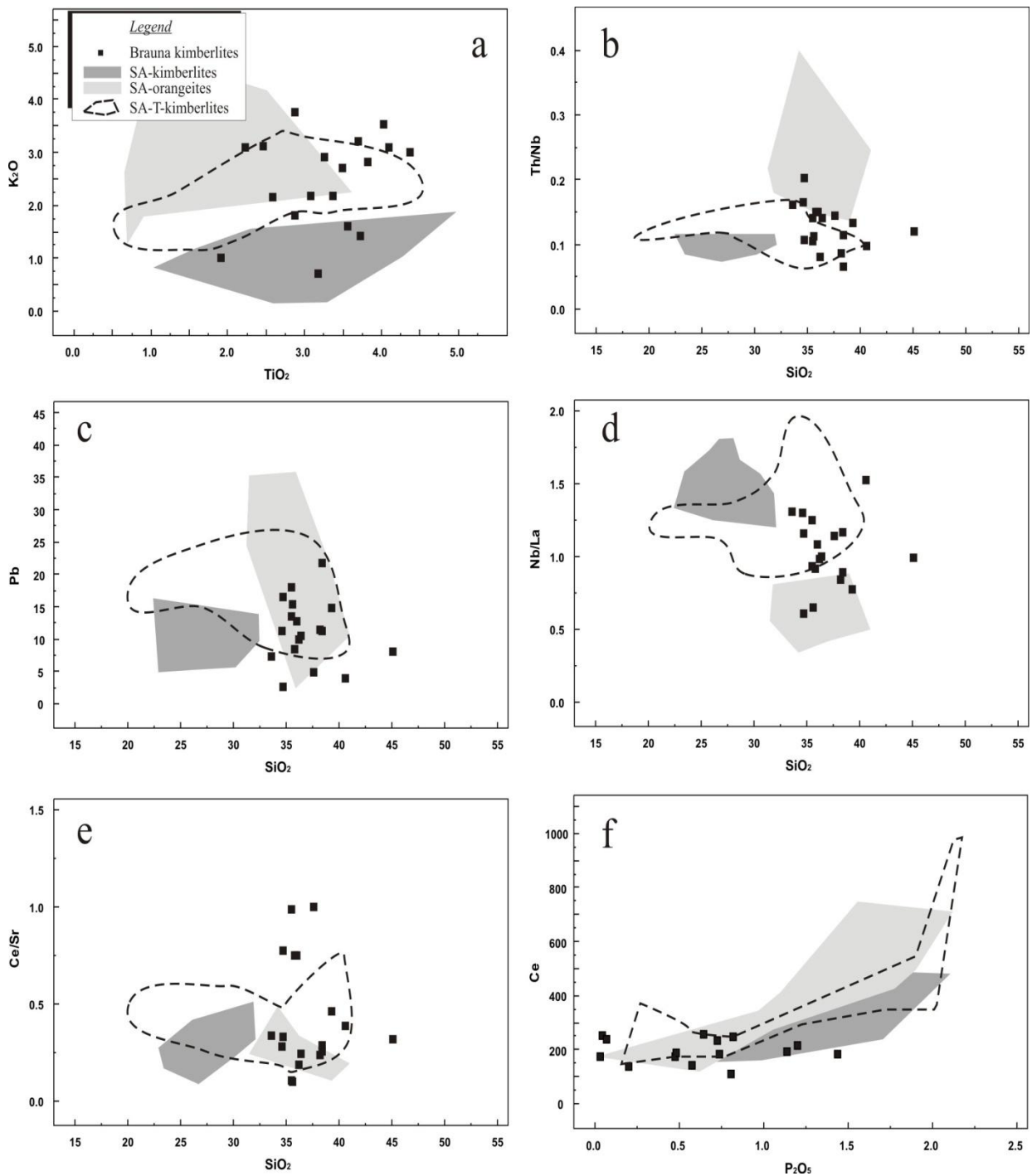
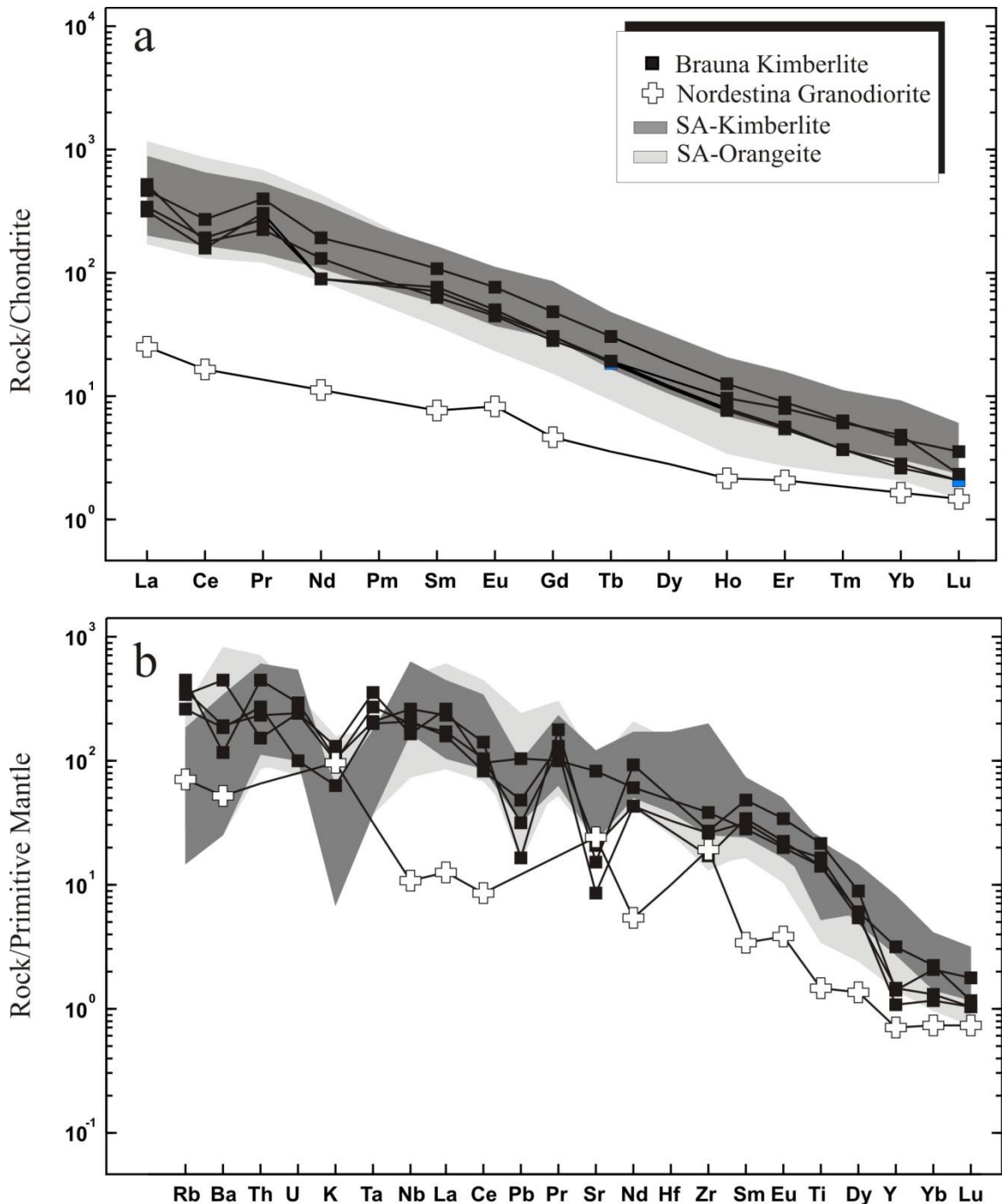


Figure 7: Geochemical characteristics of Brauna Kimberlite Field (filled square) plotted in binary discriminant diagrams from Smith (1983) and Smith et al. (1985), using the most representative major oxides and compatible trace elements. South African kimberlites and orangeites fields are from Becker and Le Roex (2006). South African Transitional kimberlites from Becker and Le Roex (2007).



8. U-Pb perovskite geochronology

Because perovskite is a common groundmass mineral in the Brauna kimberlites, and is reliable for kimberlite age dating (Kramers and Smith, 1983; Allsopp et al. 1989; Heaman, 2003; Batumike et al., 2008), perovskite grains were selected from Brauna-07 pipe for conventional U-Pb thermal ionization mass spectrometry (TIMS) analysis at the University of Alberta, Canada. Fresh euhedral perovskite grains devoid of visible inclusions were handpicked for electron microscopy confirmation and subsequent U-Pb isotopic analysis. The perovskite U-Pb sample preparation and age dating followed the procedures of Heaman and Kjarsgaard (2000) and Tappe et al. (2009). The U-Pb data for two perovskite fractions are listed in Table 2.

Table 2: U-Pb perovskite results for hypabyssal kimberlite from the Brauna 07 pipe, São Francisco Craton, Bahia state, Brazil

Description*	Weight (μg)	U (ppm)	Th (ppm)	Pb (ppm)	Th/U	TCPb (pg)	apparent ages (Ma)						Discordance [%]
							$^{206}\text{Pb}/^{238}\text{U}$	$^{207}\text{Pb}/^{235}\text{U}$	$^{207}\text{Pb}/^{206}\text{Pb}$	$^{206}\text{Pb}/^{238}\text{U}$	$^{207}\text{Pb}/^{235}\text{U}$	$^{207}\text{Pb}/^{206}\text{Pb}$	
Brauna-7													
1. dark brown-to-black octahedrons (120)	100	61	755	37	12.3	819	0.10552±77	0.9476±237	0.06514±169	646.7±4.5	676.9±12.3	778.7±53.6	17.8
2. dark brown-to-black octahedrons (80)	56	74	801	39	10.8	477	0.10402±66	0.9363±204	0.06528±147	637.9±3.9	670.9±10.6	783.4±46.7	19.5
												WA 641.7±3.0	

*Perovskite grains selected from magnetic fraction of Full Frantz Free Fall; Numbers in parentheses are numbers of grains analysed.

**Atomic ratios corrected for fractionation (0.105%/amu Pb and 0.123%/amu U), blank (5 pg Pb; 1 pg U), isotopic tracer, and initial common Pb.

Thorium concentrations calculated based on amount of 208Pb present and 207Pb/206Pb model age.

TCPb is estimated total initial common Pb based on the Stacey & Kramers (1975) terrestrial Pb evolution model.

All uncertainties in this table are quoted at 1-sigma.

For the Brauna-07 sample, two multi-grain perovskite fractions were selected from kimberlite drill core at 60 m depth: Brauna-07-1 and Brauna-07-2 fractions, respectively with 120 and 80 dark brown-to-black octahedrons. These perovskite fractions have moderate U contents (61-74 ppm) and Th/U ratios (10.8-12.3) compared with other kimberlitic perovskite. Brauna-07-1 and Brauna-07-2 fractions yielded $^{206}\text{Pb}/^{238}\text{U}$ ages of 646.7±9.0 Ma and 637.9±7.8 Ma (2-sigma), respectively, which are identical within analytical uncertainties (Fig. 9). The weighted average $^{206}\text{Pb}/^{238}\text{U}$ age of 641.7±6.0 Ma (2-sigma) is considered the best estimate for emplacement of Brauna Kimberlite Field.

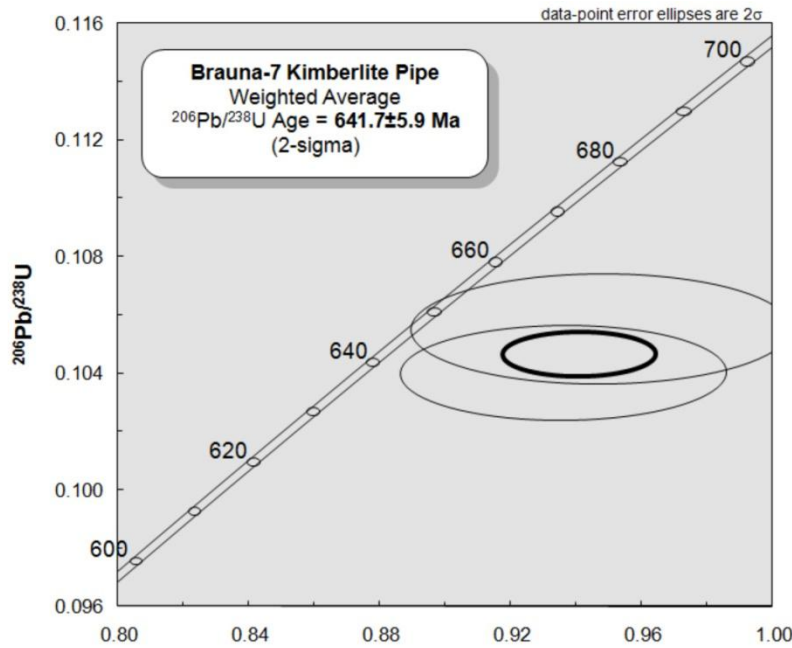


Figure 9: Perovskite U-Pb data from Brauna 07 pipe. Concordia diagram showing the $^{206}\text{Pb}/^{238}\text{U}$ age of 641.7 ± 6 Ma, interpreted as the best estimate for the timing of BKF emplacement. Error is quoted at 2σ .

9. Sr-Nd isotope

Sr and Nd isotopes are a powerful tool to help understand kimberlite petrogenesis. Five samples from Brauna 03, 04 and 07 pipes were analysed for whole-rock Sr-Nd isotopes in the Geochronology Laboratory of the University of Brasília following the analytical techniques of Gioia and Pimentel (2000). The samples were selected on the basis of petrographic evidence of minimal contamination, avoiding country rock xenoliths. Approximately 60 mg of powdered rock samples were dissolved for Sr, Sm, and Nd extraction in successive acid dissolution with concentrated HF, HNO₃, and HCl. A mixed ^{149}Sm - ^{150}Nd spike was added to the solution before the first acid attack. Sr and the REE group were separated from the whole-rock solutions using a conventional ion exchange. Isotopic measurements were carried out on a multicollector Finnigan MAT-262 mass spectrometer in static mode. Mass fractionation corrections were made using a $^{88}\text{Sr}/^{86}\text{Sr}$ ratio value of 8.3752.

The initial isotopic ratios of the Brauna kimberlites were calculated using the emplacement age of 642 Ma determined in this study. The results are presented in Table 3 and

shown in Figure 10. The samples exhibit a large range of initial $^{87}\text{Sr}/^{86}\text{Sr}$ ratios between 0.7045 and 0.7063, and a relatively wide range of negative $\epsilon\text{Nd(i)}$ values from -5.8 to -8.1.

Because perovskite has the potential to record the primary isotopic signature of the magma prior to contamination, precise Sr-Nd isotopic data are important information to help place constraints on the evolution of kimberlitic rock source. With the objective to check the quality and the reliability of whole rock Sr-Nd isotope data, which may have been modified by virtually non-observed xenolithic material, we also analysed groundmass perovskite for Nd isotope composition from the dated Brauna 07 pipe (Table 3). The procedures and measurements were carried out following the methods described in Tappe et al. (2011). The results were corrected for the age of Brauna 07 pipe (i.e. 642Ma) and they are very similar to the whole-rock data (perovskite $\epsilon\text{Nd(i)} = -7.7$; average whole-rock $\epsilon\text{Nd(i)} = -7.2$). The data similarity indicates the very robust data quality for whole-rock Sr-Nd measurements.

Table 3: Whole-rock Sr and Nd isotope analyses and perovskite Nd isotope analysis of the Brauna kimberlites

Sample	Rb*	Sr*	Sm _{ID}	Nd _{ID}	$^{87}\text{Sr}/^{86}\text{Sr}_{(\text{m})}$	$^{143}\text{Nd}/^{144}\text{Nd}_{(\text{m})}$	$\pm 2\sigma$	$^{143}\text{Nd}/^{144}\text{Nd}_{(642\text{Ma})}$	$\epsilon\text{Nd}_{(642\text{Ma})}$	$^{87}\text{Sr}/^{86}\text{Sr}_{(642\text{Ma})}$	$\epsilon\text{Sr}_{(642\text{Ma})}$
Kimberlite											
B3D34 123,3	128.3	499.4	13.91	112.03	0.712560	0.5117350	10	0.5114191	-7.6	0.705748	25.9
B3D34 186,6	194.8	1775.9	11.00	83.79	0.709040	0.5117300	6	0.5113959	-8.1	0.706132	31.4
B4D1 75	133.6	995.6	15.91	122.20	0.709320	0.5117820	15	0.5114506	-7.0	0.705762	26.1
B7D15 45	199.4	351.0	19.83	153.79	0.719550	0.5118410	14	0.5115128	-5.8	0.704476	7.8
B7D15 30	191.4	220.4	13.23	99.18	0.729320	0.5117590	16	0.5114195	-7.6	0.706252	33.1
Perovskite											
BR7-UOFA1	n.a.	n.a.	392.42	3258.1	n.a.	0.5117239	8.2E-06	0.5114165	-7.7	n.a.	n.a.

* ICPMS analysis; ID = isotope dilution; m = measured; n.a. = not analysed

Figure 10 also includes data for several kimberlites and lamproites worldwide, mantle reservoir (OIB, EM1, EM2), and the Nordestina Granodiorite, a potential wall-rock contaminant. As shown, the Brauna kimberlites plot between the South African orangeites and kimberlites groups, and barely touch the South African transitional kimberlite field. Brauna samples are isotopically similar to the anomalous Guaniamo kimberlite in Venezuela and the transitional Arkhangelsk kimberlite in Russia. Yet, the Brauna samples are isotopically not too distinct of olivine lamproites although their mineralogy and geochemistry are fairly different.

It is interesting to note that the Brauna kimberlite samples display a trend that does not suggest any significant contamination with the Nordestina granodiorite, indicating that the selected samples have not been significantly contaminated with the continental crust. This is also

supported by the concordant negative ϵ Nd value (-7.7) from the analysed groundmass perovskite. Consequently, the data may be used to place constraints on likely mantle sources for the Brauna kimberlites, which will be recalled later.

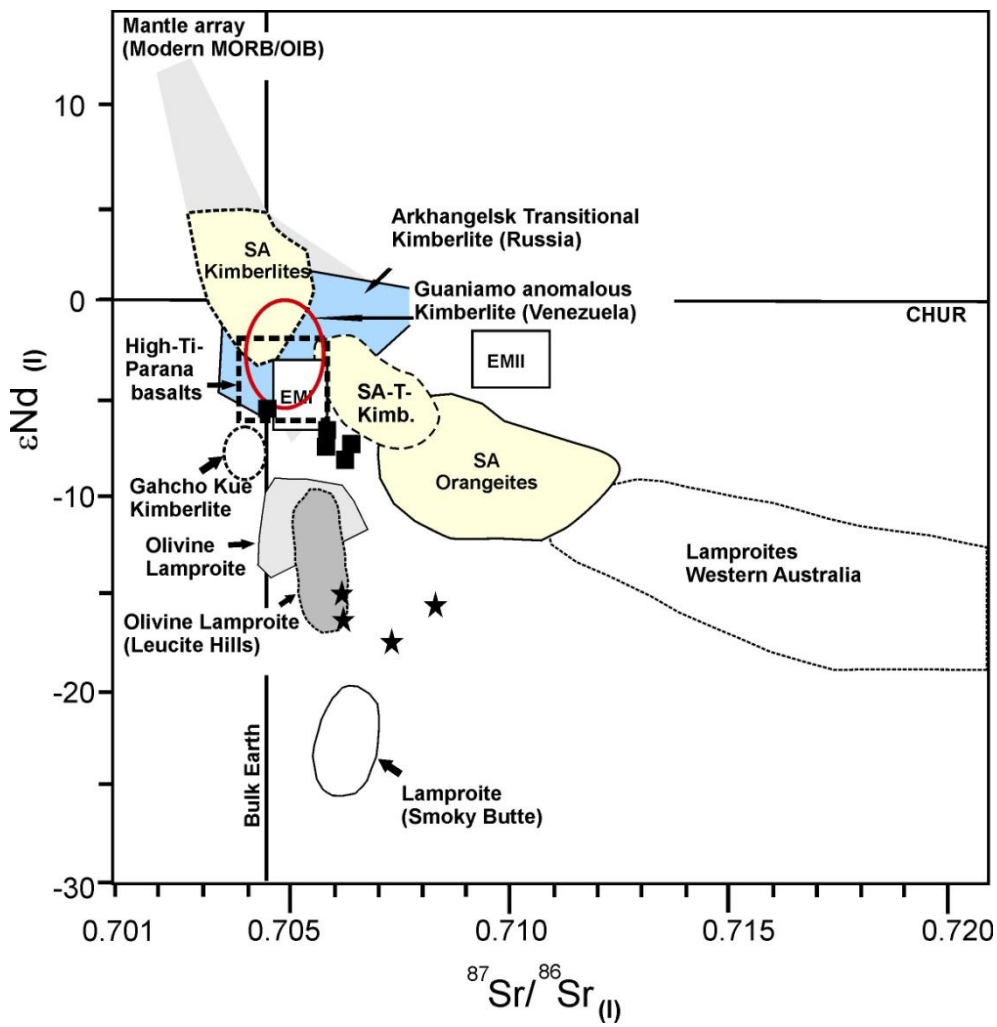


Figure 10: ϵ Nd versus $^{87}\text{Sr}/^{86}\text{Sr}$ isotopic diagram for Brauna kimberlites (filled square) and their host rocks, Nordestina granodiorite (black star), corrected for the emplacement age of the Brauna kimberlite field (642 Ma). Compositional fields in the diagram: lamproites from Greenland (Nelson, 1989; Tappe et al. 2007); Leucite Hills, Smoky Butte and Western Australia lamproites (Vollmer et al., 1984; Fraser et al., 1985); South African kimberlites and orangeites (Nowell et al., 2004; Becker and Le Roex, 2006); Guaniamo anomalous kimberlites (Kaminsky et al., 2004); Gahcho Kue kimberlites (Caro et al., 2004); South African Transitional kimberlites (Becker and Le Roex, 2007). Arkhangelsk transitional kimberlites (Beard et al., 2000); High-Ti basalts from Parana Igneous Province (Peate and Hawkesworth, 1996); The postulated EMI and EMII compositions after Zindler and Hart (1986). Data for Nordestina granodiorite from Cruz Filho et al. (2005).

10. Discussion

10.1. Brauna kimberlite classification

Kimberlites have been identified from most continents in Archean cratons and Proterozoic terranes whereas orangeites appear to be confined to the Archean Kaapvaal craton of southern African (Skinner, 1989). Mitchell and Bergman (1991) and Mitchell (1995) have argued that Group II kimberlites are not actually kimberlites and have suggested they be renamed orangeite. However, kimberlites with Group I affinity is described worldwide (e.g. India, Canada, USA, Russia, Brazil), and new evidence shows that orangeites may also occur in India (Rao et al., 2010). A third, relatively rare group of transitional kimberlites on the Kaapvaal craton, and also within the Proterozoic Namaqua-Natal mobile belt was reported (e.g. Skinner et al., 1992; Becker and Le Roex, 2007). A forth kimberlite type, not uncommon, was found in kimberlite provinces or fields that generally display relatively heterogeneous or anomalous geochemical, mineralogical and isotopic compositions compared to the well defined South African kimberlites, South African Orangeites, and lamproites.

Brauna kimberlites show relatively heterogeneous mineralogy, geochemistry and isotopic compositions. Following Mitchell (1995) mineralogical classification of South African kimberlites and orangeites, the Brauna kimberlites show transitional mineralogy between the two main South African groups. Brauna samples are similar to South African orangeites if the occurrence of groundmass tetraferriphlogopite, diopside and calcite are considered. Conversely, the occurrence of spinel and apatite as common phase in the studied samples is a characteristic of South African kimberlites. Additionally, ilmenite xenocrysts are typically absent in orangeites, and they are present in the Brauna samples. These mixed petrographic characteristics of BKP are similar to some kimberlite examples in the world such as the South African transitional kimberlites (Becker and Le Roex, 2007), Arkhangelsk transitional kimberlite in Russia (Beard et al., 2000; Lapin et al., 2007) and Guaniamo anomalous kimberlite in Venezuela (Kaminsky et al., 2007). The peculiar petrographic features of the above kimberlite types indicate that they are intermediate between the South African kimberlites and orangeites, with special regard to variable phlogopite contents, groundmass tetraferriphlogopite, dominance of calcite, serpentine

and monticellite as groundmass phases, relative size and abundance of groundmass opaque oxides, and perovskite with variable REE contents.

In addition to the mineralogical differences, the BKP isotopic composition shares little similarity with the two main South African kimberlitic groups. Indeed, orangeite has more radiogenic Sr and lesser radiogenic Nd and Pb than the kimberlite group. Moreover, the South African transitional group has distinct isotopic signature, generally showing Sr and Nd isotope ratios intermediate between kimberlites and orangeites (Fig. 6). As shown in Figure 10, the Brauna kimberlite samples have neither the isotope characteristics of the South African kimberlite nor of orangeite. Furthermore, the Brauna kimberlites have less radiogenic Sr than the South African transitional kimberlites. Yet the Brauna kimberlites plot in between the fields of these three groups, and in this aspect the BKF samples are more akin to the anomalous kimberlites described elsewhere, for example, the South African transitional kimberlites, Guaniamo anomalous kimberlite in Venezuela and Arkhangelsk kimberlite.

10.2. Petrogenesis

For petrogenetic hypothesis to be reliable, it is necessary that secondary alteration/contamination effects and fractional crystallization are minimal. Also, it is commonly accepted that the macrocryst population in kimberlites is to a large extent mantle-derived and that the macrocrystic-bearing kimberlites do not represent liquid compositions but rather random accumulations of mantle xenocrysts and early-stage liquidus phases (dominantly olivine) together with a liquid component (e.g., Le Roex et al. 2003; Kjarsgaard et al. 2009, Mitchell and Tappe 2010). On these grounds, the aphanitic kimberlite variety from the pipes is considered the most closely representative of the Brauna kimberlite magma composition rather than the porphyritic and xenocryst-rich kimberlite varieties (including the breccia facies) from pipes and dykes.

The source of the Brauna kimberlites was enriched in incompatible elements, with high La/Sm (8.29-14.93) and Gd/Yb (7.05-14.58), and enriched in the highly incompatible LIL- and HFS-elements (e.g. Th = 15.3 – 32.2 ppm, Yb = 0.75 – 0.9 ppm, Zr = 162 – 1304 ppm, Nb = 110 – 182 ppm). The Brauna kimberlites exhibit also relatively higher La/Nb ratios (0.7 – 1.5) than the average asthenospheric mantle-derived rocks, indicating a transitional and/or heterogeneous source that was probably formed between the asthenospheric mantle (i.e. La/Nb<1) and the

lithospheric mantle (i.e. $\text{La}/\text{Nb} > 1$) (Fig. 11). The Brauna kimberlites have La/Nb ratios similar to ratios described for fertile phlogopite-bearing mantle nodules from North China Craton, interpreted as the product of various degrees of metasomatism coupled with infiltration of fluids sourced mainly from deeply subducted supracrustal rocks (Zhang et al., 2011). Notably, the data distribution for the anomalous and heterogeneous Arkhangelsk kimberlite (Beard et al., 2000) and the Guaniamo anomalous kimberlite (Kaminsky et al., 2007) were also interpreted as products of metasomatized mantle sources; they are remarkably similar to BKF kimberlite compositions.

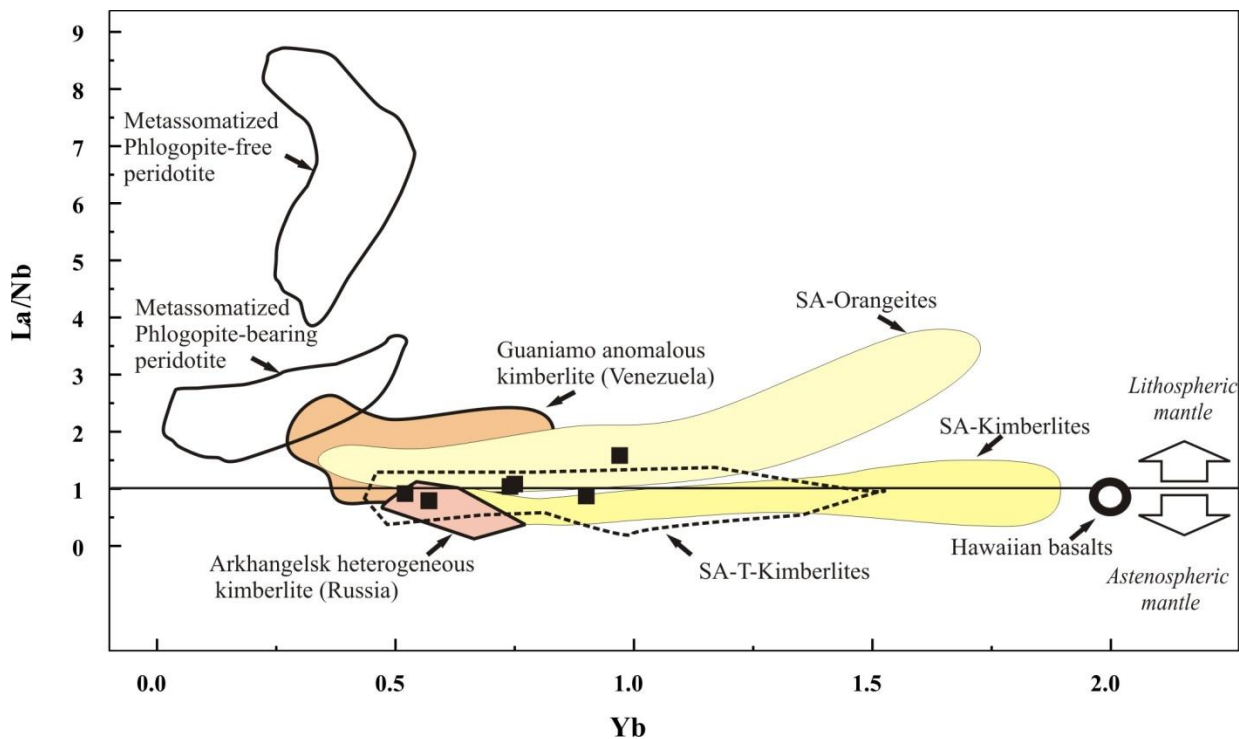


Figure 11: La/Nb versus Yb mantle source discriminant diagram for Brauna kimberlites (filled square) compared with similar rocks. Data sources: Arkhangelsk kimberlite (Beard et al., 2000); Guaniamo kimberlites (Kaminsky et al., 2007); South African (SA) kimberlites and orangeites (Becker and Le Roex, 2006); South African transitional (SA-T) kimberlites (Becker and Le Roex, 2007); Metasomatized mantle peridotites from north China craton (Zhang et al., 2011); Hawaiian basalts (Wilson, 1997). La/Nb mantle data from DePaolo and Daley (2000).

When compared to known mafic and ultramafic rock suites worldwide (Figure 12), the Brauna kimberlites exhibit geochemical signatures akin to uncontaminated magmas originated from the sub-continental lithospheric-asthenospheric mantle. Indeed, the Brauna kimberlites

show a steep mantle-normalized multi-element pattern probably owing to their origin as low-degree melts of a mantle source with garnet, olivine, phlogopite, and pyroxene.

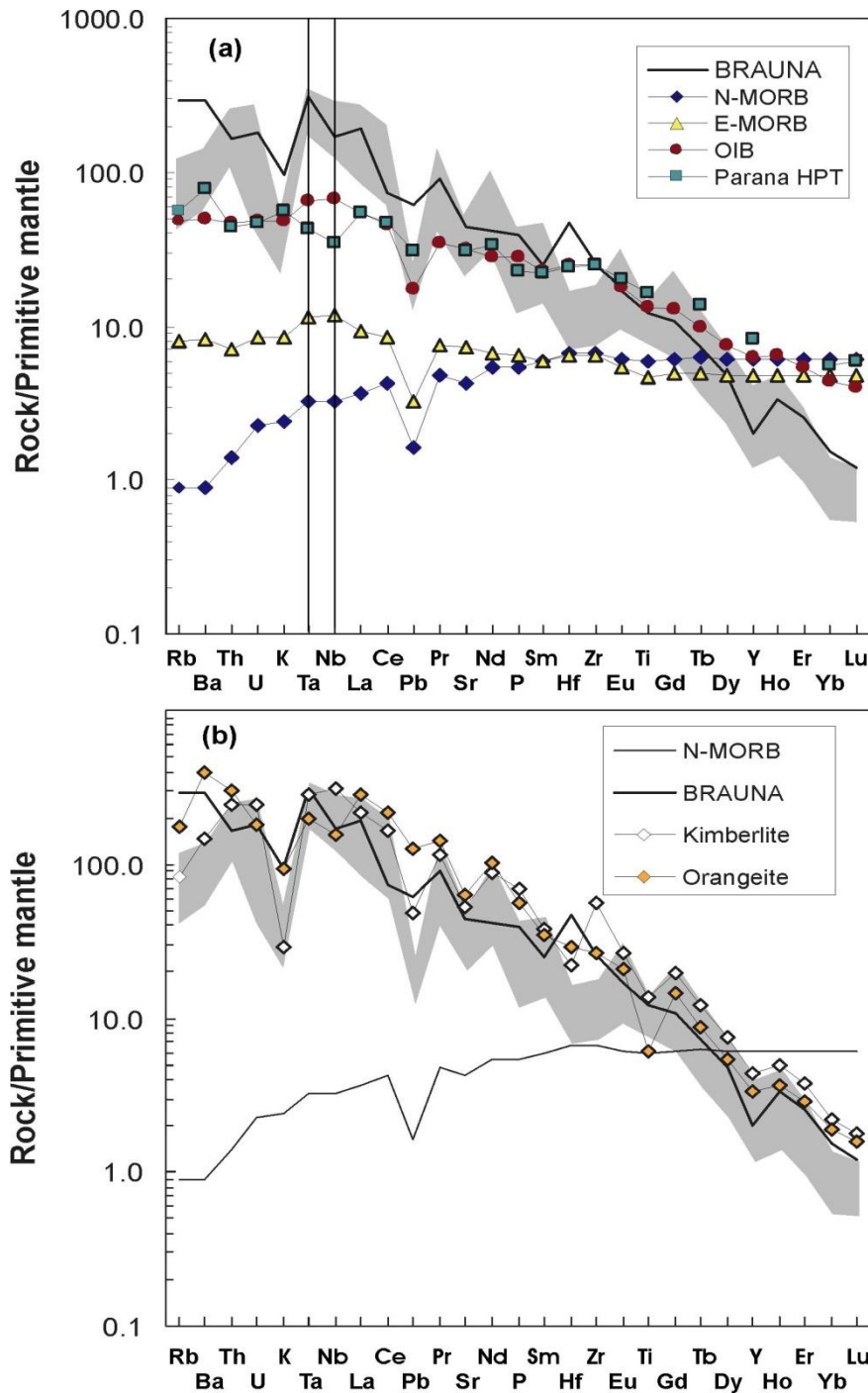


Figure 12: Primitive mantle normalized multi-element diagrams for Brauna kimberlites and related rocks. **a)** Average Brauna aphanitic kimberlite compared with oceanic basalts, Parana uncontaminated basalt from the sub-continental lithospheric mantle, and asthenosphere-derived, ca. 600 Ma West Greenland kimberlites (grey field); vertical bars highlight the Nb- and Ta anomalies; **b)** the Brauna kimberlite compared with the South African kimberlite and orangeite. N-MORB, E-MORB and OIB after Sun & McDonough (1989); Parana high-P, high-Ti basalt (HPT) after Peate et al. (1999); West Greenland kimberlite after Gaffney et al. (2007), South African kimberlite and orangeite after Becker and LeRoex (2006).

The Brauna kimberlites also show positive to negative Nb-Ta anomalies, a characteristic of magmas derived from the asthenospheric mantle (positive Nb-Ta anomalies, e.g. ocean island basalts; Fig. 12) or from the sub-continental lithospheric mantle (negative Nb-Ta anomalies, e.g. the Paraná high-Ti, high-P continental flood basalts; see Fig. 12). The Brauna kimberlites have trace elements characteristics extremely similar to the ca. 600 Ma West Greenland kimberlites (Fig. 12), which were interpreted as originated from within the asthenosphere or lower mantle on the basis of their high ${}^3\text{He}/{}^4\text{He}$ ratios (Tashibana et al., 2006). These features are all consistent with mixing between asthenospheric and lithospheric sources, or plume activity.

10.3. Brauna kimberlite magma classification

The Brauna Kimberlite Field is composed of relatively heterogeneous kimberlites with La/Nb ratios suggesting origin from within the metasomatized asthenospheric mantle, probably with subsequent contribution from the sublithospheric mantle by decompression and thermal perturbations during lithosphere extension. Regarding magma composition, the Brauna kimberlites are more similar in composition to orangeite and lamproite magma types rather than to formerly South African kimberlites owing to their high phlogopite content and high SiO₂, Al₂O₃, Rb, Ba, and K₂O abundances. On this basis, the BKF kimberlites could qualify as a member of the “metasomatized lithospheric mantle magma group” of Mitchell (1995, 2006). However, their chemical compositions are very complex given their anomalous signature, exhibiting moderate ${}^{87}\text{Sr}/{}^{86}\text{Sr}$ (0.7045 – 0.7063) and negative ϵ_{Nd} values (-5.8 to -8.1). These features suggest that the magma source regions for the BKF were metasomatically enriched to different degrees before kimberlite magma generation. Therefore, the depletion in Sr, Pb and K relative to elements of similar incompatibility observed in the multi-element diagram is probably a feature of the primary kimberlite magma that was inherited from the metasomatized source region. Donatti Filho et al. (2008) suggested that the Brauna kimberlites may be low degree partial melts, approximately 0.2-0.75% melting of a depleted garnet lherzolite source that was enriched in volatiles and highly incompatible elements prior to melting, probably formed at pressure conditions of up to 5 GPa. This is consistent with their diamond-bearing characteristics. However, the kimberlites high MgO contents, the presence of harzburgitic and lherzolitic

xenoliths, G12 garnet xenocrysts, and intense serpentinization require all a more refractory olivine-rich harzburgitic mantle source.

Several studies have described kimberlites and related rock as a consequence of metasomatism of the mantle source region, as for instance the Koidu kimberlite in Sierra Leone (Taylor et al., 1994), Aries kimberlite in Western Australia (Downes et al., 2006), Alto Paranaiba kimberlites in Brazil (Gibson et al., 1995), the olivine lamproites of Western Australia (Fraser et al., 1985), and other lamproitic occurrences. Depletion of HFSE is a common characteristic of magmatic rocks related to subduction processes (Saunders et al., 1980; Thirlwall et al. 1994). Brauna kimberlites exhibit relatively high Ba/Nb (3.76 – 26.52) and varying La/Nb (0.66 - 1.76) ratios, suggesting that the mantle sources could have also been contaminated/metasomatized by fluids released from subducted crust with the addition of sediments(?), thereby increasing Ba (LILE) and La (HREE) in the initial kimberlitic magma composition.

Furthermore, eclogitic paragenesis was also observed in BKF rocks including garnet xenocrysts (G9) and eclogite xenoliths, supporting the heterogeneous kimberlitic magma nature. As addressed before, the Nordestina granodiorite (i.e. wall-rock) did not contribute significantly to the trace elements budget, as illustrated in the mantle-normalized trace element diagram (Fig. 8) and in the Sr-Nd isotopic diagram (Fig. 10). Consequently, though the kimberlitic magma did incorporate xenoliths from the wall-rock the magma probably has not had enough time to melt them and eventually to modify its mantle-inherited composition. Furthermore, the heterogeneous magma composition of the BKF could be related to partial melting at high depth, coupled with lithosphere recycling.

11. Conclusions

The Brauna Kimberlite Field (BKF) comprises three kimberlite pipe-like bodies and nineteen kimberlite dykes as predominantly hypabyssal facies of root zone. The $^{206}\text{Pb}/^{238}\text{U}$ age of 642 ± 6.0 Ma for the Brauna-07 kimberlite pipe is the best estimate for the time of BKF magma emplacement. BKF kimberlite pipes and dykes have similar mineralogical, geochemical and textural characteristics, such as aphanitic, porphyritic, segregationary and brecciated types. The BKF kimberlites host a significant portion of altered mantle-derived xenoliths, including high magnesium garnet-phlogopite peridotites and abundant megacrysts: clinopyroxene,

orthopyroxene, and garnet. The kimberlite bodies are slightly iron-enriched and have heterogeneous mineralogy, major and trace element compositions relatively to South African orangeites, kimberlites and lamproites as described in the literature.

The evolution of the BKF magma is consistent with a single emplacement (from a single magma batch?) of relatively volatile-rich magma coupled with trapment and/or confinement process. The low Al_2O_3 , HREE, relatively high La to Sm, Ni and Cr contents, high Mg# (80.12 - 90.11), residual olivine (Fo₈₈), and pervasively serpentinization in the Brauna kimberlites indicate strongly depleted, very refractory peridotitic mantle source.

The above characteristics coupled with isotopic variations (moderate radiogenic ⁸⁷Sr and negative ϵ_{Nd}) support a model whereby the Brauna kimberlite magma appears to have been generated in the heterogeneous metasomatized lithospheric/asthenospheric mantle, subsequently erupted through a relatively disturbed cratonic lithosphere, however suitable for diamond preservation. We also suggest that Neoproterozoic-related lithospheric accretion during the São Francisco craton stabilization may be the cause of the heterogeneity of Brauna kimberlite source, perhaps caused by slab subduction beneath the São Francisco Craton combined with diapiric upwelling of the mantle and thermal perturbation by convection. The proposed model for the BKF is shown in Figure 13.

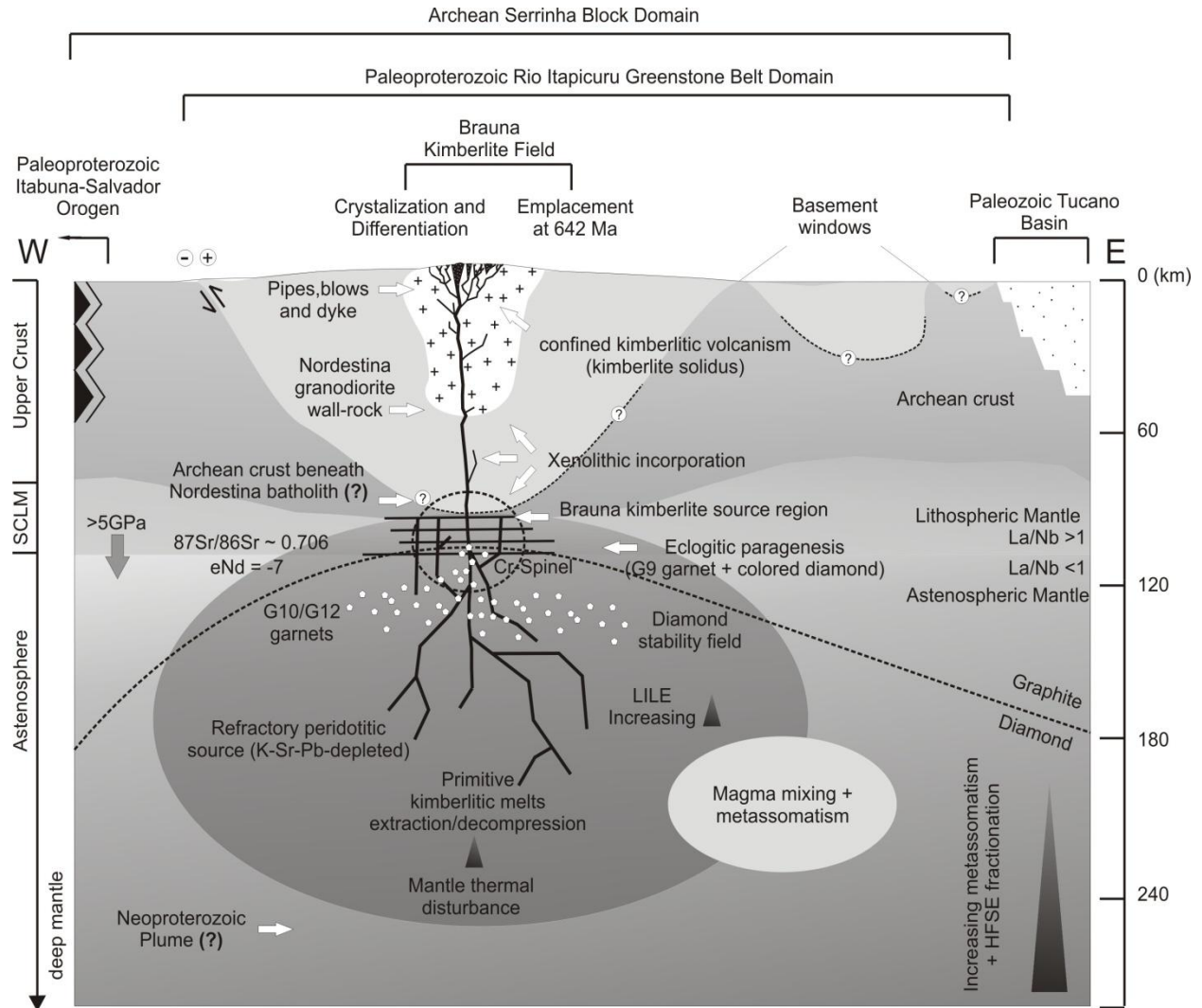


Figure 13: Proposed tectonic model for the Brauna Kimberlite Field.

Acknowledgements

The authors wish to thank Fundação de Amparo à Pesquisa do Estado de São Paulo - FAPESP for research grant to JPDF (# 07/537989) and the Brazilian research Council - CNPq for grants to EPO (# 301025/2005-3, 78989/04-0). We are grateful to Vaaldiam Resources Ltd. for fieldwork support and access to the kimberlite samples. The comments of Kenneth Tainton and Roger H. Mitchell greatly improved the manuscript. José Ricardo Pisani and Fernanda Prendin Ochika from Vaaldiam Resources Ltd. for their collaboration.

References

- Allsopp, H.L., Bristow, J.W., Smith, C.B., Brown,R., Gleadow, A.J.W.,Kramers, J.D., Garvie,O.G., 1989. A summary of radiometric dating methods applicable to kimberlite and related rocks. In: Ross, J. (Ed.), Proceedings of the Fourth International Kimberlite Conference, v. 1, Kimberlites and Related Rocks: Their Composition, Occurrence, Origin and Emplacement. Geological Society of Australia Special Publication, vol. 14. Blackwell Scientific Publications, Oxford, pp. 343–357.
- Barbosa J.S.F. & Sabaté P. 2004. Archean and Paleoproterozoic crust of the São Francisco Craton, Bahia, Brazil: geodynamic features. *Precambrian Res.*, 133:1-27.
- Bardet, M.G., 1977. Géologie du diamant. Memoires Du BRGM, pg. 177.
- Batumike, J.M., Griffin,W.L., Belousova, E.A., Pearson, N.J., O, ' Reilly, S.Y., Shee, S.R., 2008. LAM–ICPMS U–Pb dating of kimberlitic perovskite: Eocene-Oligocene kimberlites from the Kundelungu Plateau, D. R. Congo. *Earth. Planet. Sci. Let.* 267, 609–619.
- Beard, A.D., Downes, H., Hegner, E., Sablukov, S..M., 2000. Geochemistry and mineralogy of kimberlites from the Arkhangelsk Region, NW Russia: evidence for transitional kimberlite magma types. *Lithos* 51: 47-73.
- Becker, M., Le Roex, A.P., 2006. Geochemistry of South African On- and Off craton, Group I and Group II Kimberlites: Petrogenesis and Source Region Evolution. *J Petrol* 47: 673–703.
- Becker, M., Le Roex, A.P., 2007. Geochemistry and petrogenesis of South African transitional kimberlites located on and off the Kaapvaal Craton. *Sout. Afr. J. Geol.* (110): 631-646.
- Bizzi, L.A., Smith, C.R., Meyer, H.O.A., Armstrong, R., de Wit, M.J., 1994. Mesozoic kimberlites and related rocks in southwestern São Francisco craton, Brazil: a case for local mantle reservoirs and their interaction. In: Meyer, H.O.A. & Leonards, O.H. (eds) *Proceedings of the 5th International Kimberlite Conference*, Araxá, Brasilia, DF: CPRM, Special Publication 2/91, 156-171.
- Caro, G., Kopylova, M.G., 2004. The hypabyssal 5034 kimberlite of the Gahcho Kue cluster, southeastern Slave craton, northwest territories, Canada: a granite-contaminated group-I kimberlite. *Can Mineral* 42: 183-207.

Chaves, M.L.S.C., Karfunkel, J., Hoppe, A., Hoover, D.B., 2001. Diamonds from the Espinhaço Range (Minas Gerais, Brazil) and their redistribution through the geologic record. *Journal of South American Earth Sciences*, Chicago, v. 14, n. 4, p. 277-289.

Clement, C.R., Skinner, E.M., Scott, H., 1977. Kimberlite redefined. 2nd International Kimberlite Conference. Santa Fe, NM. Expanded Abstract.

Clement, C.R., Skinner, M.W., 1979. Textural genetic classification of kimberlites. *Transactions of the Geol Soc S Afr* 88: 403–410.

Costa F.G., Oliveira E.P., McNaughton, N., 2011. The Fazenda Gavião Granodiorite and Associated Potassic plutons as evidence for Palaeoproterozoic Arc-continent Collision in the Rio Itapicuru Greenstone Belt, Brazil. *J. South American Earth Sci.* 32: 127-141. Doi: 10.1016/j.jsames.2011.04.012

Cruz Filho, B.E., Conceição H., Rios D.C., Rosa M.L.S., Marinho M.M., 2003. *Geologia, petrografia e litogeoquímica do batólito trondjemítico Nordestina, Núcleo Serrinha, Nordeste da Bahia*. Revista Brasileira de Geociências 33: 175-186.

Dawson JP (1980) Kimberlite and their xenoliths. New York, Springer. 250pp.

DePaolo D. J., Daley, E., E., 2000. Neodymium isotopes in basalts of the southwest basin and range and lithospheric thinning during continental extension. *Chem. Geol.* (169): 157–185.

Donatti Filho, J.P., Oliveira, E.P., Pisani, J.R.T., Ochika, F.P., 2008. Geochemistry and mineralogy of kimberlites from the Brauna Kimberlite Province, São Francisco Craton, NE Brazil. 9º Int Kimberlite Conf Ext Abstr, Frankfut, Germany, 9IKC-A-00316.

Donnelly, K.E., Goldstein S.L., Langmuir, C.H., Spiegelman, M., 2004. Origin of enriched ocean ridge basalts and implications for mantle dynamics. *Earth. Planet. Sci. Let.* 226: 347– 366.

Downes, P.J., Wartho, J., Griffin, B.J., 2006. Magmatic Evolution and Ascent History of the Aries Micaceous Kimberlite, Central Kimberley Basin, Western Australia: Evidence from Zoned Phlogopite Phenocrysts, and UV Laser $^{40}\text{Ar}/^{39}\text{Ar}$ Analysis of Phlogopite–Biotite. *J Petrol* 47: 1751–1783.

Fipke, C.E., Gurney, J.J., Moore, R.O., 1995. Diamond exploration techniques emphasising indicator mineral geochemistry and Canadian examples; Geological Survey of Canada, Bulletin 423, 86 pp.

Fraser, K. J., Hawkesworth, C. J., Erlank, A. J., Mitchell, R. H., Scott-Smith, B. H., 1985. Sr, Nd and Pb isotope and minor element geochemistry of lamproites and kimberlites. *Earth and Planetary Sci. Lett.* 76, 57–70.

Gibson, S.A., Thompson R.N., Leonardos O.K., Dickin A.P., Mitchell J.G. 1995. The Late Cretaceous impact of the Trindade mantle plume - evidence from large-volume, mafic, potassic magmatism in SE Brazil. *J. Petrol.* (36):189-229.

Gioia, S. M. C. L., Pimentel, M. M., 2000. The Sm-Nd Isotopic Method in the Geochronology Laboratory of the University of Brasília. *An. Acad. Bras. Ci.*, (2): 72.

Grütter, H.S., Gurney, J.J., Menzies, A.H., Winter, F., 2004. An updated classification scheme for mantle-derived garnet, for use by diamond explorers. *Lithos* 77: 844–857.

Gurney, J.J., Zweistra, P., 1995. The interpretation of the major element compositions of the mantle minerals in diamond exploration. *J Geochem Exp* 53: 293-309.

Heaman, L.M., Kjarsgaard, B.A., 2000. Timing of eastern North American kimberlite magmatism: continental extension of the Great Meteor hotspot track? *Earth Planet Sci Lett* 178: 253–268.

Heaman, L.M., Kjarsgaard, B.A., Creaser, R.A., 2003. The timing of kimberlite magmatism in North America: implications for global kimberlite genesis and diamond exploration. *Lithos* 71: 153-184.

Jakubec, J. 2008. Kimberlite emplacement models — The implications for mining projects. *J. Volcanol. Geotherm. Res.* 174: 20-28.

Kaminsky, F.V., Sablukov, S.M., Sablukova, L.I., Channer, D.M.DeR., 2004. Neoproterozoic ‘anomalous’ kimberlites of Guaniamo, Venezuela: mica kimberlites of ‘isotopic transitional’ type. *Lithos* 76: 565– 590.

- Kjarsgaard, B.A., Pearson, D.G., Tappe, S., Nowell, G.M., Dowall, D., 2009. Geochemistry of hypabyssal kimberlites from Lac de Gras, Canada: comparisons to a global database and applications to the parent magma problem. *Lithos* 112: 236–248.
- Kramers, J.D., Smith, C.B., 1983. A feasibility study of U–Pb and Pb–Pb dating of kimberlites using groundmass mineral fractions and whole-rock samples. *Chem. Geol.* 1, 23–38.
- Lapin, A.V., Tolstov, A.V., Vasilenko, V.B., 2007. Petrogeochemical Characteristics of the Kimberlites from the Middle Markha Region with Application to the Problem of the Geochemical Heterogeneity of Kimberlites. *Geochemistry International*, 45:1197–1209.
- Le Roex, A.P., Bell, D.R., Davis, P., 2003. Petrogenesis of group I kimberlites from Kimberley, South Africa: evidence from bulk-rock geochemistry. *J Petrol* 44: 2261–2286.
- Lorenz, V., Kurszlaukis, S., 2007. Root zone processes in the phreatomagmatic pipe emplacement model and consequences for the evolution of maar–diatreme volcanoes. *J. Volcanol. Geotherm. Res.* 159: 4–32.
- McDonough, W.F., Sun S.S., 1995. The composition of the Earth. *Chem. Geol.*, 120:223-253.
- Mitchell, R.H., 1986. Kimberlites, Mineralogy, Geochemistry and Petrology. Plenum Press., New York, 442 pp.
- Mitchell, R.H., 1995. Kimberlites, orangeites, and related rocks. Plenum Press., New York, 410 pp.
- Mitchell, R.H., Bergman, S.C., 1991. Petrology of lamproites. Plenum Press, New York, 447 pp.
- Mitchell, R.H., Tappe, S., 2010. Discussion of “Kimberlites and aillikites as probes of the continental lithospheric mantle”, by D. Francis and M. Patterson (*Lithos* v. 109, p. 72–80). *Lithos* 115: 288-292.
- Navarro, M.S., Andrade, S., Ulbrich, H., Gomes, C.B., Girardi, V.A.G., 2008. The Direct Determination of Rare Earth Elements in Basaltic and Related Rocks using ICP-MS: Testing the Efficiency of Microwave Oven Sample Decomposition Procedures. *Geostand Geoanal Res* 32: 167-180.
- Nelson, D.R., 1989. Isotopic characteristics and petrogenesis of the lamproites and kimberlites of central West Greenland. *Lithos* 22, 265–274.

- Nowell, G.M., Pearson, D.G., Bell, D.R., Carlson, R.W., Smith, C.B., Kempton, P.D., Noble, S.R., 2004. Hf isotope systematics of kimberlites and their megacrysts: new constraints on their source regions. *Journal Petrol.* 45, 1583–1612.
- Oliveira E.P., Souza Z. S., McNaughton N. J., Lafon J-M., Costa F. G., Figueiredo A. M., 2011. The Rio Capim Volcanic-Plutonic-Sedimentary Belt, São Francisco Craton, Brazil: Geological, Geochemical and Isotopic Evidence for Oceanic Arc Accretion During Palaeoproterozoic Continental Collision. *Gondwana Research* 19: 735–750, doi:10.1016/j.gr.2010.06.005.
- Oliveira EP, Carvalho MJ, McNaughton NJ (2004) Evolução do segmento norte do orógeno Itabuna-Salvador-Curaçá: cronologia da acresção de arcos, colisão continental e escape de terrenos. *Geologia USP, Série Científica.* 4: 41-53.
- Oliveira, E.P., McNaughton, N.J., Armstrong, R., 2010. Mesoarchaean to Palaeoproterozoic Growth of the Northern Segment of the Itabuna-Salvador-Curaçá Orogen, São Francisco Craton, Brazil. In: Kusky, T. M., Zhai, M.-G., Xiao, W. (eds) *The Evolving Continents: Understanding Processes of Continental Growth.* Geol Soc London, Spec Publ 338: 263–286.
- Pearce, J.A., 1983. Role of the sub-continental lithosphere in magma genesis at active continental margins. In: C.J. Hawkesworth and M. J. Norry (editors), *Continental Basalts and Mantle Xenoliths.* Shiva, Nantwich, pp. 230-249.
- Peate, D.W., Hawkesworth, C.J., 1996. Lithospheric to asthenospheric transition in low-Ti flood basalts from southern Parana, Brazil. *Chemical Geology* 127, 1–24.
- Pisani, J.R.T., Tainton, K.M., Allan, A.F., Silva, S.B., Miranda, J.V., 2001. Geology and exploration of the Brauna Diamantíferous Kimberlites, Serrinha Block, Bahia, Brazil. *Rev Bras Geoc* 31(4): 663-664.
- Ramsey, R.R., Tompkins, L.A., 1994. The geology, heavy mineral concentrate mineralogy, and diamond prospectivity of Boa Esperanca and Cana Verde pipes, Corrego D'anta, Minas Gerais, Brazil; in *Kimberlites, Related Rocks and Mantle Xenoliths, Proceedings of the 5th International Kimberlite Conference, Companhia de Pesquisa de Recursos Minerais - CPRM,* 2, 329-345.

- Rao, N.V.C., Srivastava, R.K., 2010. Petrology and geochemistry of diamondiferous Mesoproterozoic kimberlites from Wajrakarur kimberlite field, Eastern Dharwar craton, southern India: genesis and constraints on mantle source regions. Contributions to Mineral Petrol 157: 245-265.
- Regelous, M., Hofmann, A.W., Abouchami, W., Galer, S.J.G., 2003. Geochemistry of lavas from the Emperor Seamounts, and the geochemical evolution of Hawaiian magmatism from 85 to 42 Ma. J. Petrol. 44: 113-140.
- Rios, D.C., Conceição, H., Davis, D.W., Plá Cid, J., Rosa, M.L.S., Macambira, M.J.B., McReath, I., Marinho, M.M., Davis, W.J., 2007. Paleoproterozoic potassic-ultrapotassic magmatism: Morro do Afonso sienite pluton, Bahia, Brazil. Precambrian Res 154: 1-30.
- Santos J.O.S., Potter P.E., Reis N.J., Hartmann L.A., Fletcher I.R., McNaughton N.J., 2003. Age, source, and regional stratigraphy of the Roraima Supergroup and Roraima-like outliers in northern South America based on U-Pb geochronology. GSA Bulletin 115: 331–348.
- Saunders, A.D., Tarney, J., and Weaver, S.D. 1980. Transverse chemical variations across the Antarctic peninsula: implications for the genesis of calc-alkaline magmas. Earth Planet Sci Lett (46): 344–360.
- Schulze, D.J., 2003. A classification scheme for mantle-derived garnet in kimberlite: a tool for investigating the mantle and exploring for diamonds. Lithos 71: 195–213.
- Scott Smith, B, H, 2008. Canadian kimberlites: Geological characteristics relevant to emplacement. J. Volcanol. Geotherm. Res. 174: 9–19.
- Shulze, D.J., 2001. Origins of chromian and aluminous spinel macrocrysts from kimberlites in southern Africa. Canadian Mineralogy 39: 361-376.
- Skinner, E., M., W., 1989. Proc. 4th Int. Kimberlite Conf. Kimberlites and related rocks. (eds) J. Ross, A. L. Jaques, J. Ferguson, D. H., Green, S.Y. O'Reilly, R.V. Danchin and A.J.A. Jause, Geol. Soc. Austrl. Spl. Publ. 14 528—544.
- Skinner, E.M.W., Clement, C.R., 1979. Mineralogical classification of southern African kimberlites. In: Boyd, F.R., Meyer, H.O.A. (Eds.), Proceedings of 2nd International Kimberlite Conference, Washington D.C. AGU, pp. 129–139.
- Skinner, E.M.W., Marsh, J.S., 2004. Distinct kimberlite pipe classes with contrasting eruption processes. Lithos 76: 183– 200.

- Skinner, E.M.W., Smith, C.B., Viljoen, K.S. and Clark, T.C. (1992). The petrography, tectonic setting and emplacement ages of kimberlites in the south western border region of the Kaapvaal Craton, Prieska area, South Africa. In: H.O.A. Meyer and O.H. Leonards (Editors), Kimberlites, Related rocks and Mantle Xenoliths. Companhia de Pesquisa de Recursos Minerais, Rio de Janeiro, 80-97.
- Smith CB (1983) Pb, Sr and Nd isotopic evidence for sources of southern African Cretaceous kimberlites. *Nature* 304:51–54.
- Smith CB, Gurney JJ, Skinner EMW, Clement CR, Ebrahim N (1985) Geochemical character of the southern African kimberlites: a new approach based on isotopic constraints. *Trans Geol Soc S Afr* 88:267–280.
- Sobolev, N.V., 1977. Deep-Seated Inclusions in Kimberlites and the Problem of the Composition of the Upper Mantle. (English translation of Russian edition, 1974. Izdatel'stvo Mauka) American Geophysical Union, Washington. 279 pp.
- Sobolev, N.V., Lavrent'ev, YuG., Pokilenko, N.P., Usova, L.V., 1973. Chrome-rich garnets from the kimberlites of Yakutia and their paragenesis. *Contributions to Mineral Petrol* 40: 39–52.
- Souza, J.D., Kosin, M., Melo, R., Oliveira, E.P., Carvalho, M.J., Leite, C.M.M., 2003. Guia de excursão – Geologia do segmento norte do orógeno Itabuna-Salvador-Curaçá. *Rev. Bras. Geoc.* 33 (Suplemento): 27-32.
- Sun, S.S., McDonough, W.F., 1989. Chemical and isotopic systematics of oceanic basalts: implications for mantle composition and processes. In: A.D. Saunders and M.J. Norry (eds.) *Magmatism in the Ocean Basins*. *Geol Soc Spec Publ* 42: 313-345.
- Svisero, D.P., 1995. Distribution and origin of diamonds in Brazil: an overview. *Journal of Geodynamics* Vol. 20, No. 4, pp. 493-514.
- Tappe S., Foley S. F., Stracke A., Romer R. L., Kjarsgaard B. A., Heaman L. M. and Joyce N. (2007) Craton reactivation on the Labrador Sea margins: $^{40}\text{Ar}/^{39}\text{Ar}$ age and Sr–Nd–Hf–Pb isotope constraints from alkaline and carbonatite intrusives. *Earth Planet. Sci. Lett.* 256, 433–454.
- Tappe, S., Foley, S.F., Jenner, G.A., Kjarsgaard, B.A., 2005. Integrating ultramafic lamprophyres into the IUGS classification of igneous rocks: rational and implications. *J Petrol* 46 (9), 1893–1900.

- Tappe, S., Steenfelt, A., Heaman, L.M., Simonetti, A., 2009. The newly discovered Jurassic Tikiusaaq carbonatite-aillikite occurrence, West Greenland, and some remarks on carbonatite-kimberlite relationships. *Lithos* 112: 385-399.
- Tappe, S., Pearson, D.G., Nowell, G., Nielsen, T., Milstead, P., Muehlenbachs., K. 2011. A fresh isotopic look at Greenland kimberlites: Cratonic mantle lithosphere imprint on deep source signal. *Earth Planet. Sci. Lett.* 305, 235-248.
- Tashibana Y, Kaneoka I, Gaffney A, Upton B (2006) Ocean-island basalt-like source of kimberlite magmas from West Greenland revealed by high $^{3}\text{He}/^{4}\text{He}$ ratios. *Geology* (34): 273-276.
- Taylor, W.R., Tompkins, L.A., Haggerty, S.E., 1994. Comparative geochemistry of West African kimberlites: evidence for a micaceous end member of sublithospheric origin. *Geochim. Cosmochim. Acta* 58 (19), 4011 – 4037.
- Thirlwall M. F., Smith T. E., Graham A. M., Theodorou N., Hollings P., Davidson J. P., Arculus R. J., 1994. High Field Strength Element Anomalies in Arc Lavas: Source or Process? *J. Petrology* 35: 819-838.
- Vendemiatto, M.A., Enzweiler, J., 2001. Routine control of accuracy in silicate rock analysis by X-ray fluorescence spectrometry. *Geostandards Newsletter - J Geostand Geoanal* 25: 283-291.
- Vollmer, R., Ogden, P., Schilling, J. G., Kingsley, R. H., Waggoner, D. G., 1984. Nd and Sr isotopes in ultrapotassic volcanic rocks from the Leucite Hills, Wyoming. Contributions to Mineralogy and Petrology 87, 359–368.
- Wilson, Wilson, S.A., 1997. Data compilation for USGS reference material BHVO-2, Hawaiian Basalt, U.S. Geological Survey Open-File Report xxxxx.
- Wyatt, B.A., Baumgartnerb, M., Anckarc, E., Grutter, H., 2004, Compositional classification of “kimberlitic” and “non-kimberlitic” ilmenite. *Lithos* 77, 819– 840.
- Zhang, Z.M., Dong, X., Liou, J.G., Liu, F., Wang, W., Yui, F., 2011. Metasomatism of garnet peridotite from Jiangzhuang, southern Sulu UHP belt: constraints on the interactions between crust and mantle rocks during subduction of continental lithosphere. *J. Metamorphic Geol.*
- Zindler A., Hart S. R., 1986. Chemical geodynamics. *Annual Review of Earth and Planetary Sciences* 14:493-523.

ANEXO 2:

“Zircon xenocrysts U-Pb dating from the Neoproterozoic Brauna Kimberlite Field, São Francisco Craton, Brazil: geodynamic implications for kimberlitic intrusion”

Zircon xenocrysts U-Pb dating from the Neoproterozoic Brauna Kimberlite Field, São Francisco Craton, Brazil: geodynamic implications for kimberlitic intrusion

José Paulo Donatti Filho^a, Elson Paiva Oliveira^a, Neal McNaughton^b

^a *Institute of Geosciences, P.O. Box 6152, University of Campinas – UNICAMP, 13083-970 Campinas, SP, Brazil*

^b *John de Laeter Centre of Mass Spectrometry, School of Applied Physics, Curtin University of Technology, Perth, WA 6845, Australia*

Abstract

The 642 Ma-old Brauna Kimberlite Field is located on the northeastern part of the São Francisco Craton and forms part of a limited Neoproterozoic kimberlitic event of the northern part of South America. In this study, zircons from the volumetric most important kimberlitic pipes Brauna 03, Brauna 07 and Brauna 04, were used as a tool to identify different components of the lithosphere beneath the northeast region of the São Francisco craton, Brazil. Eight representative and distinct drill holes were used for the sampling. Furthermore, the Brauna Kimberlite Field host-rock, the Paleoproterozoic Nordestina granodiorite, was also analysed for zircon U-Pb age dating in order to compare the inherited results and improve the tectonic model. Fifty-four inherited zircon grains from the kimberlites, and sixty zircon phenocrysts from three distinct facies of the granodiorite, were analysed using the Sensitive High Resolution Ion Microprobe (SHRIMP II). The obtained ages were compared with the available precise age data on the regional rocks. The Brauna kimberlites zircon ages spread the time span 2107-2223 Ma. The zircon $^{207}\text{Pb}/^{206}\text{Pb}$ ages indicate eight distinct populations (i.e. 2,107-2,117 Ma; 2127-2138 Ma; 2138-2148 Ma; 2148-2161 Ma; 2161-2168 Ma; 2168-2199 Ma; 2199-2209 Ma and 2209-2223 Ma). The most frequent populations (2150-2160 Ma) are related to the host-rock Nordestina granodiorite that yielded three distinct results: the western is 2132 Ma; the central part is 2139 Ma and the eastern border is 2155 Ma. The second and the third most frequent populations are 2125 Ma and 2200 Ma respectively, may represent others regional granodiorites, however no

rocks were found so far with these ages. The younger 2029-2107 Ma population shows a concordance outside of 100+/-10%, however the data are very reliable on the basis of ages of regional granites and felsic volcanic sequence. The presented data shows that only the Palaeoproterozoic Rio Itapicuru greenstone belt has contributed material to the Brauna Kimberlite Field, whereas Archaean basement was not sampled by the kimberlitic magma either by structural control of the lithosphere, or there is no Archean crust beneath the kimberlitic region, suggesting that perhaps the cratonic root was recycled during the Neoproterozoic time.

Keywords: São Francisco Craton lithosphere, kimberlite emplacement; U-Pb zircon geochronology.

Corresponding author. Tel.: +55 19 97732250

E-mail address: donatti@ige.unicamp.br (José Paulo Donatti Filho)

1. Introduction

Kimberlites are the main host for economic diamond deposits. They are formed at depths greater than 100 km and are transported quickly from the mantle to the Earth's surface. During ascent from their sources, kimberlitic magmas may interact with the mantle and crust and capture fragments of these materials. Kimberlites are thus one of the most reliable probe to samples of the mantle and crust beneath continental areas.

In the northern area of the São Francisco craton, in Brazil (Fig. 1a), several kimberlite bodies make up the Brauna Kimberlite Field (BKF). The kimberlites were intruded into the Nordestina granodiorite batholith, which is one of several granitic bodies of the Paleoproterozoic Rio Itapicuru greenstone belt (Fig. 1b). However, little is known about the lithosphere underlying this region. In order to place constraints on the crustal evolution of the BKF area, we use the kimberlite zircon xenocrysts as time capsules or messengers of the lithosphere beneath the Serrinha Block.

This paper presents new U-Pb SHRIMP data for inherited zircon grains entrained in the volumetric most important kimberlite bodies of the Brauna Kimberlite Field (BKF), represented by the Brauna 03-pipe, Brauna 07-pipe and Brauna 04-pipe. In addition to this data we also

collected samples from the BKF host-rock (i.e Nordestina granodiorite) to comprehend their relationship during the kimberlitic ascent history. The zircon grains are xenocrysts in the Brauna kimberlites because they differ in age from the kimberlite emplacement age of 642 Ma (Donatti Filho et al. 2011 submitted), thus they are derived from the underlying basement. In the Nordestina granodiorite, zircon grains exhibit the crystallization age of the batholith.

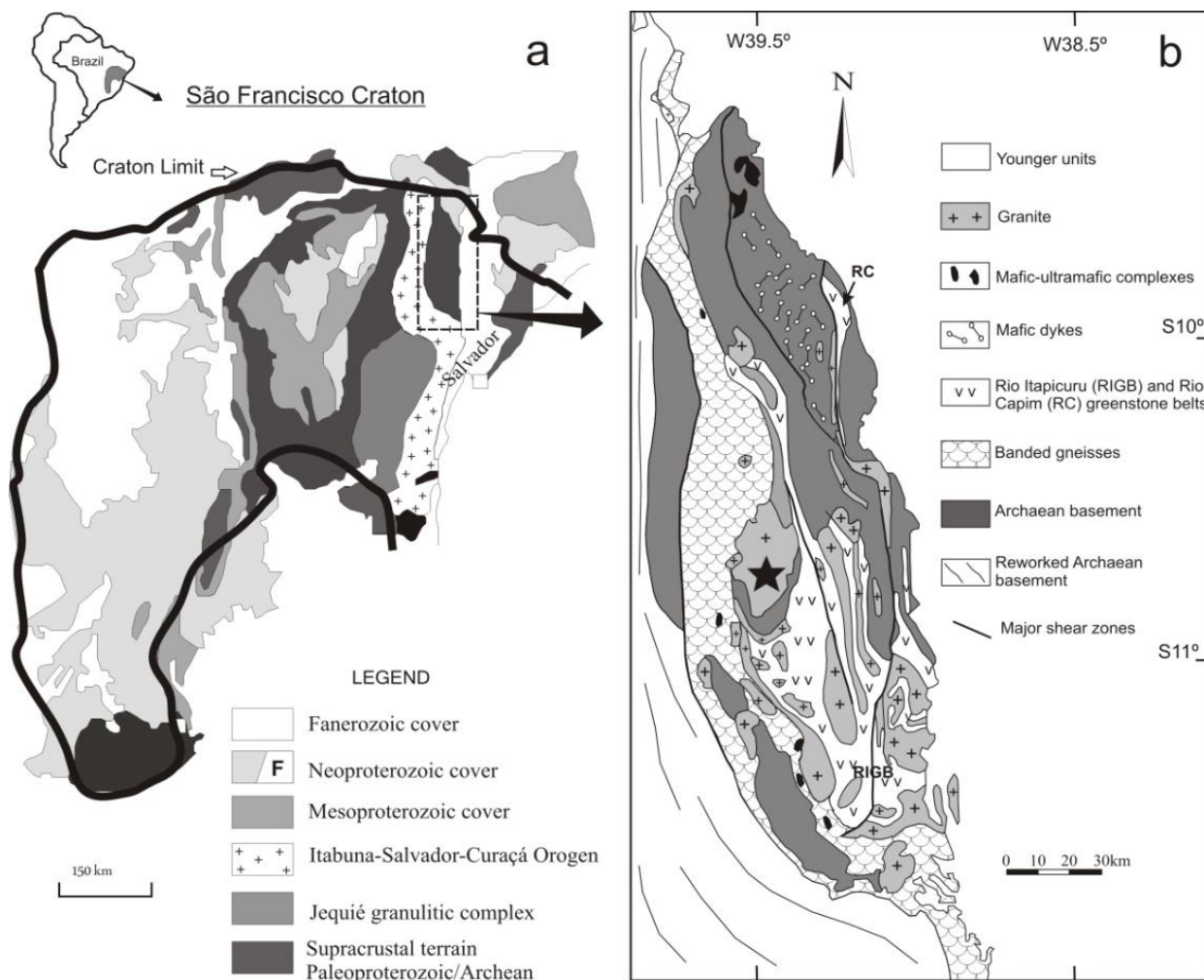


Fig. 1 Geological setting of the Brauna Kimberlite Field. **A)** Geological map of the São Francisco Craton and the location of the Serrinha block (after Souza et al., 2003). **B)** Geological map of the Serrinha Block and the Rio Itapicuru greenstone belt (modified after Oliveira et al., 2011) with location of the Brauna kimberlite field (black star). RIGB: Rio Itapicuru greenstone belt. RC: Rio Capim greenstone belt.

Previous work on kimberlite zircon provenance elsewhere has used zircon xenocrysts collected from drainages (e.g. Batumike et al., 2007). Our study differs from the others on the sampling technique. Here we use fresh kimberlite samples from drill holes for analysis. Our new data improve the geodynamic model for the Brauna Kimberlite Field magmatism and also contribute to place constraints on the age and nature of the cratonic root beneath the Serrinha Block. Furthermore, the data provides new insights for the Rio Itapicuru greenstone belt geodynamic evolution identifying zircon ages that have not been found in the area so far.

2. Geological Settings

The São Francisco craton is composed by numerous Archean blocks bounded by Neoproterozoic orogenic belts and is partially covered by Mesoproterozoic and Neoproterozoic sedimentary basins (Fig. 1a). The Archean basement in the Brauna Kimberlite Field area is represented by migmatites and gneisses of the Serrinha Block. This Block forms a mega-ellipsoidal structure ($> 21,000 \text{ km}^2$) that has remained relatively rigid during Paleoproterozoic collision of at least three blocks to form the Itabuna-Salvador-Curaçá orogen (Barbosa and Sabaté, 2004; Oliveira et al., 2010). The lithostratigraphic succession of the Serrinha Block consists dominantly of: (i) an Archean basement of migmatitic gneisses and calc-alkaline to tonalite-trondhjemite-granodiorite (TTG) plutons, mostly granodiorite with N-S foliation; (ii) volcano-sedimentary sequences of the Rio Itapicuru greenstone belt and the Rio Capim greenstone belt; and, (iii) granitic intrusions (Silva et al. 2001; Mello et al. 2006; Oliveira et al. 2010). Syenites make up a distinct but volumetrically minor rock assemblage in the western part of the Serrinha block; they post-date the major volcanic-plutonic cycles and much of the early deformation (Rios et al. 2007).

The Paleoproterozoic basement in the Brauna Kimberlite Field area is represented by the Rio Itapicuru greenstone belt (RIGB). The RIGB is the volumetric most important volcano-sedimentary sequence in the Serrinha Block, comprising a N-S elongate structure along 100 km long and 60 km wide and 9.5 km thick (Davison et al., 1988). This belt is made up of a basal unit of massive and pillow basalts, andesites, dacites and pyroclastic rocks of the felsic unit, and by clastic and chemical sedimentary rocks of the upper unit, all of them showing greenschist-facies metamorphism (Kishida & Riccio 1980; Davison et al. 1988). Several granitoids intrude the belt,

especially the basalts and the sedimentary rocks, and together they form a regional pattern of domes and keels, like Archaean granite–greenstone terranes (Kishida, 1979; Kishida and Riccio, 1980; Mello, 1999; Mello et al., 2000; Silva et al., 2001; Rios et al., 2009; Oliveira et al., 2010; Costa et al., 2011).

The compilation of available U-Pb age data for the Serrinha Block and Rio Itapicuru greenstone belt is shown in Table 1.

Table 1 U-Pb ages for rock units of the Serrinha Block.

Sample	Tectonic Unit	Age (Ma)	error	(+/-)	Methodology	Reference
Caldeirão Belt Orthogneiss	Basement of Serrinha Block	3152	5		U-Pb zircon	Oliveira et al., 2002
Valente Gneiss	Basement of Serrinha Block	3102	5		U-Pb zircon	Rios et al., 2009
Retirolandia Gneiss	Basement of Serrinha Block	3085	6		U-Pb zircon	Oliveira et al., 2010
Vale do Jacurici G1 Tonalite	Basement of Serrinha Block	2983	6		U-Pb zircon	Oliveira et al., 2010
Eficeas Granodiorite	Rio Itapicuru greenstone belt	2163	5		U-Pb zircon	Rios et al., 2009
Nordestina Granodiorite (west border)	Rio Itapicuru greenstone belt	2155	8		U-Pb zircon	this paper
Nordestina Granodiorite	Rio Itapicuru greenstone belt	2.153	9		Pb-evaporation zircon	Cruz Filho et al., 2003
Trilhado Granodiorite	Rio Itapicuru greenstone belt	2152	6		U-Pb monazite	Mello et al., 2006
Tholeiitic Basalt	Rio Itapicuru greenstone belt	2145	8		U-Pb zircon	Oliveira et al., 2010
Tholeiitic Basalt	Rio Itapicuru greenstone belt	2143	6		U-Pb zircon	Oliveira et al., 2010
Nordestina Granodiorite (center)	Rio Itapicuru greenstone belt	2139	7		U-Pb zircon	this paper
Nordestina Granodiorite (east border)	Rio Itapicuru greenstone belt	2132	11		U-Pb zircon	this paper
Teofilândia Granodiorite	Rio Itapicuru greenstone belt	2130	7		U-Pb zircon	Mello et al., 2006
Barrocas Granodiorite	Rio Itapicuru greenstone belt	2127	5		Pb-evaporation zircon	Chauvet et al. 1997
Morro do Afonso Sienite	Rio Itapicuru greenstone belt	2111	10		U-Pb zircon	Rios et al., 2007
Itareru Tonalite	Rio Itapicuru greenstone belt	2109	5		U-Pb zircon	Carvalho and Oliveira, 2003
Fazenda Gavião Granodiorite	Rio Itapicuru greenstone belt	2106	6		U-Pb zircon	Costa et al., 2011
Dacite	Rio Itapicuru greenstone belt	2081	9		U-Pb zircon	Oliveira et al., 2010
Pedra Vermelha Granite	Rio Itapicuru greenstone belt	2080	8		U-Pb zircon	Rios et al., 2005
Ambrosio Granodiorite	Rio Itapicuru greenstone belt	2080	2		U-Pb xenotime	Mello et al., 2006
Morro do Lopes Granite	Rio Itapicuru greenstone belt	2072	1		U-Pb zircon isotopic dilution	Rios et al., 2000
Brauna Kimberlites	Rio Itapicuru greenstone belt	642	5		U-Pb perovskite	Donatti Filho et al., submitted

The Brauna Kimberlite Field is a confined Neoproterozoic (i.e. 642 Ma U-Pb perovskite) ultrapotassic igneous complex that forms part of the Archean Serrinha block (Donatti Filho et al. submitted). BKF occurs as intrusions into the Paleoproterozoic Nordestina granodiorite batholith (Pisani et al., 2001; Donatti Filho et al., 2008), which is one of the oldest granites of the Paleoproterozoic Rio Itapicuru greenstone belt rock sequence. The BKF is controlled by a NW-SE fracture system hosting three kimberlite pipes and nineteen contemporaneous kimberlitic dykes (0.5 to 5 meters wide) that can be traced over a strike length of 15 kilometers; all of them are diamondiferous (Donatti Filho et al. 2008) (Fig. 2).

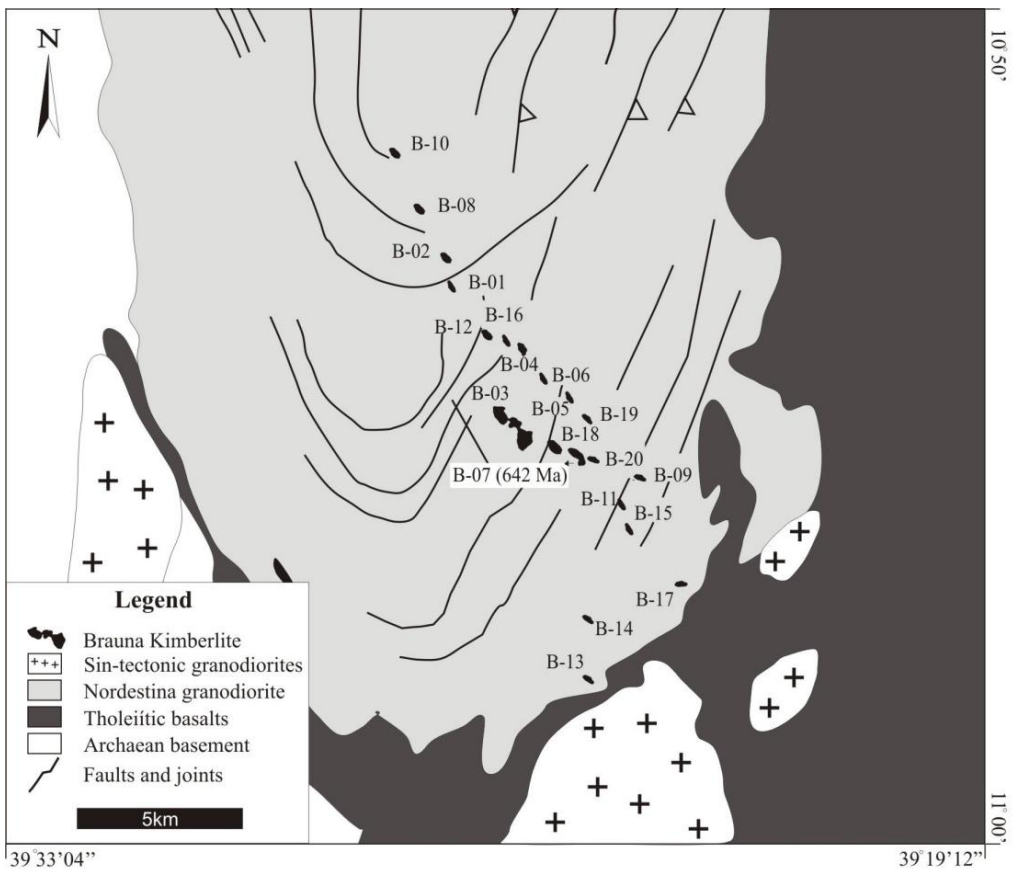


Fig. 2 Geological map and surface exposure of the Brauna Kimberlite Field (Donatti Filho et al. 2011 submitted).

3. Brauna kimberlite zircon sources

Zircon xenocrysts for this study potentially come from crustal and mantle xenoliths captured by the kimberlitic magma during its ascent. Typically, the most abundant population of crustal xenoliths in the BKF is represented by granodiorite xenoliths of the host rock Nordestina granodiorite batholith (Fig. 2). The host rock fragments vary from fresh to kimberlitzed granodiorite that can reach up to 4 meters long (Fig. 2a) or occur as small fragments in the kimberlitic matrix (Fig. 2b) (Donatti Filho et al. 2011 submitted). In the Brauna kimberlites, granodiorite xenoliths occur as large boulders surrounded by serpentine and/or a very fine grained phlogopite-bearing kimberlite crosscut by calcite + pyrite + serpentine veins including polygonal serpentine (serphophite). In the contact zone between the kimberlite and the granodiorite, the kimberlitzation process was very expressive, and the xenoliths exhibits less transported by magma flow, and/or locally more confined.

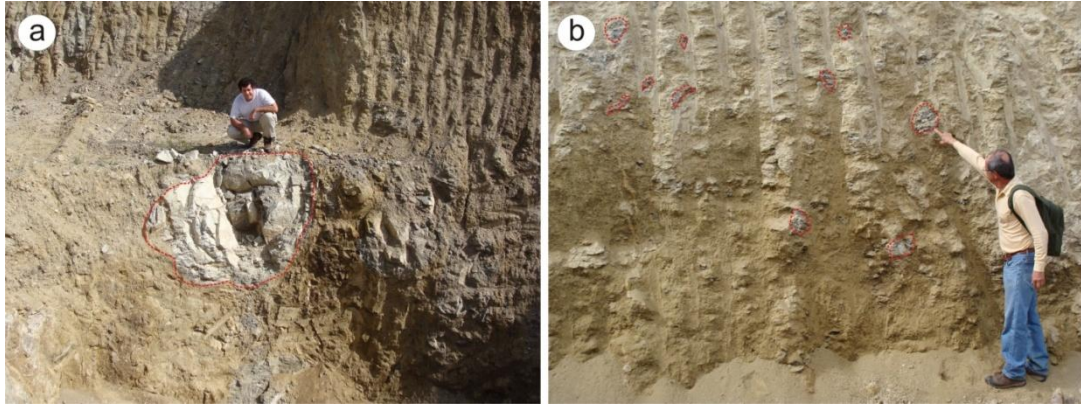


Fig. 2 Field aspect of the Paleoproterozoic Nordestina granodiorite xenoliths in the Brauna 03 kimberlite northern pipe. Size and shape of xenoliths highlighted by red lines.

Different xenoliths from the lower and upper crust were also recognized, such as altered granitic and granulitic rocks, respectively. They are clearly less abundant than the granodiorite host-rock. On the other hand, they are an important zircon xenocryst source for the Brauna kimberlites and also carry important information about the underlying basement. Generally their textures are obliterated by pervasively alteration caused by the metassomatism (Fig. 3a). Other important xenolith occurrences are rocks from the Rio Itapicuru greenstone belt sequence such as basalt, andesite, gneisses, granites, chemical and clastic sediments, however they are rarely preserved.

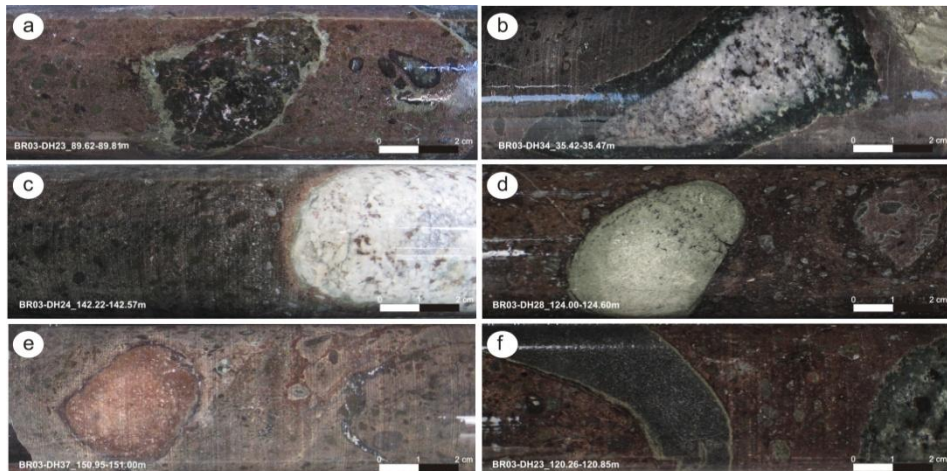


Fig. 3 Crustal xenoliths collected from drill holes of the Brauna Kimberlite Field. **a.** Kimberlitzed granodiorite xenolith; **b.** preserved Nordestina granodiorite xenolith with serpentine halo; **c.** altered gneiss xenolith with phlogopite halo; **d.** altered sediment xenolith (?) with phlogopite halo and surrounded by serpentinized olivine macrocrysts; **e.** altered granite xenolith; **f.** preserved basalt xenolith.

Mantle xenoliths in the Brauna kimberlites are relatively rare comparing with the crustal xenoliths. Mantle xenoliths are rounded to subangular and small in size, varying from 0.2 to 6 cm in some cases. In general, they are highly altered and are represented by garnet-bearing serpentinised peridotites (Fig. 4). Primary textures are obliterated by the kimberlitic magma metassomatism. The more refractory mantle xenoliths are harzburgitic rocks, and the less refractory are represented by garnet-free and garnet-bearing lherzolitic rocks.

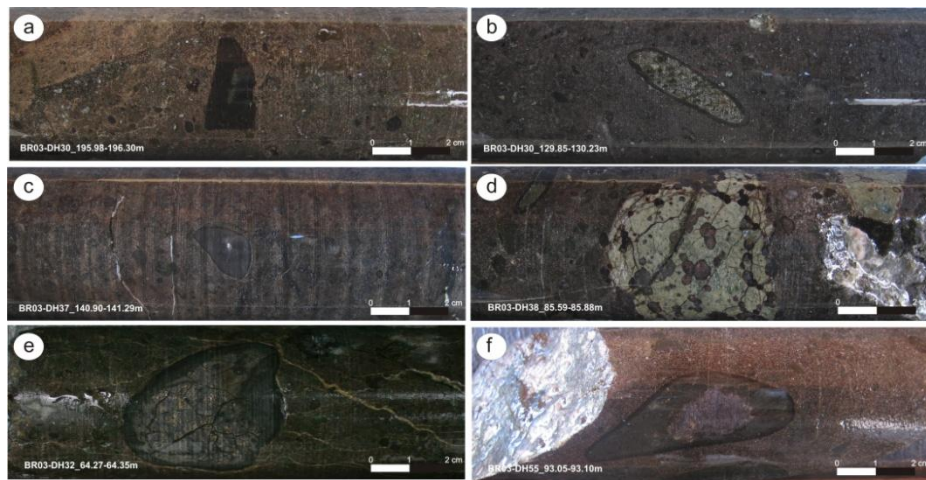


Fig. 4 Mantle xenolith examples collected from the Brauna Kimberlite Field drill holes. **a.** altered angular peridotite xenolith; **b.** serpentinised garnet harzburgite xenolith; **c.** obliterated peridotite xenolith; **d.** altered garnet lherzolite xenolith; **e.** obliterated garnet harzburgite xenolith with very fine grained phlogopite border; **f.** serpentinised peridotite xenolith; **g.** pervasively altered garnet peridotite xenolith; **h.** altered harzburgite xenolith.

4. U-Pb SHRIMP zircon dating

Mineral separation was carried out in the University of Campinas using conventional magnetic and density techniques to concentrate the non-magnetic, heavy fractions. From the volumetric most important kimberlites (i.e. Brauna 03 and 07 pipes; and Brauna 08 dyke) all zircon grains were extracted by hand-picking under a binocular microscope, whereas from samples of the Nordestina batolith only representative zircon populations were selected. After separation the zircon grains were mounted with epoxy resin along with chips of BR266 zircon standard ($U=550$ ppm; $^{206}\text{Pb} / ^{238}\text{U}=0.0914$). External form and internal structure were imaged using combined cathodoluminescence/BSE techniques in a Jeol 6400 scanning electron

microscope at Curtin University of Technology - Australia, and at University of Campinas – Brazil.

Zircon analyses were carried out on the SHRIMP II at Curtin University of Technology, Australia, based on the operation procedures described by Compston et al. (1984) and operation conditions described by Smith et al. (1998). Common Pb corrections were made assuming Broken Hill common-Pb compositions for all sample analyses. The data were reduced using the SQUID software (Ludwig, 1999a) and ISOPLOT (Ludwig, 1999b).

The ages reported here are for $^{207}\text{Pb}/^{206}\text{Pb}$ with between 95% and 105% concordance.

4.1. Nordestina Granodiorite zircon geochronology

Precise age data for the Nordestina granodiorite i.e. host rock of the Brauna Kimberlite Field are not available. Cruz Filho et al. (2003) presented a Pb-Pb evaporation age of 2.153 Ma for zircon grains of the Nordestina batholith. For this study we selected three distinct samples for U-Pb geochronology, one from the western deformed border (Nord1-W), one from the non-deformed eastern border (FM-170), and another from the non-deformed, central area of the granodiorite batholith (CGF-12). The results are shown in the Table 2.

The western border granodiorite sample Nord1-W contains euhedral zircon grains with oscillatory zoning, or diffuse zoning. This sample also contains zircon grains exhibiting generally high U-contents, which for zircons of this age resulted in significant metamictization, Pb-loss and discordance. Using a cutoff for concordance of 100+/-7% as the best data, seven analyses have an MSWD of 1.19 which indicates slightly more scatter than expected for a population with a single age. For these seven analyses, one (#9-1) was significantly younger than the others and omitting this analysis yielded an acceptable MSWD of 0.30 and an age of 2155 ± 8 Ma ($n = 6$), which is considered to be the primary age of the zircons (Fig. 5). It is noted that six other discordant analyses are within error of this age, and one slightly discordant analysis (#2-1) is significantly older and is interpreted as a xenocryst.

Table 2: SHRIMP U-Pb zircon results for the Nordestina granodiorite (BKF kimberlites host rock).

Mount 0929A=Nord1-W (granodiorite western border)													
Grain-spot	ppm U	ppm Th	232Th /238U	% comm	207Pb /206Pb	207Pb /235U	206Pb /238U	207Pb /206Pb	Age (Ma)	+/-s	Conc		
1-1#	436	137	0.33	0.19	0.1336	0.0008	6.69	0.06	0.363	0.003	2146	10	93
1-Feb	1316	690	0.54	0.4	0.1375	0.0005	8.65	0.06	0.456	0.003	2196	6	110
1-Mar	325	126	0.4	0.71	0.1327	0.0011	6.16	0.07	0.336	0.003	2134	15	88
4-1#	287	77	0.28	0.05	0.1341	0.0007	7.34	0.07	0.397	0.003	2152	9	100
1-May	1264	396	0.32	0.47	0.128	0.0006	5.04	0.04	0.285	0.002	2070	8	78
6-1#	240	49	0.21	0.08	0.1345	0.0008	7.51	0.08	0.405	0.004	2158	10	102
1-Aug	647	297	0.47	0.43	0.1187	0.0008	3.7	0.04	0.226	0.002	1937	12	68
9-1#	403	84	0.22	0.45	0.1318	0.001	6.59	0.07	0.363	0.003	2122	13	94
15-1	935	318	0.35	0.18	0.1055	0.0006	2.33	0.02	0.16	0.001	1724	11	55
16-1	846	513	0.63	0.18	0.1063	0.0007	2.34	0.03	0.16	0.001	1737	12	55
17-1	361	164	0.47	0.12	0.1262	0.0008	4.76	0.06	0.273	0.003	2046	11	76
19-1#	436	187	0.44	0.1	0.1344	0.0007	7.07	0.08	0.381	0.004	2157	9	97
20-1	984	492	0.52	0.33	0.1043	0.0007	2.2	0.03	0.153	0.001	1702	13	54
21-1#	508	124	0.25	0.49	0.1348	0.0008	7	0.08	0.377	0.004	2161	10	95
22-1	584	131	0.23	0.84	0.1284	0.0012	3.73	0.05	0.211	0.002	2076	17	59
23-1	340	168	0.51	0.83	0.1333	0.0013	5.34	0.07	0.29	0.003	2143	17	77
24-1	491	150	0.31	0.99	0.1265	0.0013	4.38	0.06	0.251	0.002	2050	18	70
25-1#	355	52	0.15	0.19	0.1342	0.0012	6.83	0.09	0.369	0.004	2154	16	94
28-1	241	61	0.26	0.32	0.1361	0.0012	6.51	0.1	0.347	0.004	2178	16	88
30-1	372	68	0.19	0.66	0.1349	0.0013	5.41	0.08	0.291	0.003	2163	17	76
31-1	275	84	0.32	0.21	0.1316	0.0012	5.81	0.09	0.32	0.004	2120	16	84
33-1	276	71	0.27	0.22	0.1341	0.0011	6.26	0.09	0.339	0.004	2152	14	87
34-1	344	49	0.15	0.13	0.1355	0.0011	6.3	0.09	0.337	0.004	2170	14	86
Mount 0929B=CGF-12 (granodiorite central part)													
Grain-spot	ppm U	ppm Th	232Th /238U	% comm	207Pb /206Pb	207Pb /235U	206Pb /238U	207Pb /206Pb	Age (Ma)	+/-s	Conc		
2-1#	265	69	0.27	0.41	0.1311	0.001	6.94	0.1	0.384	0.004	2113	14	99
3-1#	240	49	0.21	0.35	0.1325	0.001	7.65	0.11	0.419	0.005	2131	13	106
4-1#	233	45	0.2	0.25	0.1325	0.001	7.55	0.11	0.413	0.005	2132	13	105
1-6*	267	69	0.27	1.67	0.1319	0.0018	7.84	0.14	0.431	0.005	2124	24	109
1-8*	377	46	0.13	0.16	0.1359	0.0007	9.24	0.11	0.493	0.006	2175	8	119
1-10#	323	64	0.2	0.21	0.1326	0.0009	8.02	0.1	0.439	0.005	2132	12	110
1-11#	216	50	0.24	0.26	0.1328	0.001	7.9	0.11	0.431	0.005	2136	13	108
1-12#	339	59	0.18	0.63	0.133	0.0011	7.17	0.1	0.391	0.004	2138	15	99
1-13#	299	60	0.21	0.48	0.1332	0.0009	7.49	0.1	0.408	0.004	2141	12	103
1-14*	578	178	0.32	0.42	0.1356	0.0007	8.58	0.09	0.459	0.004	2172	9	112
1-17#	366	75	0.21	0.15	0.1335	0.0007	8.12	0.09	0.441	0.005	2144	9	110
1-18#	371	53	0.15	0.06	0.1339	0.0006	8.07	0.09	0.437	0.004	2150	8	109
1-19#	561	108	0.2	0.28	0.1339	0.0006	8.07	0.09	0.437	0.004	2150	8	109
1-20#	221	50	0.23	0.34	0.1313	0.0011	7.6	0.11	0.42	0.005	2116	14	107
1-21*	225	44	0.2	0.1	0.1327	0.0008	8.39	0.11	0.459	0.006	2134	11	114
Mount 0929C=FM-170 (granodiorite eastern border)													
Grain-spot	ppm U	ppm Th	232Th /238U	% comm	207Pb /206Pb	207Pb /235U	206Pb /238U	207Pb /206Pb	Age (Ma)	+/-s	Conc		
1-1#	276	70	0.26	0.51	0.1331	0.0011	7.06	0.1	0.385	0.004	2139	14	98
1-2#	319	84	0.27	0.18	0.1312	0.0007	7.48	0.09	0.413	0.004	2114	10	105
1-3#	114	30	0.28	0.42	0.1336	0.0016	7.43	0.14	0.403	0.006	2146	21	102
4-1#	124	44	0.36	0.31	0.1326	0.0014	7.92	0.14	0.434	0.006	2132	18	109
7-1#	243	62	0.26	0.06	0.1352	0.0008	7.94	0.11	0.426	0.005	2166	11	106
8-1*	261	100	0.39	0.58	0.1264	0.0012	5.31	0.08	0.305	0.003	2049	16	84
9-1*	226	125	0.57	0.41	0.1359	0.0012	8.57	0.12	0.457	0.005	2175	15	112
11-1#	169	44	0.27	0.1	0.1337	0.0009	8.1	0.12	0.439	0.005	2147	12	109
12-1#	141	32	0.23	0.43	0.1327	0.0017	6.74	0.13	0.368	0.005	2135	23	95
15-1	258	104	0.42	0.07	0.1339	0.0008	8.21	0.11	0.445	0.005	2150	10	110
18-1	246	44	0.18	0.2	0.1317	0.001	7.74	0.11	0.426	0.005	2121	13	108
19-1	166	36	0.23	0.44	0.1304	0.0012	7.41	0.12	0.412	0.006	2103	17	106
20-1#	390	127	0.34	0.19	0.1283	0.0007	6.05	0.07	0.342	0.003	2075	10	91
21-1	337	76	0.23	0.27	0.1326	0.0008	6.55	0.08	0.358	0.004	2132	11	93
22-1*	118	18	0.16	0.59	0.1324	0.002	6.2	0.13	0.34	0.005	2130	26	89

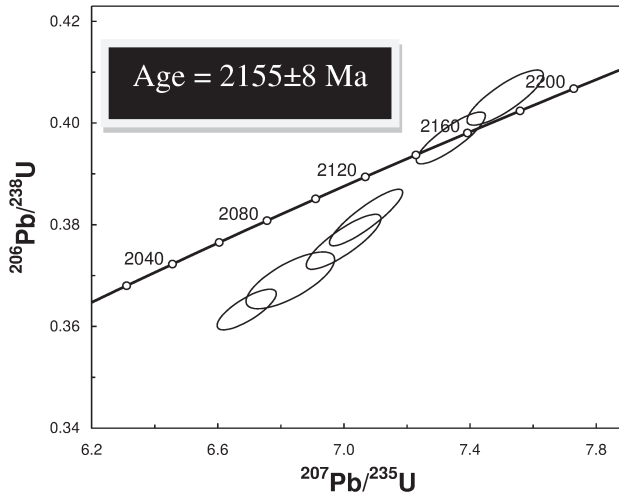


Fig. 5: Concordia diagram for sample Nord1-W from the western border of the Nordestina granodiorite. All data $100\pm7\%$ concordant; error ellipses are $\pm 1 \sigma$.

The sample from the central area of the granodiorite batholith (CGF-12) contains zircon grains with rounded to euhedral morphology and oscillatory internal structure. Some zircon grains exhibit moderate U-contents, which for zircons of this age resulted in some metamictization, Pb-loss and discordance. Omitting one analysis with high common Pb and using a cutoff for concordance of $100\pm10\%$ as the best data, 11 of 15 analyses gave an age of 2139 ± 7 Ma (MSWD = 1.12), which is considered to be the primary age of the zircons (Fig. 6).

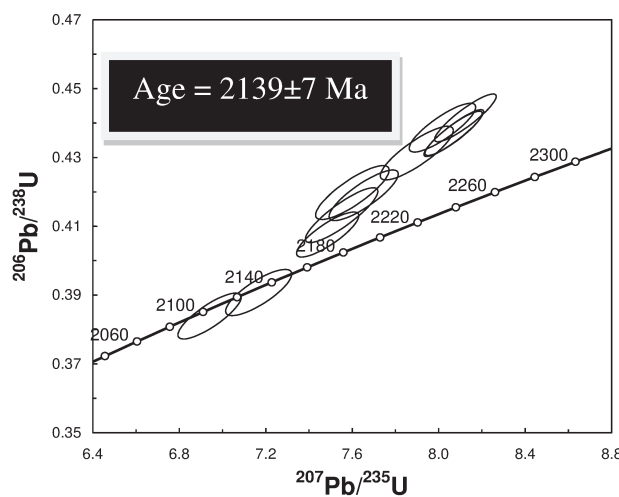


Fig. 6: Concordia diagram for granodiorite sample CGF-12 from the central area of the Nordestina batolith. All data $100\pm10\%$ concordant; error ellipses are $\pm 1 \sigma$.

Granodiorite sample FM-170 from the eastern border of the granodiorite batholith contains zircon grains with rounded to euhedral morphology and oscillatory internal. Omitting three analyses using a cutoff for concordance of $100\pm10\%$ as the best data, the remaining 12 analyses yielded an MSWD of 5.0, indicating outlier analyses. Analysis #7-1 is older than the main population and interpreted as a xenocryst, and #20-1 is younger, suggestive of Pb-loss. Omitting these two, 10 analyses gave an age of 2132 ± 11 Ma (MSWD = 1.4). Omitting the most discrepant analysis (#19-1) reduces the MSWD slightly to 1.14 but does not significantly change the age, so 2132 ± 11 Ma is considered to be the primary age of the zircon grains (Fig. 7).

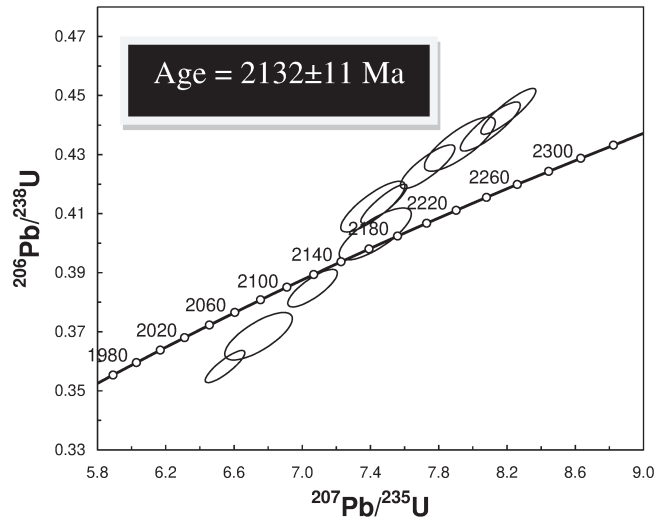


Fig. 7: Concordia diagram for granodiorite sample FM-170 from the eastern border of the Nordestina batholith. All data $100\pm10\%$ concordant; error ellipses are $\pm1\sigma$.

4.2. Brauna Kimberlite Field zircon geochronology

Brauna Kimberlite Field has an emplacement age of 642 Ma (U-Pb perovskite, Donatti Filho et al., submitted) and was not affected by any significant deformation or metamorphism. Therefore, we considered all zircon grains older than the perovskite age as xenocrysts in the Brauna kimberlites. The kimberlite sample used contains rounded to euhedral zircon grains with internal structures varying from oscillatory, laminated and no zoning. Zircon grains in the analysed sample had generally medium to high U-contents, which for zircons of this age resulted in significant metamictization, Pb-loss and discordance. It is noteworthy that most zircons with

>400 ppm U are more than 10% discordant, reflecting enhanced metamictization and Pb-loss. Using a cutoff for concordance of $100\pm10\%$ and a common Pb correction of <1.0% to identify the best data, 33 of 54 analyses show a spread of ages between ca. 2.22 and 2.12 Ga. The age data is shown in Table 3. The zircon $^{207}\text{Pb}/^{206}\text{Pb}$ ages indicate eight distinct populations (i.e. 2107-2117 Ma; 2127-2138 Ma; 2138-2148 Ma; 2148-2,161 Ma; 2161-2168 Ma; 2168-2199 Ma; 2199-2209 Ma and 2209-2223 Ma) (Fig. 8). The results are shown in the Table 3.

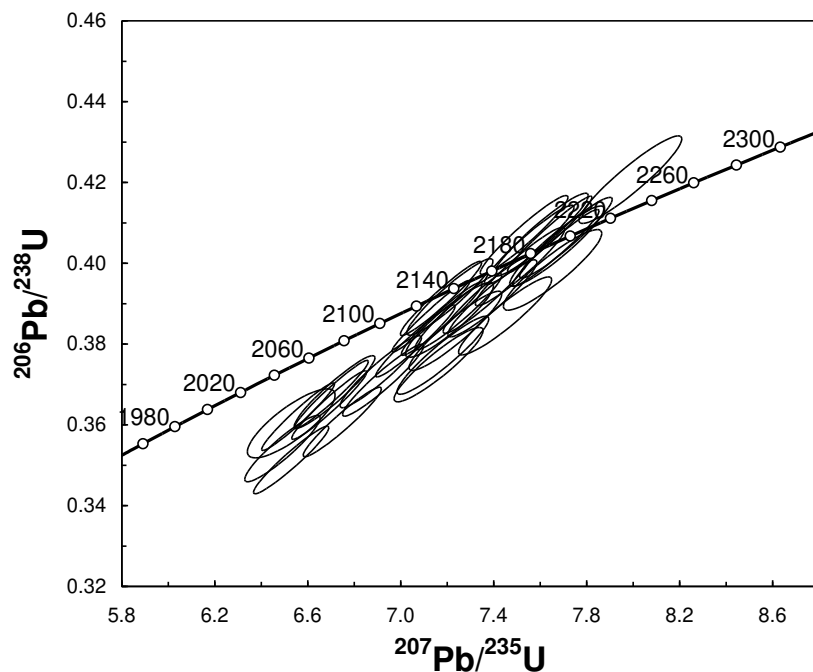


Fig. 8: Concordia diagram for zircon xenocrysts from the Brauna kimberlite sample (Brauna 0940A). All data $100\pm10\%$ concordant and common Pb correction <1.0%; error ellipses are $\pm 1 \sigma$.

Table 3: SHRIMP U-Pb zircon results for the inherited zircons from the Brauna Kimberlite Field.

Mount 0940A: ranked by 207Pb/206Pb age.													
Grain-spot	ppm	ppm	232Th	%	207Pb	207Pb	206Pb	207Pb	Age (Ma)	+/‐1s	Conc		
	U	Th	/238U	comm	/206Pb	/235U	/238U	/206Pb					
33-1	156	41	0.27	-0.27	0.1396	0.0009	7.45	0.13	0.387	0.006	2223	11	95
20-1	163	48	0.31	-0.28	0.1393	0.0011	7.65	0.14	0.398	0.007	2219	13	97
54-1	181	53	0.31	0.46	0.1386	0.001	7.16	0.13	0.375	0.006	2209	12	93
53-1	129	31	0.25	-0.08	0.1381	0.0009	7.18	0.13	0.377	0.006	2203	11	94
27-1	139	37	0.28	-0.2	0.1377	0.0009	7.99	0.15	0.421	0.007	2199	12	103
40-1	302	140	0.48	-0.09	0.1377	0.0006	7.67	0.12	0.404	0.006	2198	7	99
47-1	177	67	0.39	-0.25	0.1376	0.0009	7.67	0.13	0.404	0.007	2198	11	100
4-1	216	71	0.34	-0.06	0.1376	0.0007	7.71	0.13	0.406	0.007	2198	9	100
30-1	195	54	0.28	-0.08	0.137	0.0008	7.39	0.13	0.391	0.006	2190	10	97
32-1	129	31	0.25	0.13	0.1369	0.0009	7.24	0.13	0.383	0.006	2189	12	96
44-1	199	92	0.48	-0.14	0.1365	0.0007	7.51	0.13	0.399	0.006	2183	9	99
7-1#	225	60	0.27	-0.03	0.1363	0.0007	7.37	0.12	0.392	0.006	2181	9	98
13-1	412	142	0.36	-0.09	0.1361	0.0005	7.64	0.12	0.407	0.006	2178	7	101
37-1#	353	108	0.32	8.23	0.136	0.0119	6.72	0.6	0.358	0.007	2177	152	91
14-1#	310	111	0.37	1.97	0.1357	0.0024	6.76	0.16	0.361	0.006	2173	30	92
23-1	244	71	0.3	-0.02	0.1357	0.0007	6.75	0.11	0.361	0.006	2173	8	91
50-1#	193	52	0.28	3.94	0.1357	0.0075	7.22	0.42	0.386	0.007	2173	96	97
25-1	252	68	0.28	-0.1	0.1355	0.001	7.21	0.12	0.386	0.006	2170	12	97
52-1	147	31	0.22	-0.03	0.1355	0.0008	7.6	0.13	0.407	0.007	2170	10	101
26-1	211	79	0.39	-0.06	0.1355	0.0007	7.25	0.12	0.388	0.006	2170	9	97
21-1	201	74	0.38	0.1	0.1354	0.0007	7.55	0.13	0.405	0.006	2169	9	101
16-1	255	83	0.34	0.12	0.1353	0.0007	6.92	0.12	0.371	0.006	2168	9	94
17-1	281	72	0.27	-0.01	0.1348	0.0006	6.53	0.11	0.351	0.006	2161	8	90
34-1	318	139	0.45	-0.12	0.1348	0.0006	7.18	0.12	0.386	0.006	2161	8	97
2-1	356	111	0.32	0.09	0.1345	0.0006	7.06	0.11	0.381	0.006	2158	7	96
.11-1	266	90	0.35	0.33	0.1344	0.0007	6.91	0.12	0.373	0.006	2156	10	95
42-1	221	59	0.27	0.04	0.1342	0.0007	7.53	0.12	0.407	0.006	2154	8	102
.8-1	487	176	0.37	0.06	0.1337	0.0005	7.13	0.11	0.387	0.006	2147	6	98
36-1	231	111	0.5	0.3	0.1335	0.0008	7.21	0.12	0.392	0.006	2145	10	99
15-1	358	143	0.41	-0.04	0.133	0.0006	6.69	0.11	0.365	0.006	2138	7	94
45-1	298	86	0.3	0.02	0.133	0.0006	7.17	0.12	0.391	0.006	2137	8	100
41-1	352	111	0.33	0.6	0.1329	0.0008	6.49	0.11	0.354	0.005	2137	11	91
.1-1	223	55	0.25	0.2	0.1323	0.0008	6.72	0.11	0.368	0.006	2129	10	95
.6-1	450	176	0.4	-0.12	0.1323	0.0005	6.7	0.11	0.368	0.006	2128	7	95
12-1*	339	91	0.28	0.51	0.132	0.0009	5.36	0.09	0.295	0.005	2125	12	78
51-1	264	79	0.31	0.69	0.1314	0.0014	6.53	0.12	0.36	0.006	2117	19	94
48-1	373	68	0.19	0.08	0.1314	0.0005	6.56	0.1	0.362	0.006	2117	7	94
39-1*	367	118	0.33	0.1	0.1306	0.0006	6.09	0.1	0.338	0.005	2107	8	89
18-1*	365	118	0.33	0.11	0.1304	0.0006	6.1	0.1	0.339	0.005	2104	8	89
.3-1*	406	194	0.49	0.68	0.1302	0.0008	5.94	0.1	0.331	0.005	2101	11	88
43-1*	459	196	0.44	0.56	0.1264	0.0007	5.53	0.09	0.317	0.005	2049	10	87
46-1*	464	212	0.47	0.3	0.125	0.0008	5.21	0.09	0.302	0.005	2029	11	84
22-1*	671	169	0.26	0.13	0.1247	0.0005	3.58	0.06	0.208	0.003	2025	7	60
49-1*	571	284	0.51	-0.04	0.1236	0.0005	4.59	0.07	0.27	0.004	2008	7	77
10-1*	589	312	0.55	0.92	0.1226	0.0012	4.63	0.08	0.274	0.004	1994	18	78
35-1*	620	186	0.31	0.55	0.1207	0.0007	4.01	0.06	0.241	0.004	1966	11	71
9-1*	625	264	0.44	0.28	0.1206	0.0006	4.44	0.07	0.267	0.004	1965	9	78
24-1#*	490	222	0.47	1.02	0.1206	0.0011	4.61	0.08	0.278	0.004	1964	16	80
19-1*	493	191	0.4	0.31	0.1192	0.0006	4.43	0.07	0.27	0.004	1944	9	79
28-1*	282	919	3.36	0.09	0.1126	0.0007	3.4	0.06	0.219	0.003	1842	11	69
38-1*	835	274	0.34	0.25	0.1095	0.0005	3.02	0.05	0.2	0.003	1791	8	66
29-1*	837	389	0.48	0.78	0.1094	0.0008	3.15	0.05	0.209	0.003	1789	13	68
5-1#*	737	501	0.7	1.71	0.104	0.0017	2.67	0.06	0.186	0.003	1698	29	65
31-1*	1218	771	0.65	0.19	0.104	0.0005	2.3	0.04	0.161	0.002	1697	9	57

5. Discussion

In kimberlites, zircon phenocrysts and macrocrysts frequently occur as a minor constituent in the mineral phase (e.g. some South African Group I kimberlites, Belousova et al., 2001; Belousova et al., 2002). On the other hand, zircon xenocrysts are far to be rare because kimberlitic magmatism occurs crossing the Earth's crust carrying up pieces of the mantle and crust.

Figure 9 shows the histogram for the analysed zircon xenocrysts sampled by the Brauna kimberlites. Comparing the regional age data (Tab. 1) with the analysed Brauna kimberlite zircon xenocrysts, the most frequent population varies from 2150 Ma to 2170 Ma, and it interpreted to be related to the Palaeoproterozoic Nordestina granodiorite batholith, that exhibits three distinct crystallization ages (i.e. 2155 Ma, 2139 and 2132 Ma). The second and the third most frequent populations are around 2125 Ma and 2200 Ma respectively, and we suggest that they may represent other regional source rocks in the Rio Itapicuru greenstone belt. The Barrocas granodiorite was dated at 2127+5 Ma and as is the closest source for zircon grains of the 2125 Ma age population. However no rocks with ages older than 2163 Ma have been found so far in the Rio Itapicuru greenstone belt and as such sources for the 2200 Ma zircon xenocryst population remain to be discovered. The younger 2029 Ma to 2107 Ma population shows a concordance outside of $100\pm10\%$, however the data are very reliable on the basis of ages of regional granites and felsic volcanic sequence (see Table 1), thus we assume that these data must be used.

Previous work on zircon provenance in metasedimentary rocks of the Rio Itapicuru greenstone belt sequence has recognized the presence of Paleoproterozoic xenocystic zircon grains only (Grisolia and Oliveira, 2011 in prep.). The absence of Archean zircon grains in the sedimentary rocks led these authors to conclude that at the timing of sediment deposition the Archean basement was not available for erosion, or more likely Archean and Paleoproterozoic sources were distinct terranes geographically far from each other (Fig. 9). They also provide evidence of a rock sequence exhibiting ages older than 2180 Ma that was not found in the area. Notably, the zircon xenocrysts sampled by the BKF magma also exhibits similar age intervals, where the oldest zircons yielded an age of 2230 Ma (Fig. 9).

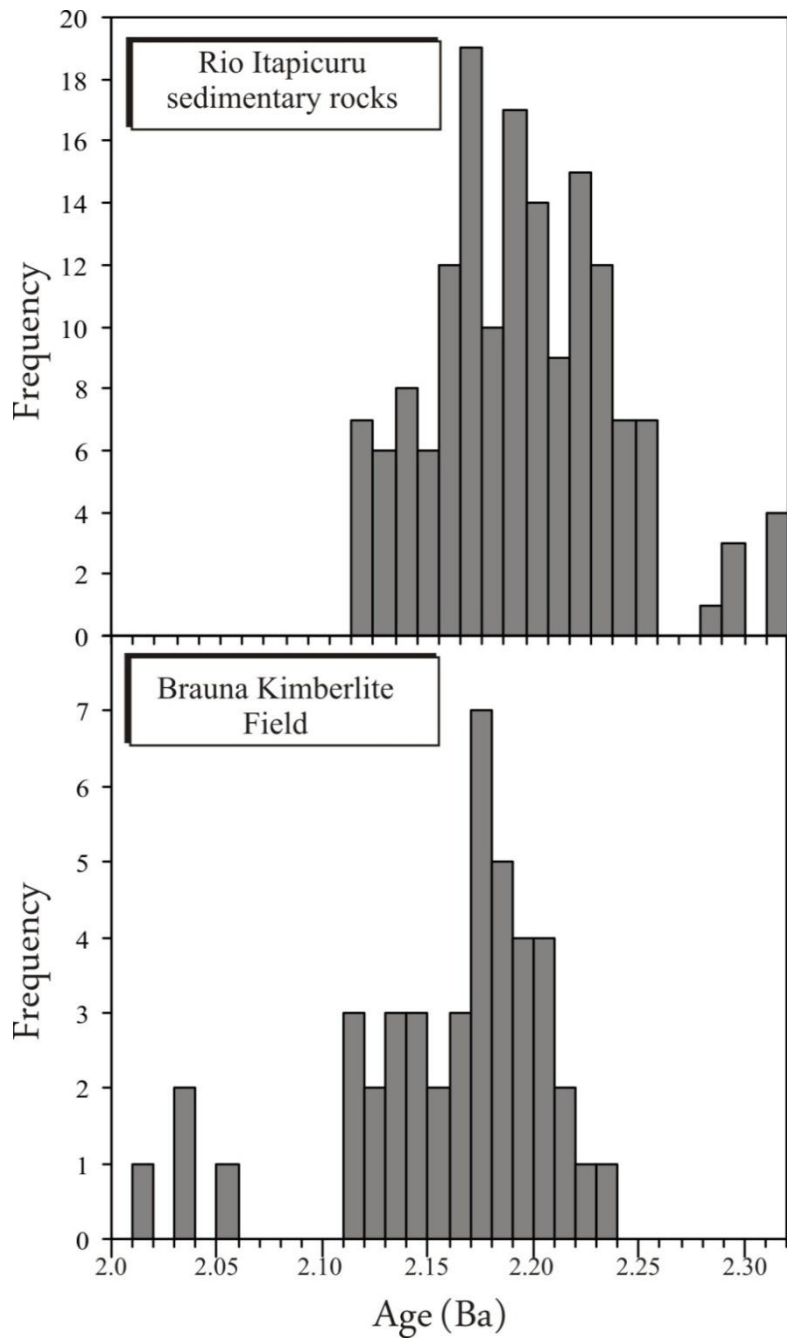


Fig. 9: Variation histogram using frequency versus U-Pb ages (Ba) for the zircon xenocrysts from the Brauna Kimberlite Field (this study) and from the sedimentary rocks from the Rio Itapicuru greenstone belt (Grisólia and Oliveira 2011, *in prep.*). Note the younger zircon population between 2010 Ma and 2060 Ma from Brauna Kimberlite field and the oldest population between 2240 Ma and 2302 Ma from sedimentary rocks of the Rio Itapicuru greenstone belt. These population ages were not found in the area so far.

In order to improve our understanding about the crustal evolution of the Serrinha Block and the tectonic model for the Brauna Kimberlite Field intrusion, we propose a simplistic tectonic model for the lithosphere beneath the Brauna Kimberlite Field (Fig. 5). The model is based on zircon analysis from this study and supported by previous work presented by Donatti Filho et al. (2011, submitted). Our new data indicate that the Paleoproterozoic basement is likely to be the

dominant rock unit beneath Brauna kimberlites and that either the older Archean crust is not present or it has not been sampled by the kimberlite magma.

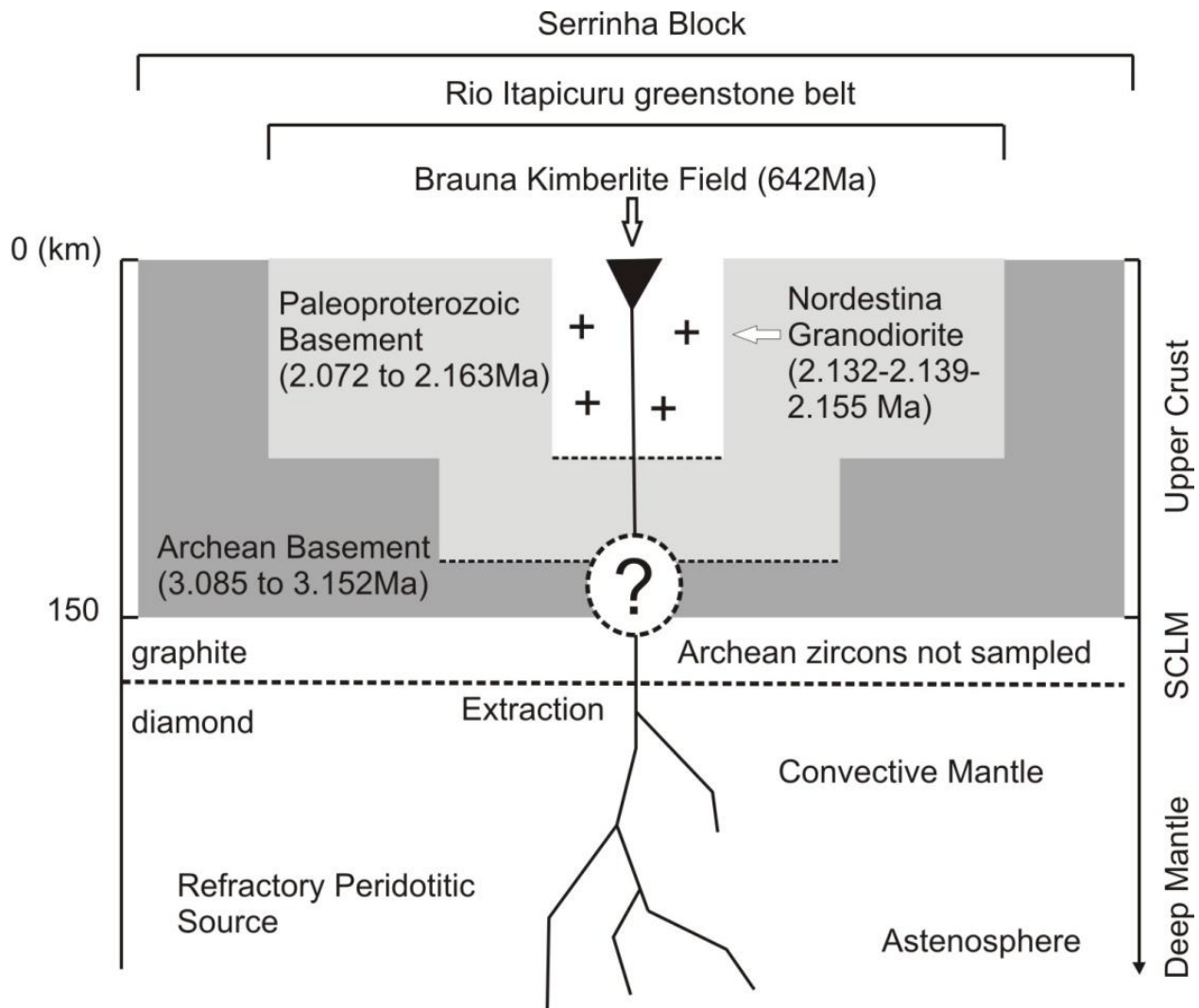


Fig. 5: Proposed tectonic model for the lithosphere beneath Brauna Kimberlite Field based on inherited zircon xenocrysts.

Acknowledgements

The authors wish to thank Fundação de Amparo à Pesquisa do Estado de São Paulo - FAPESP (grants No. 07/537989) for research grant to JPDF and the Brazilian research Council - Conselho Nacional de Desenvolvimento Científico e Tecnológico - CNPq (grants No.

301025/2005-3, 78989/04-0) for grants to EPO. We are grateful to Vaaldiam Resourced Ltd. for fieldwork support, and access to the kimberlite samples for analytical analysis.

References

- Barbosa, J.S.F. & Sabaté P. 2004. Archean and Paleoproterozoic crust of the São Francisco Craton, Bahia, Brazil: geodynamic features. *Precambrian Res.*, 133:1-27.
- Batumike, J.M., O'Reilly, S.Y., Griffin, W.L., Belousova, B.L. 2007. U-Pb and Hf-isotope analyses of zircon from the Kundelungu Kimberlites, D.R. Congo: Implications for crustal evolution. *Prec. Res.* (156): 195–225.
- Belousova, E.A., Griffin, W.L., Shee, S.R., Jackson, S.E., O'Reilly, S.Y., 2001. Two age populations of zircons from the Timber Creek kimberlites, Northern Territory, Australia, as determined by laser ablation-ICPMS analysis. *Aust. J. Earth Sci.* 48, 757– 766.
- Belousova, E.A., Walters, S., Griffin, W.L., O'Reilly, S.Y., Fisher, N.I., 2002. Zircon trace-element compositions as indicators of source rock type. *Contrib. Miner. Petrol.* 143, 602– 622.
- Carvalho, M.J., Oliveira EP (2003) Geologia do Tonalito Itareru, bloco Serrinha, Bahia: uma intrusão sin-tectônica do início da colisão continental no segmento norte do Orógeno Itabuna-Salvador-Curaçá. *Revista Brasileira de Geociências* 33 (suplemento): 55-68.
- Chauvet, A., Alves da Silva, F.C., Faure, M., Guerrot, C. 1997 Structural evolution of the paleoproterozoic Rio Itapicuru Greenstone Belt (Bahia, Brazil): the role of synkinematic plutons in the regional tectonics. *Prec. Res.* (84): 139-162.
- Compston, W., Williams, I.S., Meyer, C. 1984. U-Pb geochronology of zircons from lunar breccia 73217 using a sensitive hight massresolution ion microprobe. *Journal of Geoph. Res.* (89): 252-534.
- Costa, F.G., Oliveira, E.P., McNaughton N.J. 2011. The Fazenda Gavião Granodiorite and Associated Potassic plutons as evidence for Palaeoproterozoic Arc-continent Collision in the Rio Itapicuru Greenstone Belt, Brazil. *J. South. Amer. Earth Sci.* (32): 127-141.

Cruz Filho, B.E., Rosa, M.L.S., Conceição, H., Macambira, M.J.B., Scheller, T., Rios, D.C., Marinho, M.M., 2003. New Pb-Pb evaporation age on zircon of Nordestina batholith, northeast of Bahia state, Brazil. IV South American Symposium on Isotope Geology, vol.II, 532-534.

Davison I, Teixeira JBG, Silva MG, Rocha Neto MB, Matos, FMV (1988) The Itapicuru Belt, Bahia, Brasil: structure and stratigraphical outline. Prec. Res. (44):1-17.

Donatti Filho, J.P., Oliveira, E.P., Pisani, J.R.T., Ochika, F.P., 2008. Geochemistry and mineralogy of kimberlites from the Brauna Kimberlite Province, São Francisco Craton, NE Brazil. 9º Int Kimberlite Conf Ext Abstr, Frankfut, Germany, 9IKC-A-00316.

Kishida, A. 1979. Característica geológica e geoquímica da seqüência vulcão-sedimentar do médio Rio Itapicuru, Bahia. Instituto de Geociências, Universidade Federal da Bahia. Dissertação de Mestrado, 98 p.

Kishida, A., Riccio, L. 1980. Chemostratigraphy of lava sequences from the Rio Itapicuru Greenstone Belt, Bahia, Brazil. Prec. Res. 11: 161-178.

Ludwig, K.R., 1999a. Squid, version 1.02. Berkeley Geochron. Center Spec. Pub. No. 2, 16 pp.

Ludwig, K.R., 1999b. Isoplot/Ex version 2.00, a geochronological toolkit for Microsoft Excel. Berkeley Geochron. Center Spec. Pub. No. 2, 46 pp.

Mello, E.F., Lacerda CMM, Oliveira EP, McNaughton N (1999) SHRIMP U-Pb geochronology on xenotime and zircon from the Ambrosio dome, Rio Itapicuru Greenstone Belt, Brazil: a major syntectonic granodiorite intrusion. Actas II South American Symposium on Isotope Geology, Córdoba, Argentina, September 12-16, 1999, pp.331-334.

Mello, E.F., Xavier R.P., McNaughton N.J., Hagemann S.G., Fletcher I., Snee L. 2006. Age constraints on felsic intrusions, metamorphism and gold mineralisation in the Paleoproterozoic Rio Itapicuru greenstone belt, NE Bahia State, Brazil. Miner. Deposita, 40:849-866.

Oliveira, E.P., Mello E.F., McNaughton N., Choudhuri A. 2002. SHRIMP U-Pb age of the basement to the Rio Itapicuru Greenstone Belt, NE São Francisco Craton. In: SBG, Congr. Bras. Geol., 41, João Pessoa, Anais, 522.

- Oliveira, E.P., Carvalho, M.J., McNaughton, N.J. 2004. Evolução do segmento norte do orógeno Itabuna-Salvador-Curaçá: cronologia da acresção de arcos, colisão continental e escape de terrenos. *Geologia USP, Série Científica.* 4: 41-53.
- Oliveira, E.P., McNaughton, N.J., Armstrong, R., 2010. Mesoarchaean to Palaeoproterozoic Growth of the Northern Segment of the Itabuna-Salvador-Curaçá Orogen, São Francisco Craton, Brazil. In: Kusky, T. M., Zhai, M.-G., Xiao, W. (eds) *The Evolving Continents: Understanding Processes of Continental Growth.* Geol Soc London, Spec Publ 338: 263–286.
- Oliveira E. P., Souza Z. S., McNaughton N. J., Lafon J-M., Costa F. G., Figueiredo A. M., 2011. The Rio Capim Volcanic-Plutonic-Sedimentary Belt, São Francisco Craton, Brazil: Geological, Geochemical and Isotopic Evidence for Oceanic Arc Accretion During Palaeoproterozoic Continental Collision. *Gondwana Research* 19: 735–750, doi:10.1016/j.gr.2010.06.005
- Pisani, J.R.T., Tainton, K.M., Allan, A.F., Silva, S.B., Miranda, J.V., 2001. Geology and exploration of the Brauna Diamantíferous Kimberlites, Serrinha Block, Bahia, Brazil. *Rev Bras Geoc* 31(4): 663-664.
- Rios, D.C., Davis, D.W., Conceição, H., Macambira, M.J.B., Peixoto, A.A., Cruz Filho, B.E., Oliveira, L.L. 2000. Ages of granites of the Serrinha Nucleus, Bahia (Brazil): an overview. *Revista Brasileira de Geociências*, 30: 74-77.
- Rios, D.C., Conceição, H., Davis, D.W., Rosa, M.L.S., Marinho, M.M. 2005. Expansão do magmatismo granítico pós-orogênico no núcleo Serrinha (NE Bahia), cráton do São Francisco: idade U-Pb do maciço granítico Pedra Vermelha. *Revista Brasileira de Geociências*, 35(3):423-426.
- Rios, D.C., Conceição, H., Davis, D.W., Plá Cid, J., Rosa, M.L.S., Macambira, M.J.B., McReath, I., Marinho, M.M., Davis, W.J. 2007. Paleoproterozoic potassic-ultrapotassic magmatism: Morro do Afonso sienite pluton, Bahia, Brazil. *Prec. Res.* (154): 1-30.
- Rios, D.C., Davis D.W., Conceição, H., Davis, W.J., Rosa, M.L.S., Dickin, A.P. 2009. Geologic evolution of the Serrinha nucleus granite-greenstone terrane (NE Bahia, Brazil) constrained by U-Pb single zircon geochronology, Brazil. *Prec. Res.* (170): 175-201.

- Silva, M.G., Coelho, C.E.S., Teixeira, J.B.G., Alves da Silva, F.C., Silva, R.A., Souza, J.A.B. 2001. The Rio Itapicuru greenstone belt, Bahia, Brazil: geologic evolution and review of gold mineralization. *Mineral. Dep.* (36): 345-357.
- Souza, J.D., Kosin M., Melo R., Oliveira E.P., Carvalho M.J. & Leite C.M.M. 2003. Guia de excursão - Geologia do segmento norte do orógeno Itabuna-Salvador-Curaçá. *Rev. Bras. Geoc.*, 33 (I-Suplemento):27-32.